

REMOVAL OF BASELINE WANDERING FROM THE
ELECTROCARDIOGRAM

A THESIS SUBMITTED TO
THE GRADUATE SCHOOL OF NATURAL AND APPLIED SCIENCES
OF
MIDDLE EAST TECHNICAL UNIVERSITY

BY

VOLKAN TANRIVERDİ

IN PARTIAL FULFILLMENT OF THE REQUIREMENTS
FOR
THE DEGREE OF MASTER OF SCIENCE
IN
ELECTRICAL AND ELECTRONICS ENGINEERING

SEPTEMBER 2006

Approval of the Graduate School of Natural and Applied Sciences

Prof. Dr. Canan ÖZGEN
Director

I certify that this thesis satisfies all the requirements as a thesis for the degree of
Master of Science

Prof. Dr. İsmet ERKMEN
Head of Department

This is to certify that we have read this thesis and that in our opinion it is fully
adequate, in scope and quality, as a thesis for the degree of Master of Science

Asst. Prof. Dr. Yeşim SERİNAĞAOĞLU
Supervisor

Examining Committee Members

Prof. Dr. Nevzat Güneri GENÇER (METU,EE) _____

Asst. Prof. Dr. Yeşim SERİNAĞAOĞLU (METU,EE) _____

Asst. Prof. Dr. Çağatay CANDAN (METU,EE) _____

Asst. Prof. Dr. Özgür YILMAZ (METU,EE) _____

Oğuz TANRISEVER(M.S.) (KARDİOSİS) _____

I hereby declare that all information in this document has been obtained and presented in accordance with academic rules and ethical conduct. I also declare that, as required by these rules and conduct, I have fully cited and referenced all material and results that are not original to this work.

Name, Last name :

Signature :

ABSTRACT

REMOVAL OF BASELINE WANDERING FROM THE ELECTROCARDIOGRAM

Tanrıverdi, Volkan

M.S., Department of Electrical and Electronics Engineering

Supervisor: Asst. Prof. Dr. Yeşim Serinağaoğlu

September 2006, 125 pages

ECG measures electrical potentials on the body surface via contact electrodes. Conditions such as movement of the patient, breathing, and interaction between the electrodes and skin cause baseline wandering of the ECG signal. Baseline wandering noise can mask some important features of the ECG signal; hence it is desirable to remove this noise for proper analysis of the ECG signal. This study includes an implementation and evaluation of methods to remove this noise, such as finite impulse response filters, infinite impulse response filters, interpolation filters and adaptive filters. These filters are first applied offline to simulated ECG data. The filter outputs and their frequency spectra are compared to the pure ECG signal and its frequency spectrum using visual inspection and numerical evaluation criteria such as root mean squared error and percentage root relative squared error. The best filters are then selected and applied online to the same simulated data. Finally, these best methods are used to suppress the baseline wandering noise in real ECG

recordings using both offline and online filtering. In the offline application, windowing type filters were found to be the most successful filters among the implemented filters. However, a high filter order should be used to produce such good results, which increases the computation time, thus it may not be the best method for online filtering, in which fast computation is essential. Butterworth bidirectional type is preferred for online filtering since it has lower computational complexity, and it produces acceptable results.

Keywords: Electrocardiography, Baseline wandering noise, ECG noise

ÖZ

ELEKTROKARDİYOGRAFİ SİNYALİNDEN TEMEL ÇİZGİ KAYMALARININ KALDIRILMASI

Tanrıverdi, Volkan

Yüksek Lisans, Elektrik ve Elektronik Mühendisliği Bölümü

Tez Yöneticisi: Yrd. Doç. Dr. Yeşim Serinağaoğlu

Eylül 2006, 125 sayfa

EKG cihazı ile vücut yüzeyine takılan elektrotlar kullanılarak, vücut yüzeyindeki elektrik potansiyelleri ölçülmektedir. Elektrotların vücutla etkileşimi, nefes alma ve benzeri hareketler nedeniyle EKG sinyalinin taban çizgisinde kaymalar meydana gelir. Bu kaymalar EKG den elde edilen bazı önemli bilgilerin bozulmasına neden olur. EKG yi doğru yorumlamak için bu kaymaları yok etmek gerekmektedir. Bu çalışmada gürültüyü yok etmek için sonlu tepki filtresi, sonsuz tepki filtresi, eğri uydurma ve uyarlanabilir filtreleme metotları kullanılmıştır. Bu filtreler önce gürültülü sentetik EKG sinyaline uygulanmıştır ve bu işlemin sonunda elde edilen filtrelenmiş EKG sinyali ile gürültü içermeyen EKG sinyali karşılaştırılmıştır. Bu karşılaştırmayı yaparken frekans spektrumu incelenmiş ve karekök ortalama hata ve karekök bağıl hata değerlendirme metotları da kullanılmıştır. Daha sonra en başarılı sonucu veren filtreler seçilip bu filtreler eş zamanlı filtreleme şeklinde uygulanmıştır. Son olarak eş zamanlı ve eş zamanlı olmayan filtreler gürültülü

gerçek EKG sinyaline uygulanmıştır. Eş zamanlı olmayan filtreler içinde en iyi sonucu veren filtre Blackman pencereleli sonlu tepki filtresi olarak bulunmuştur. Bu sonuca ulaşmak için seçilmiş olan filtrenin derecesi yüksektir. Bu nedenle hızlı işlem yapma gerekliliği olan eş zamanlı filtreleme yöntemi için bu filtrenin başarılı sonuç vereceği söylenemez. Diğer taraftan iki yönlü sonsuz tepki filtresi başarılı bir gürültü bastırma gerçekleştirmiştir ve işlem yoğunluğu da düşüktür. Bu nedenle eş zamanlı filtreleme metodu için bu filtreleme yöntemi tercih edilir.

Anahtar Kelimeler: Temel çizgi kayması, Eksen kayması gürültüsü, EKG gürültüsü

ACKNOWLEDGEMENTS

I would like to express my deepest gratitude to my supervisor Asst. Prof. Dr. Yeřim SERİNAĖAOĖLU for her guidance, advice, criticism and understanding throughout the research. The author would also like to thank OĖuz TANRISEVER for his criticism, comments and precious help at providing the support of KARDİOSİS firm to share the all ECG materials and WinEkgPro software. The author especially thanks to Prof. Dr. Nevzat GENÇER for his considerable guidance and precious advices, Asst. Prof. Dr. ÇaĖatay CANDAN and Asst. Prof. Dr. Özgür YILMAZ for their valuable help. I would like to thank to my friends Koray Özdal ÖZKAN, Emre BAŞESKİ and Serdar ÇULLU for their comments and precious support.

TABLE OF CONTENTS

PLAGIARISM	iii
ABSTRACT	iv
ÖZ	vi
ACKNOWLEDGEMENTS	viii
TABLE OF CONTENTS	ix
LIST OF TABLES	xiii
LIST OF FIGURES	xiv
CHAPTER	
1. INTRODUCTION.....	1
1.1 Conduction System of the Heart and the ECG.....	2
1.2 The 12-Lead Electrocardiogram Signals.....	6
1.3 ECG Stress Test	9
1.4 ECG Noises and Baseline Wandering.....	9
1.5 Problem Definition and Purpose of the Study.....	12
1.6 Literature Study.....	12
1.7 Scope of the Thesis	15
1.8 Outline of the Thesis	15
2. THEORY OF THE STUDY	16
2.1 Digital Filters	16
2.2 Digital FIR Filters	18

2.2.1	Estimation of FIR Filter Order	19
2.2.2	Computer-Based Iterative Filter Design Technique ..	20
2.2.3	FIR Windowing Method	22
2.2.3.1	Rectangular Window.....	25
2.2.3.2	Hamming Window	26
2.2.3.3	Hanning Window	27
2.2.3.4	Blackman Window	27
2.2.4	High-Pass Filter Design	27
2.3	IIR Filter Design	29
2.3.1	Butterworth Function	30
2.3.2	IIR Filters From Analog Filters	31
2.3.3	Bidirectional IIR Filtering.....	32
2.3.4	Non Causal Zero-Phase IIR Filtering	32
2.4	ECG QRS Detection and Spline Filtering.....	34
2.4.1	QRS Detection Algorithm.....	35
2.4.2	Spline Interpolation	37
2.4.2.1	Linear Spline Interpolation	37
2.4.2.2	Cubic Spline Interpolation	38
2.5	Adaptive Filters.....	39
2.5.1	LMS Algorithm.....	39
2.5.2	Normalized LMS.....	40
3.	SYNTHETIC DATA, NOISE AND THE EVALUATION CRITERIA.	42
3.1	Reference Synthetic Data.....	42

3.2	Synthetic Noisy Data	46
3.3	Evaluation Criteria	49
3.3.1	Root Mean Squared Error	49
3.3.2	Root Relative Squared Error	50
4.	RESULTS WITH SYNTHETIC DATA.....	51
4.1	Offline FIR Filters.....	51
4.1.1	Computer-Based Iterative FIR Filter	52
4.1.2	FIR Filtering With Windowing Methods.....	55
4.1.2.1	Hamming Window Filtered Data	55
4.1.2.2	Hanning Window Filtered Data	58
4.1.2.3	Blackman Window Filtered Data.....	61
4.2	Offline IIR Filter Results	64
4.2.1	Butterworth IIR Filtered Data	64
4.2.2	Butterworth Bidirectional IIR Filter	67
4.3	Offline Interpolation Filters	69
4.3.1	Correction with respect to R Peaks	70
4.3.2	Correction with respect to S Peaks	72
4.3.3	Correction with respect to Isoelectric Line	75
4.3.4	Correction with respect to Q Peaks	78
4.4	Offline Adaptive Filtering.....	80
4.4.1	NLMS Filtering	80
4.5	Summary of Offline Filtering Results.....	82
4.6	Online Filtering	87

4.6.1	Blackman Window FIR Online Filter	88
4.6.2	Bidirectional IIR Online Filter	91
4.6.3	Summary of Online Filtering Results	93
4.7	The Effect of Cut-off Frequency on the ST Segment D.Data.	95
5.	FILTERING REAL ECG DATA WITH BASELINE WANDER	102
5.1	Real ECG Data with Baeline Wander Noise	102
5.1.1	Offline Filtering Results.....	103
5.1.2	Online Filtering Results	109
6.	CONCLUSION AND DISCUSSION.....	113
6.1	Comparison of FIR Filters	113
6.2	Comparison of IIR Filters	114
6.3	Cubic Spline Interpolation Filters	115
6.4	Adaptive Filters	115
6.5	Online Filtering	115
6.6	Real ECG Data Filtering	116
6.7	Effects of the Cut-off Frequency	116
6.8	Summary of Conclusions	117
6.9	Future Work	118
	REFERENCES.....	119
	APPENDIX A. MATLAB Based Graphical User Interface.....	123

LIST OF TABLES

TABLES

Table 3.1	Magnitudes of Q, R, S Points	43
Table 4.1	The normalized values of PSD Deviation for Offline Filters.....	83
Table 4.2	The RMSE and RRSE of Offline Filters from second 10 to 30	85
Table 4.3	The RMSE and RRSE of Offlinefilters from second 0 to 50.....	86
Table 4.4	The normalized values of PSD Deviation for online Filters	94
Table 4.5	The RMSE and RRSE of the Online Filters from second 10 to 30	94
Table 4.6	The RMSE and RRSE of the Online Filters from second 0 to 50.....	95

LIST OF FIGURES

FIGURES

Figure 1.1	Action Potential with Phases	3
Figure 1.2	Conduction system of the heart and the ECG.....	3
Figure 1.3	Cardiac signal generation detected by ECG	5
Figure 1.4	ECG QRS signal	6
Figure 1.5	Positions of electrodes for 12 lead ECG.....	7
Figure 1.6	12 lead ECG signals.....	8
Figure 1.7	A baseline noisy data	11
Figure 1.8	The spectrum of the baseline noise and ECG	11
Figure 2.1	Linear phase characteristics of a digital filter.....	17
Figure 2.2	Magnitude response of a low pass filter	19
Figure 2.3	Magnitude response of an ideal filter	23
Figure 2.4	Magnitude response of an ideal window	24
Figure 2.5	Sinc function	25
Figure 2.6	Magnitude response of a low pass filter	28
Figure 2.7	Butterworth filter design parameters	31
Figure 2.8	Block diagram of a bidirectional filter.....	34
Figure 2.9	$h'(n)$ bidirectional filter	34
Figure 2.10	The Algorithm to used to detect the QRS wave	36
Figure 2.11	Base line correction with respect to R waves	36
Figure 2.12	Spline interpolation curve.....	38
Figure 2.13	Adaptive filtering block diagram.....	40
Figure 3.1	Pure(clean) ECG signal(focused)	43
Figure 3.2	Pure ECG signal.....	44
Figure 3.3	The pure data given as a reference.....	44
Figure 3.4	Power spectrum density estimation of pure ECG data	45

Figure 3.5	PSD estimate given as a reference	46
Figure 3.6	Generated noise to form baseline wandering noise model	47
Figure 3.7	Noisy ECG data	47
Figure 3.8	Noisy synthetic data from second 10 to 30.....	48
Figure 3.9	PSD estimate of the noisy data 0 to 10 Hz	48
Figure 3.10	PSD estimate of the noisy data 0 to 4 Hz	49
Figure 4.1	Optimal FIR filter's frequency response	53
Figure 4.2	Optimal FIR filtered data and difference.....	54
Figure 4.3	Power spectrum density estimation of optimal FIR filtered signal	54
Figure 4.4	Hamming window FIR filter's frequency response.....	56
Figure 4.5	Hamming window FIR filtered data and difference	57
Figure 4.6	PSD estimation of hamming window filtered signal.....	57
Figure 4.7	Hanning window FIR filter's frequency response.....	59
Figure 4.8	Hanning window FIR filtered data and reference.....	60
Figure 4.9	PSD estimation of hanning window filtered signal	60
Figure 4.10	Blackman window FIR filter's frequency response	62
Figure 4.11	Blackman window FIR filtered data and results.....	63
Figure 4.12	PSD estimation of Blackman window filtered signal.....	63
Figure 4.13	Butterworth IIR filter's frequency response	65
Figure 4.14	Butterworth IIR filtered data and difference.....	66
Figure 4.15	PSD estimation of Butterworth IIR filtered signal	67
Figure 4.16	Butterworth bidirectional IIR filtered data	68
Figure 4.17	PSD estimation of butterworth bidirectional IIR filtered signal.....	69
Figure 4.18	Cubic spline interpolation curve with R peaks	70
Figure 4.19	Cubic spline correction with respect to R peaks.....	71
Figure 4.20	PSD estimation of cubic spline correction with R peaks	72
Figure 4.21	Cubic spline interpolation curve with S peaks.....	73
Figure 4.22	Cubic spline correction with respect to S peaks	74
Figure 4.23	PSD estimation of cubic spline correction with S peaks	75

Figure 4.24 Cubic spline interpolation curve with isoelectric line	76
Figure 4.25 Cubic spline correction with respect to isoelectric line	77
Figure 4.26 PSD estimation of cubic spline cor. with isoelectric line points	77
Figure 4.27 Cubic spline interpolation curve with Q peaks	78
Figure 4.28 Cubic spline correction with respect to Q peaks.....	79
Figure 4.29 PSD estimation of cubic spline correction with Q peaks.....	80
Figure 4.30 Adaptive NLMS filtered data	81
Figure 4.31 PSD estimation of adaptive NLMS filtered signal	82
Figure 4.32 The normalized deviations from the pure data for 1 Hz and 2 Hz.....	84
Figure 4.33 The normalized deviations from the pure data for 3 Hz and 4 Hz.....	85
Figure 4.34 The percentage RRSE of the filters	86
Figure 4.35 Graphical diagram of online filtering algorithm.....	88
Figure 4.36 Blackman window online FIR filter results.....	90
Figure 4.37 PSD estimation of online Blackman window filtered signal.....	90
Figure 4.38 Bidirectional IIR online filtered data results.....	92
Figure 4.39 PSD estimation of online bidirectional IIR filtered signal	93
Figure 4.40 ST segment depressed baseline noisy data	97
Figure 4.41 PSD estimation of ST segment depressed baseline noisy data.....	97
Figure 4.42 Offline bidirectional IIR filtered data with cut-off 0.4 Hz	98
Figure 4.43 PSD estimate of Offline bid. IIR filtered data with cut-off 0.4 Hz.....	98
Figure 4.44 Offline bidirectional IIR filtered data with cut-off 0.67 Hz	99
Figure 4.45 PSD estimate of Offline bid. IIR filtered data with cut-off 0.67 Hz	99
Figure 4.46 Offline bidirectional IIR filtered data with cut-off 0.85 Hz	100
Figure 4.47 PSD estimate of Offline bid. IIR filtered data with cut-off 0.85 Hz ..	100
Figure 4.48 Offline bidirectional IIR filtered data with cut-off 1.2 Hz	101
Figure 4.49 PSD estimate of Offline bid. IIR filtered data with cut-off 1.2 Hz	101
Figure 5.1 Baseline noisy data record from ECG	104
Figure 5.2 A few consecutive beats of Baseline noisy data.....	104
Figure 5.3 PSD estimation of baseline noisy data from 0 to 60 Hz	105
Figure 5.4 PSD estimation of baseline noisy data from 0 to 6 Hz	105

Figure 5.5	Baseline noise is suppressed with Blackman window FIR filter.....	106
Figure 5.6	Blackman window FIR filtered ECG signal (focused)	106
Figure 5.7	PSD estimation of Blackman window filtered signal.....	107
Figure 5.8	Bidirectional IIR filtered data and difference	107
Figure 5.9	Bidirectional IIR filtered signal (focused).....	108
Figure 5.10	PSD estimation of bidirectional IIR filtered signal	108
Figure 5.11	Blackman window FIR online filtered signal	110
Figure 5.12	Blackman window FIR online filtered signal (focused)	110
Figure 5.13	PSD estimation of Blackman window online filtered signal.....	111
Figure 5.14	Online bidirectional IIR filtered data and difference.....	111
Figure 5.15	Online bidirectional IIR filtered signal (focused).....	112
Figure 5.16	PSD estimation of online bidirectional IIR filtered signal	112
Figure A.1	Prepared graphical user interface (GUI)	123
Figure A.2	Filter design parameters.....	124

CHAPTER 1

INTRODUCTION

Cardiac failure and cardiac diseases are among the main causes of death in the world. Therefore, it is necessary to have proper methods to determine the cardiac condition of the patient. Electrocardiography (ECG) is a tool that is widely used to understand the condition of the heart, since it records the electrical activity generated over the cardiac cycle via electrodes positioned at various locations on the body surface [1]. ECG can measure or detect the following features of the heart [2]:

- The rate and rhythm mechanism of the heart,
- How the heart is placed in the chest cavity,
- Evidence of increased thickness (hypertrophy) of the heart muscle,
- Evidence of the occurrence of a prior heart attack (myocardial infarction),
- Adverse effects of various heart diseases or systemic diseases such as high blood pressure, thyroid conditions, etc., on the heart,
- Adverse effects of certain lung conditions such as emphysema, pulmonary embolus (blood clots to lung) on the heart,
- Evidence of abnormal blood electrolytes (potassium, calcium, magnesium).

ECG of a patient is examined visually in time domain. But examining the ECG curve visually is usually inadequate. Signal processing methods are performed to examine the ECG curve accurately. Frequency domain methods, spectrum estimation and filtering are necessary to examine the ECG curve.

Conditions such as movement of the patient, breathing and interaction between the electrodes and the skin cause baseline wandering of the ECG signal. Baseline wandering can mask some important features of the ECG signal hence it is

desirable to remove this noise for proper analysis and display of the ECG signal. Examining the ECG signal only in time domain is inadequate. Frequency domain ECG signal processing methods are necessary to examine the ECG spectra. Suppression of unwanted frequencies is essential and it is required to examine the ECG correctly. There are various filters to remove the baseline wandering noise. These are finite impulse response (FIR), infinite impulse response (IIR), adaptive and spline interpolation filters. This study includes an investigation of these methods, implementation and verification of each method for offline applications. The offline filters with best performances are then selected and used in online applications. We first compare the filters using simulated data, in which we know the noise free signal, therefore we can compare the filtered output with this noise free data. Then we apply the filters that provide best results with the simulated data to real ECG recordings with baseline wander noise.

In this chapter, we provide background information on the cardiac electrical activity and its relation to ECG and baseline wandering, and we present the scope of this thesis.

1.1 Conduction System of the Heart and the ECG

The distribution of ions across the cell membrane yields a potential difference across the membrane of the cell. This difference is called the transmembrane potential. The transmembrane potential changes during impulse propagation with action potential impulses. An action potential is an essential carrier of the information code that provides the control and coordination of organs like heart. An action potential is a wave of electrical discharge that travels along the membrane of a cell. Depolarization is the rise of the membrane potential, from a negative potential value to a more positive potential. Repolarization is the return of the membrane potential to its resting potential value, as shown in Figure 1.1 [3].

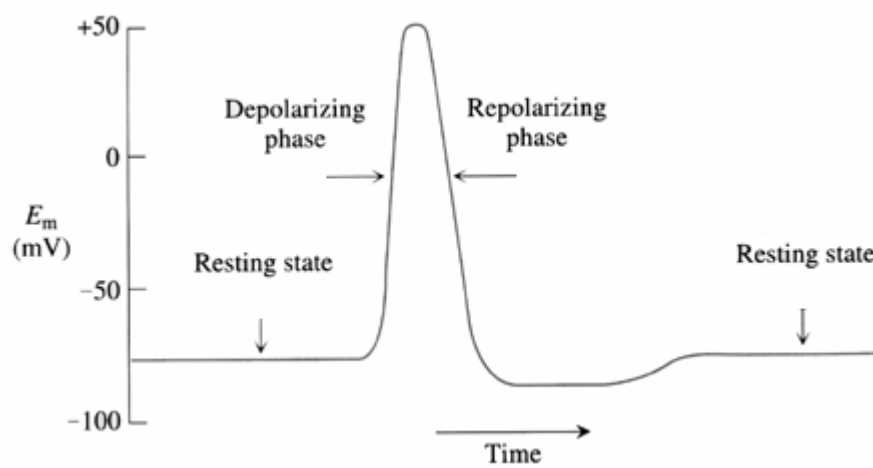


Figure 1.1: Action potential with depolarization, repolarization and the resting phases [3].

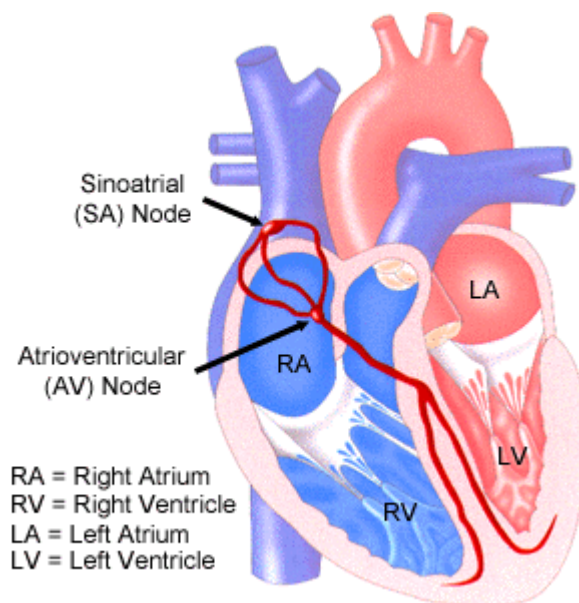


Figure 1.2: Conduction system of the heart and the ECG. The atriums, ventricles, heart muscle and the electrical nodes (SA, AV) are illustrated [4].

The heart works as a pump that pushes blood to the cells of the body. Atria, ventricles, heart muscle, electrical nodes are the main components of the heart as

shown in Figure 1.2. The electrical impulse begins in the sinoatrial (SA) node, located at the top of the right atrium. The SA node is called the heart's natural pacemaker. When an electrical impulse is released from this natural pacemaker, it causes the atria to contract (systole); this is called the atrial depolarization. The signal then passes from the SA node to atrioventricular (AV) node. The AV node receives the signal and waits for blood to pass through the heart valves into the ventricles. After this delay, AV node sends the signal to the muscle fibers of the ventricles via the “bundle of His” causing the ventricles to contract. The SA node sends electrical impulses at a certain rate, but this rate may still change depending on physical demands, stress, or hormonal factors. The contraction of any muscle is associated with electrical changes, and these changes can be detected by electrodes attached to the surface of the body. ECG is a tool to monitor the electrical activity of the heart by using electrodes positioned on the body surface [1, 4].

Figure 1.3 illustrates the relation between the heart's electrical activity and the ECG signal. In this figure, blue regions on the heart and blue coded parts of the ECG signal correspond to depolarization of the heart cells, and pink regions on the heart and pink coded parts of the ECG signal correspond to repolarization of the heart cells. Main components of an ECG signal are the P wave, QRS complex, and the T-wave. P wave corresponds to the depolarization of the atria and during this activity, atrial muscles contract. Formation of the P wave is shown in panels (a-d) of Figure 1.3. When the muscle fibers of the ventricles are excited, contraction of the ventricles starts. QRS complex occurs during the contraction of the ventricles as shown in Figure 1.3 (e-f). T wave represents the repolarization of the ventricles shown in Figure 1.3 (g) [5].

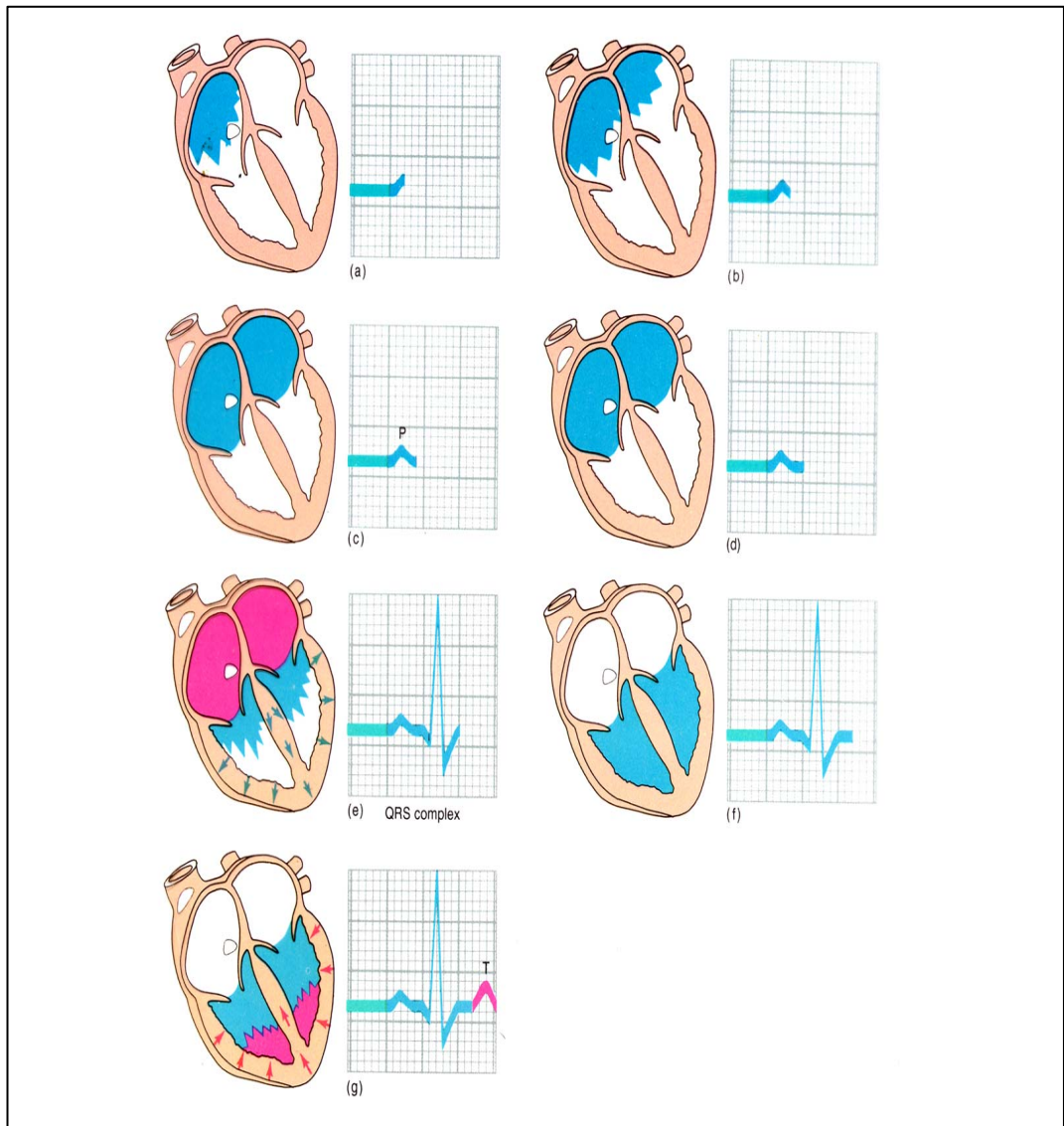


Figure 1.3: Cardiac signal generation detected by ECG. The P, QRS, T signals are generated according to the electrical activity of the heart [5].

Figure 1.4 shows a sample ECG recording with more detail. In addition to the P, QRS and T waves that we have explained above, important intervals are also shown in this figure. Among these intervals, P-R interval is the time from the beginning of the P wave to the beginning of the QRS complex. It represents the interval between the activation of the SA node and the beginning of ventricular

depolarization. Q-T interval represents the time from the beginning of the QRS complex to the end of the T wave. S-T interval starts from the end of the S wave and ends at the end of the T wave. Finally, R-R interval is the time required for 1 complete cycle, and is measured from one R-wave to the next one. This interval is used to determine heart rate [2].

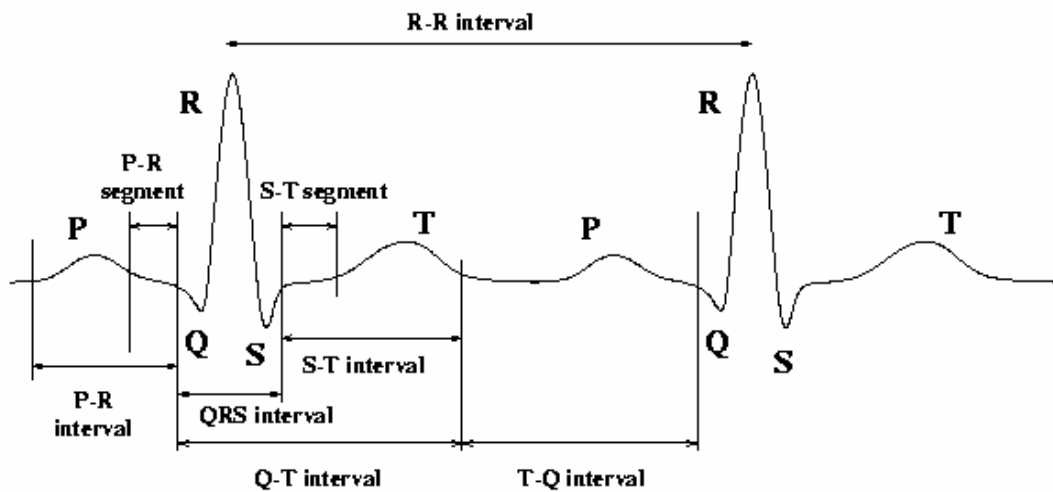


Figure 1.4: Two cycles of an ECG signal are shown in this figure. Important features and intervals are marked on this illustration [6].

P, QRS and T waves and the indicated intervals are important in diagnosis for clinicians. For instance, dead or injured cells from a myocardial infarction will generally show up as irregularities in the ECG signal as ST segment depression on the S-T interval [6].

1.2 The 12-Lead Electrocardiogram Signals

In the 19th century it became clear that the heart generated electricity. Systematical approach to the heart from an electrical view started with Augustus Waller. He found that cardiac currents could be recorded by placing surface electrodes on the body. Willem Einthoven invented the first practical ECG in 1903

[7]. Currently, small size 12 lead ECG devices are developed with interface softwares.

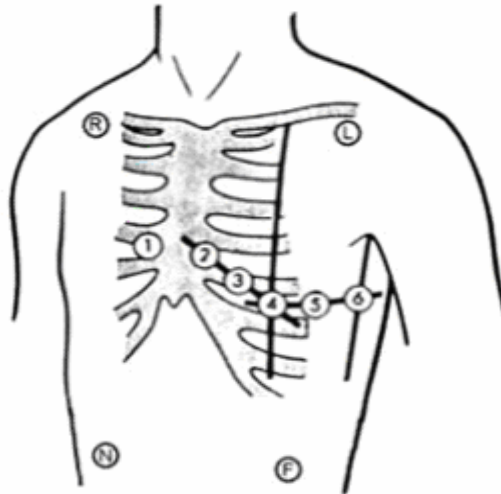


Figure 1.5: Positions of electrodes for 12 lead ECG. R (RA), right arm. L (LA), left arm. F (LL), left leg. N (RL), right leg [8].

Information about heart conditions can be inferred from the ECG recordings by positioning electrical sensing electrodes on the body in standardized locations. The locations of the electrodes for 12 lead ECG are shown in Figure 1.5. Different channels are used because on each channel, electrical activity is monitored from different horizontal and frontal planes. This is like looking at an object from different angles. ECG leads are attached to the body while the patient lies flat on a bed or table. A small amount of gel is applied to the skin, which allows the electrical impulses of the heart to be more easily transmitted to the ECG leads. The numbers 1 to 6 in Figure 1.5 are the positions of electrodes on the chest. R, L, N, and F are the positions of the limb leads where R, L, F and N represent right arm (RA), left arm (LA), left leg (LL), and right leg (RL), respectively.

A sample recording obtained from a 12-lead ECG is shown in Figure 1.6. Channels V1 to V6 are recorded from the chest leads. The other channels are

recorded from limb leads and calculated according to Einthoven triangle (I, II, III, aVR, aVL, aVF) [8].

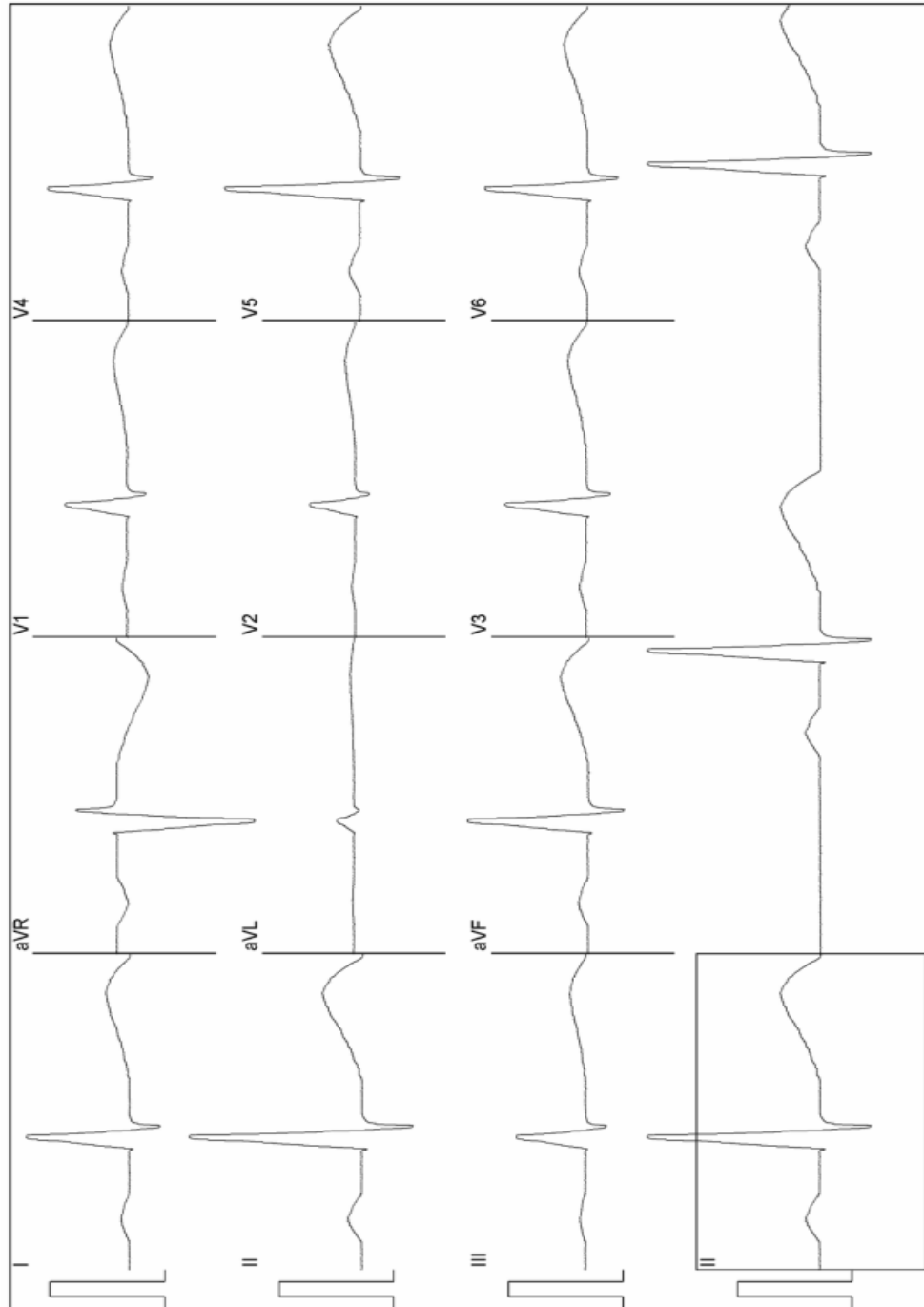


Figure 1.6: 12 lead ECG signals. Channel numbers are set on the left corner for each channel. Channel II is put in a box for more emphasis [8].

1.3 ECG Stress Test

When the body is active, it requires more oxygen than when it is at rest, and, therefore, the heart has to pump more blood. Because of the increased stress on the heart, exercise can reveal problems that are not apparent when the body is at rest. The stress test helps medical doctors determine how well the heart handles the increased demands imposed by physical activity. It is particularly useful for evaluating possible coronary artery diseases and detecting inadequate supply of oxygen-rich blood to the tissues of the heart muscle (ischemia), etc. A stress test requires exercises on a treadmill or an exercise bicycle while patient's ECG, heart rate, breathing, blood pressure are recorded. Real time visualization and real time filtering are required for the stress test [9].

1.4 ECG Noises and Baseline Wandering

Some noises can corrupt ECG signal significantly. Considerable ECG noises are power-line noise, electromyogram (EMG) noise and baseline noise. These noises can mask some important features of the ECG signal hence it is desirable to remove them for proper analysis and display of the ECG signal.

Power-line noise consists of interference in the ECG by nearby AC power supplies and power lines. This affects the ECG as sinusoidal waves which are of the same frequency as the base and harmonic frequencies of 50 or 60 Hz of the power supply.

EMG noise is caused by the contraction of other muscles besides the heart. When other muscles contract, they generate depolarization and repolarization waves that can also be detected by the ECG.

Low frequency artifacts and baseline drift may be caused in the chest lead ECG signals by coughing or breathing, with large movements of the chest, or when an arm or leg is moved during the ECG data acquisition. Poor contact of the electrodes and perspiration of the patient under the electrodes may affect the

electrode impedance which causes low frequency artifacts. Baseline drift may sometimes be caused by variations in temperature and bias in the instrumentation and amplifiers as well. This type of noise is undesired and needs to be removed before any further signal processing, for proper analysis and display of the ECG signal.

Clinicians measure slopes and time intervals in ST, RR and QT segments to predict any abnormalities in the cardiac activity [10, 11]. Therefore, the slope of the baseline should be zero for clean ECG data. When there is baseline wandering noise in the ECG signal, the slope deviates from zero, and this causes difficulties in the evaluation of ECG recordings. For example, baseline drift makes analysis of isoelectric part of the ST segment difficult especially when there is an ST segment elevation or depression, where the slope of the interval is significant. If there is baseline wandering noise, it would be hard to differentiate noise related slope from the slope of the ST segment. Also, a large baseline drift may cause the positive or negative parts in the ECG to be clipped or badly detected by the analog to digital converter (ADC) or the other hardware.

Figure 1.7 shows a sample ECG recording with baseline wandering noise. In this figure, baseline wandering noise is highest at 30 seconds; the deviation in the baseline at this time instant is approximately 0.5 mV. Moreover, the slope of the baseline is quite high from 30 to 40 seconds.

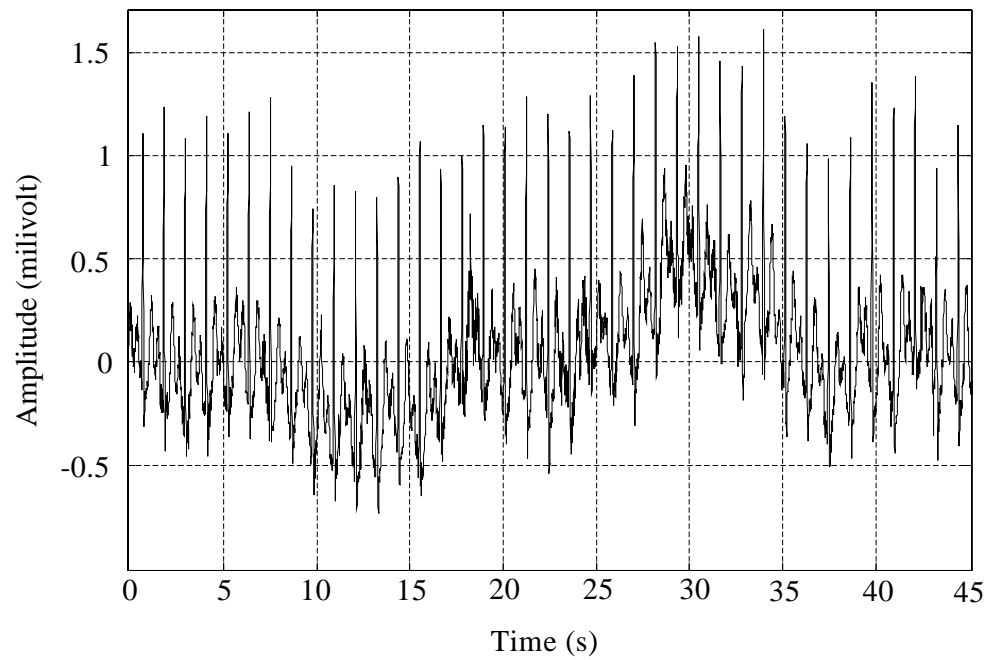


Figure 1.7: A baseline noisy data to give the low frequency artifact on the ECG data.

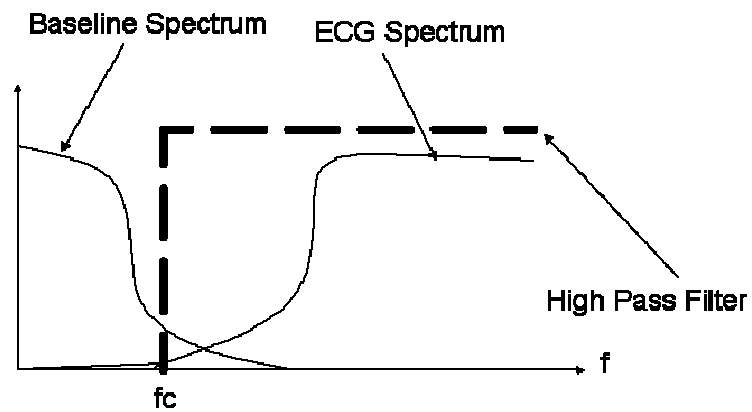


Figure 1.8: The spectrum of the baseline noise and ECG. The function of high pass filter is to suppress the baseline noise. f_c is the cut-off frequency.

1.5 Problem Definition

We have stated earlier that the baseline wander noise makes the analysis of ECG data difficult. Therefore it is necessary to suppress this noise for correct evaluation of ECG.

The baseline of an ECG waveform can vary considerably. There are both high and low amplitude wanders across a number of different frequencies. The frequency range of the ECG signal is 0 - 250 Hz and the frequency range of the baseline noise based on respiration frequency is 0- 0.3 Hz. The spectra of baseline wander and the ECG signal are close, and in some cases may overlap as shown in Figure 1.8. Therefore, a good filter should eliminate the wander while leaving the ECG signal undistorted.

Filtering of the baseline wandering noise can be carried out in two ways, offline and online. Offline filtering is the case when the whole signal is recorded and the entire record is filtered. It is useful in typical 12 channel ECG devices. Online filtering is the case when the signal is filtered as it is recorded. It is necessary when real time processing and visualization are required as in an ECG stress test, in which the signal is simultaneously filtered and monitored in order to examine the effects of stress on the electrical activity of heart.

The main purpose of this study is first to implement various offline baseline noise filters and to discuss the advantages and disadvantages of each offline filter; then to implement successful offline filters for online filtering case.

1.6 Literature Review

One of the most basic techniques for removing baseline wandering noise is known as the cubic spline method. This method is used as a reference method in many studies and performances of other filters are compared with cubic spline. In this method, first the QRS complexes are detected. Then the baseline wander is

estimated with a third order polynomial using various points on the ECG such as Q, R and S points or isoelectric baseline locations as the knots of the splines. Finally, the estimated noise is subtracted from the ECG signal. Cubic spline method has a number of disadvantages; for example, in the presence of high amplitude noise, QRS detector may not operate correctly. Also, baseline wander with sharp transitions may not be accurately described by a cubic polynomial so the order should be increased [12, 13].

A good method of correcting baseline distortion is employing a high pass filtering technique. One such filtering technique is to employ Finite Impulse Response (FIR) filters where the output of the FIR filter is combined with a group delay. As the filter order increases, the complexity of the filter increases. However, if the filter order is selected to be low, then the noise suppression performance of the filter will decrease [14, 15].

Infinite impulse response (IIR) filters, on the other hand, can achieve a sharp transition region with a small number of coefficients. However, an IIR filter that has a cutoff frequency high enough to remove baseline wander has a nonlinear phase response which distorts meaningful components of the ECG waveform. To avoid this distortion, bidirectional filters are used, in which the signal is filtered in a forward direction over a selected window and then the same window is filtered in a reverse direction. In Pottala's study [16], a filter having a nonlinear phase response is used to filter an ECG waveform. In this approach, the data are filtered both forward and backward in time thereby removing nonlinearities injected by the IIR filter. A short window was selected so that the filter could be used for real time purposes. Bidirectional IIR filter is implemented for online and offline cases by HP and DellMar-Avionics and these filters are licenced by US Patents [12, 17].

In [18], Jane implemented an adaptive filter that consists of two adaptive stages. One stage is the 0 Hz adaptive filter. Second stage is an adaptive impulse correlated least mean square (LMS) filter cascaded with a QRS detector. This method is used for online filtering but high mathematical complexity of this filter causes problems in implementation.

In [19], Rossi implemented a fast FIR filter for online filtering. He performed binomial filters like (1, 2, 1) and (1, 2, 4, 1) using moving averages. He tested the results and observed that the filters were fast but suppression performance of the filter was not adequate.

In [20], Pandit discussed a time frequency analysis such as short time fourier transform (STFT) but he showed that it is not adequate when the online filtering window is shorter than four seconds. To have a good frequency resolution, the window time should be wider.

David Cuesta Frau gave an offline baseline removal method using wavelet approximations in [21]. This approximation is based on the signal decomposition in two parts; high frequency components, and the low frequency components. He reported that the results were quite accurate with much less effort than the frequency selective filters.

Xu Lisheng performed a wavelet based cascade adaptive filter to remove the baseline wander in [22]. This cascade adaptive filter worked in two stages. The first stage was a discrete Meyer wavelet filter and the second stage was the cubic spline estimation. But the wavelet filter's edge influence needed to be improved.

In order to filter the baseline wander noise successfully, one needs to select an appropriate cut-off frequency. Previously we have stated that the frequency range of the ECG signal is 0 - 250 Hz and the frequency range of the baseline noise based on respiration frequency is 0 - 0.3 Hz and it is altering with the movement of the patient. The American Heart Association states that the filter's cut-off frequency should be on the order of 0.67 Hz, since it is generally thought that the slowest heart rate is 40 bpm, implying the lowest frequency to be 0.67 Hz. But when the heart rate increases, this frequency also changes. Thus, an adaptive cut-off frequency selection is required. Time varying cut-off frequency is especially valuable for online filtering [17]. Time varying cut-off frequency selection has been studied by a number of researchers. The motivation of these studies was concentrated on adapting the cut-off frequency, since the ECG spectra and the baseline noise spectra move towards right in the frequency axis when the heart rate and the frequency of motion artifact

increase. In [23], Aksela observed that the time varying cut-off frequency should be inversely proportional to the distance between the RR peaks, but he did not give an exact solution to the problem [23]. Sornmo implemented the time varying filter as a bank of linear low pass filters, in which each filter has a slightly differing cut-off frequency but this approach has problems when the heart rate is high [24].

1.7 Scope of the Thesis

In this thesis, we implemented various offline baseline wandering removal filters and compared performances of these offline filters using synthetically generated ECG data. Successful filters are selected and applied to online filtering and these filtering results are compared with the offline case. Then, these successful offline and online filters are used to remove the baseline wandering noise in real ECG recordings. Finally, the effects of the filter cut off frequency are studied.

We implemented all filters using Matlab. A Matlab graphical user interface (GUI) is also created for this implementation and to display the results.

1.8 Outline of the Thesis

In this thesis, after an introduction to ECG signals, baseline noise and a brief literature study in Chapter 1, the theory behind the removal of baseline noise from the ECG is given in Chapter 2. Synthetic data and noise is introduced in Chapter 3. The filters' results on the synthetic data are given in Chapter 4 for both offline and online cases. In Chapter 5 real noisy ECG data are filtered with two of the successful filters. Conclusions and discussions are given in Chapter 6. Finally, the Matlab GUI is given in Appendix A.

CHAPTER 2

THEORY OF THE STUDY

In this chapter, we provide the theoretical background for the thesis. First, we present general information on digital filters. Then we explain characteristics of FIR filters, computer based FIR filters and windowing FIR filters. Next, we discuss IIR filter design and bidirectional IIR filtering. QRS detection and spline interpolation with respect to different points on the ECG signal is introduced. Finally, a brief theory on adaptive filters with least mean square (LMS) algorithm is given.

2.1 Digital Filters

In signal processing, the function of a filter is to remove unwanted parts of a signal, such as random noise, or to specify useful parts of the signal, such as components lying in a certain important frequency range. There are two main kinds of filters; analog and digital. An analog filter uses analog electronic circuits made up from components such as resistors, capacitors and operational amplifiers to produce the required filtering effect. An analog filter can only be changed by redesigning the filter circuit.

A digital filter uses a digital processor to perform numerical calculations on sampled values of the signal for filtering. The processor may be a general purpose computer, or a specialized digital signal processor (DSP) chip. A digital filter is realized by a program stored in the processor's memory. This means the digital filter can simply be changed without affecting the circuitry (hardware). Because of

flexibility in their design, digital filters are commonly used for filtering. Digital filters are discrete time systems and are characterized by their impulse responses. An impulse response can either have a finite or an infinite duration. A finite impulse response 'h(n)' has values extending over a finite time interval from 0 to N and it is zero beyond that interval. The finite impulse response

$$h(n) = (h_0, h_1, \dots, h_N) \quad (2.1)$$

has values in the interval (0 to N) and it is referred to as a finite impulse response system or filter of order N. So an N'th order digital filter has an impulse response with a size of (N+1) samples. The samples of the impulse response function h(n) are also called the filter coefficients [25, 26].

The digital filter has linear phase characteristics as shown in Figure 2.1. This means that the phase response is a linear function of frequency and it has a constant group delay response.

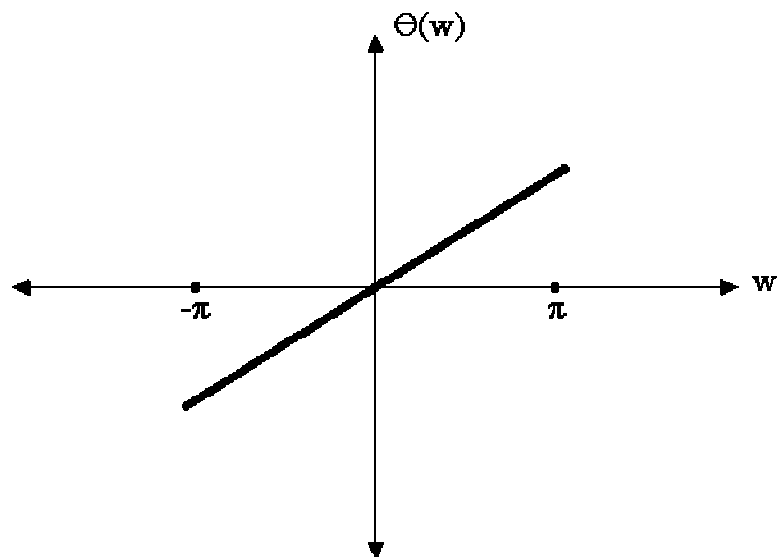


Figure 2.1: Linear phase characteristics of a digital filter. The y-axis is the phase; the x-axis is the frequency axis.

General digital filter design process can be divided into four main steps:

- Approximation (Estimation of the suitable filter parameters for the digital filter.).
- Synthesis and realization (Implementation and realization of the filter).
- Performance analysis (Performance test of filter for given specifications and adjusting the filter characteristics in order to design required filter.).
- Implementation (Implementation of the adequate filter on the noisy data and the realization of the suppression process.).

Both digital FIR and IIR filters are designed with using this filter design procedure in order to approach the required filter specifications.

2.2 Digital FIR Filters

FIR filters are linear discrete time systems, in which the output sequence is related to the input and the impulse response of the filter by the convolution sum:

$$y(n) = \sum_{m=0}^N x(m) \cdot h(n-m) \quad (2.2)$$

The summation on the right hand side is a convolution between the input sequence, $x(n)$, and the impulse response of the filter, $h(n)$. The frequency response of an N 'th order FIR filter is given by:

$$H(w) = \sum_{n=0}^{N-1} h(n) \cdot e^{-j \cdot w \cdot n} \quad (2.3)$$

2.2.1 Estimation of FIR Filter Order

Estimation methods are performed for the approximation of the filter order in order to achieve adequate filter specifications. The magnitude response of the low pass filter is given in Figure 2.2 with the important parameters considered in the design process. In this figure, $H(w)$ is the frequency response of the filter. The regions (0 to w_p), (w_p to w_s) and (w_s to infinity) are called the pass band, the transition band, and the stop band, respectively. δ_{pass} is the pass band ripple, δ_{stop} is the stop band ripple. Then, the order of the FIR filter is estimated by:

$$N = \frac{-20 \cdot \log_{10} \left(\sqrt{\delta_{pass} \cdot \delta_{stop}} \right) - 13}{14.6 \cdot \frac{(w_s - w_p)}{2 \cdot \pi}} \quad (2.4)$$

According to this equation the filter length of an FIR filter is inversely proportional to the transition bandwidth, ($w_s - w_p$). When the designed filter does not give the desired result, the order (N) is increased [27, 28].

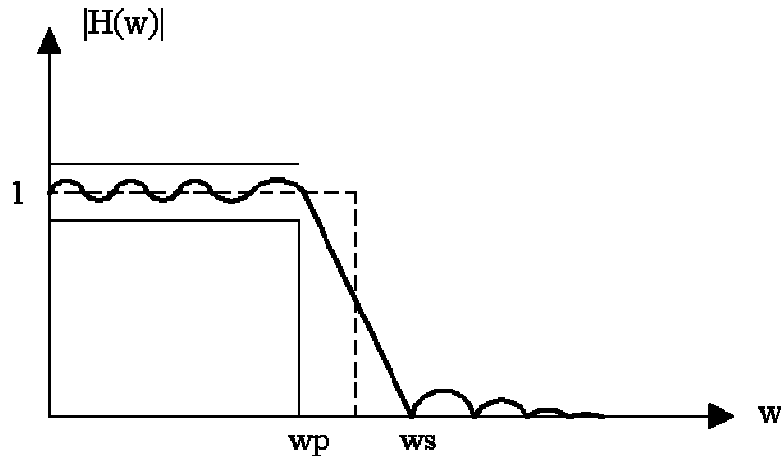


Figure 2.2: Magnitude response of low pass filter. The interval between 0 to w_p is pass-band. The interval between w_p to w_s is transition-band. The interval after w_s is called stop-band. Deviation from magnitude 1 in the pass-band is (δ_{pass}) pass-band ripple. Deviation in the stop-band is (δ_{stop}) stop-band ripple.

2.2.2 Computer-Based FIR Iterative Filter Design Technique

Computer-based iterative methods are performed to design digital filters. Desired filter characteristics are determined and the filter design process starts according to an approximation algorithm using iteration. Desired filter has the magnitude response, $D(\omega)$, and let $|H(e^{j\omega})|$ denote the magnitude response of the digital transfer function to approximate the desired magnitude response $D(\omega)$. The objective is to determine the transfer function coefficients so that the difference between $|H(e^{j\omega})|$ and $D(\omega)$ for all values of ω , which is in the range of $0 \leq \omega \leq \pi$, is minimized [29]. This difference is specified as a weighted error function $E(\omega)$ given by:

$$E(\omega) = P(\omega) \cdot [|H(e^{j\omega})| - D(\omega)] \quad (2.5)$$

where $P(\omega)$ is the weighting function. The mini-max criterion is used as an approximation method, in which the peak absolute value of the error $E(\omega)$, is denoted as ϵ :

$$\epsilon = \max |E(\omega)| \quad 0 \leq \omega \leq \pi \quad (2.6)$$

The linear-phase FIR filter obtained by minimizing the peak absolute value of the weighted error is called the “optimum FIR filter”. The Parks-McClellan algorithm [4] is used for designing the optimum linear-phase FIR filter. The frequency response of a linear phase FIR filter $H(e^{j\omega})$ with order N is given by:

$$H(e^{j\omega}) = e^{-j(N-1)\frac{\omega}{2}} \cdot e^{j\beta} \cdot H_a(\omega) \quad \beta = 0 \text{ or } \pi/2 \quad (2.7)$$

where the amplitude response $H_a(\omega)$ is a real function of ω which is given in equation 2.8. In equation 2.7, type-1 linear-phase FIR filter is considered. Type-1

linear phase FIR filter has a symmetric impulse response of order N equals to 2M+1. Amplitude response of this type of FIR filter is calculated as:

$$Ha(w) = \sum_{n=0}^M a(n) \cdot \cos(w \cdot n) \quad (2.8)$$

where the coefficients a(n) are related to the filter's impulse response coefficients h(n) according to the relation given in equation 2.9:

$$A(0) = h(M) \quad a(n) = 2 \cdot h(M-n) \quad (2.9)$$

The amplitude function Ha(w) is minimizing the error if there exists 'M+2' angular frequencies w_1, w_2, \dots, w_{M+2}

$$0 \leq w \leq \pi \quad \text{such that} \quad w_1 < w_2 < \dots < w_{M+1} < w_{M+2}$$

$$E(w_i) = -E(w_{i+1}) \quad \text{with} \quad 1 \leq i \leq M+1 \quad (2.10)$$

$$|E(w_i)| = \varepsilon \quad \text{with} \quad 1 \leq i \leq M+2$$

The optimum solution can be obtained by solving the set of M+2 equations.

$$P(w_i) (Ha(w_i) - D(w_i)) = (-1)^i \cdot \varepsilon \quad 1 \leq i \leq M+2 \quad (2.11)$$

In order to find unknowns a(i) and ε , equation 2.11 can be rewritten in a matrix form:

$$\begin{bmatrix}
1 & \cos(w_1) & \dots & \cos(M \cdot w_1) & \frac{1}{P(w_1)} \\
1 & \cos(w_2) & \dots & \cos(M \cdot w_2) & \frac{-1}{P(w_2)} \\
\cdot & \cdot & \dots & \cdot & \cdot \\
\cdot & \cdot & \dots & \cdot & \cdot \\
\cdot & \cdot & \dots & \cdot & \cdot \\
1 & \cos(w_{M+1}) & \dots & \cos(M \cdot w_{M+1}) & \frac{(-1)^M}{P(w_{M+1})} \\
1 & \cos(w_{M+2}) & \dots & \cos(M \cdot w_{M+2}) & \frac{(-1)^{M+1}}{P(w_{M+2})}
\end{bmatrix}
\begin{bmatrix}
a(0) \\
a(1) \\
\cdot \\
\cdot \\
\cdot \\
a(M) \\
\varepsilon
\end{bmatrix}
=
\begin{bmatrix}
D(w_1) \\
D(w_2) \\
\cdot \\
\cdot \\
\cdot \\
D(w_{M+1}) \\
D(w_{M+2})
\end{bmatrix} \quad (2.12)$$

which can be solved for the unknowns if the locations of the ‘M+2’ frequencies are known. Remez algorithm [27], which is an iterative procedure, is used to determine the locations of the frequencies.

2.2.3 FIR Windowing Method

FIR filters can also be designed using the windowing method. The ideal filter has infinite number of samples in time domain given in equation 2.15. Windows are performed in order to have finite number of samples in time domain for realizable filter design.

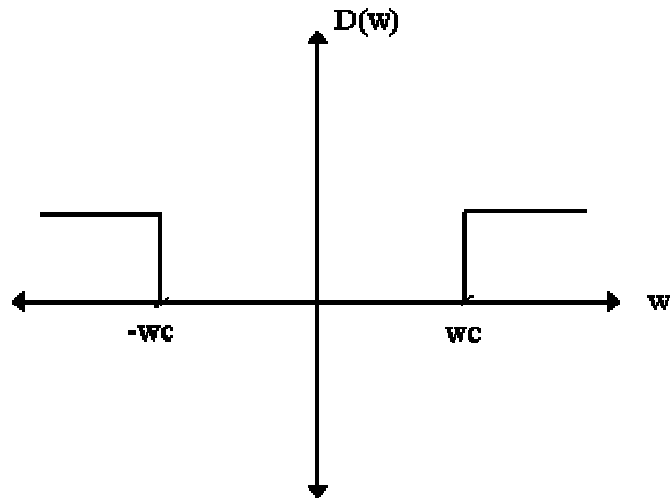


Figure 2.3: Magnitude response of an ideal filter. The cut-off frequency is ω_c .

The ideal high pass filter characteristic is given in Figure 2.3. The continuous frequency response and the discrete-time impulse response are related by the equation 2.13. The aim is giving the relation between ideal frequency domain filter and its impulse response in time domain and to show the importance of windowing method.

$$D(\omega) = \sum_{k=-\infty}^{\infty} d(k) \cdot e^{-j\omega k}$$

$$d(k) = \int_{-\pi}^{\pi} \frac{D(\omega)}{2\pi} e^{j\omega \cdot k} d\omega \quad (2.13)$$

The filter's impulse response can be obtained by using the inverse fourier transform. The filter coefficients will simply be the impulse response samples. The desired low pass filter's response is given by equation 2.14:

$$D(w)=1, \text{ if } |w|<w_c$$

$$= 0, \text{ elsewhere} \quad (2.14)$$

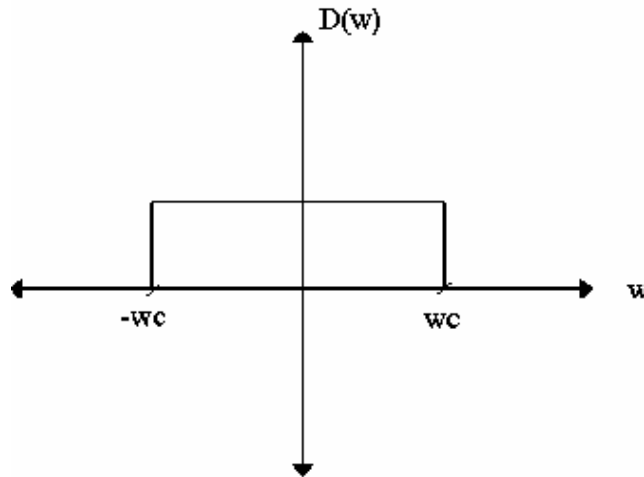


Figure 2.4: Magnitude response of an ideal window. A window function from $-w_c$ to w_c is employed to show the windowing effect.

The impulse response of the ideal window, $d(k)$, is determined in equation 2.15:

$$d(k) = \int_{-\pi}^{\pi} \frac{D(w)}{2 \cdot \pi} e^{j \cdot w \cdot k} dw$$

$$d(k) = \int_{-w_c}^{w_c} \frac{1}{2 \cdot \pi} e^{j \cdot w \cdot k} dw \quad (2.15)$$

$$d(k) = \int_{-w_c}^{w_c} \frac{1}{(2 \cdot \pi) \cdot j \cdot k} (e^{j \cdot w \cdot k} - e^{-j \cdot w_c \cdot k}) dw$$

$$d(k) = \frac{\sin(w_c \cdot k)}{\pi \cdot k} \quad -\infty < k < \infty$$

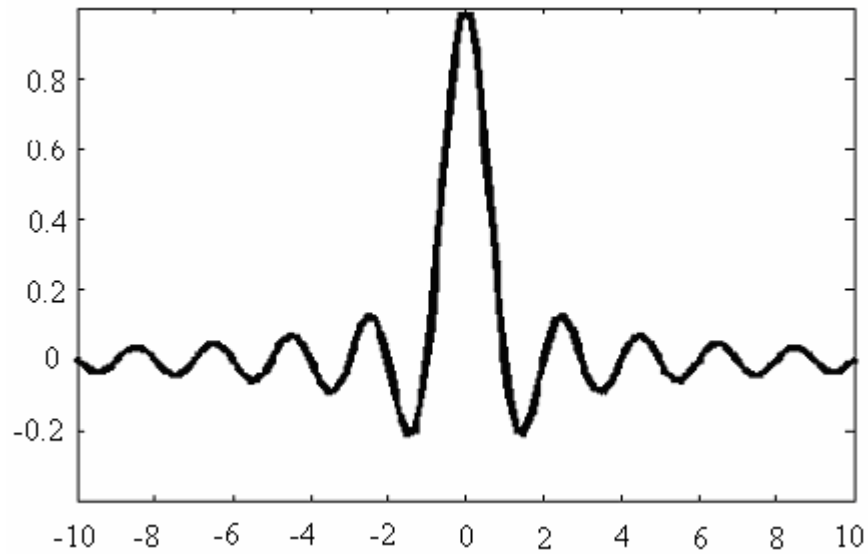


Figure 2.5: Sinc function, $d(k)$ function with k from -10 to 10.

In order to compute the impulse response of a finite duration, a window function is employed. The ideal impulse response, $d(k)$, is multiplied by a window function, $w(n)$, which results in a finite duration. There are different windowing functions. The important window functions are rectangular window, Hamming, Hanning, Blackman windows.

2.2.3.1 Rectangular Window

The filter is required to have finite number of values within a certain interval, from $-M$ to M . This is equivalent to multiplying $d(k)$ by a rectangular function given by:

$$\begin{aligned} w(n) &= 1, \quad |n| < M \\ w(n) &= 0, \quad \text{otherwise} \end{aligned} \tag{2.16}$$

2.2.3.2 Hamming Window

Discontinuities in the time function cause ringing in the frequency domain. The rectangular window is replaced by a window function ending smoothly at both ends which will cause reduction in ripples. The hamming window is an important window function. The hamming window is defined as:

$$w(n) = 0.54 - 0.46 \cdot \cos\left(\frac{2\pi n}{N-1}\right) \quad (2.17)$$
$$n=0,1,\dots,N-1$$

where N is the order of the filter and M is the window length. This equation defines the window samples as already shifted (indices from 0 to 'N-1'). So the impulse response of the FIR low pass filter designed using the hamming window is:

$$h(n) = w(n) \cdot d(n-M)$$
$$h(n) = \left(0.54 - 0.46 \cdot \cos\left(\frac{2\pi n}{N-1}\right)\right) \cdot \frac{\sin((n-M) \cdot \omega_c)}{(n-M) \cdot \pi} \quad (2.18)$$

The ripples that occur in rectangular windowing in both the pass band and the stop band are virtually eliminated. Thus, the filtered data will have a wider transition width.

2.2.3.3 Hanning Window

The Hanning window is defined mathematically as:

$$w(n) = 0.5 - 0.5 \cos\left(\frac{2\pi n}{N-1}\right) \quad (2.19)$$
$$n=0,1,\dots,N-1$$

The difference of Hanning window is performed window function. This function is quite similar to the Hamming window.

2.2.3.4 Blackman Window

The Blackman window exhibits a lower maximum stop band ripple in the resulting FIR filter than the Hamming window. It is defined mathematically as:

$$w(n) = 0.42 - 0.5 \cos\left(\frac{2\pi n}{N-1}\right) + 0.08 \cos\left(\frac{4\pi n}{N-1}\right) \quad (2.20)$$

The width of the main lobe in the magnitude response is wider than that of the Hamming window.

2.2.4 High Pass Filter Design

The amplitude response of a low pass filter is shown in Figure 2.6. Low pass filter is first applied, and with simple transformations the high pass filter can then be easily performed.

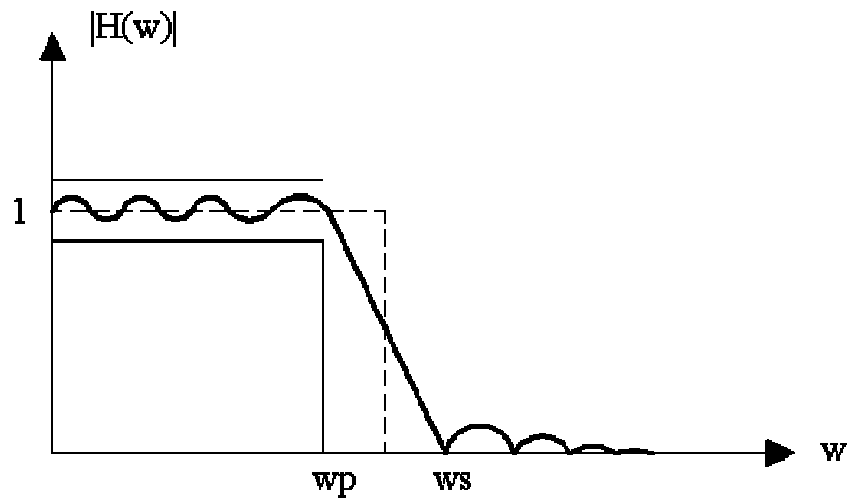


Figure 2.6: Magnitude response of a low pass filter. Pass-band and stop-band regions are illustrated with equation 2.21 and equation 2.22.

The derivation of the transformation is specified with the following equations:

$$w_p = \frac{2 \pi f_{\text{pass}}}{f_s}$$

$$w_s = \frac{2 \pi f_{\text{stop}}}{f_s} \tag{2.21}$$

$$w_c = \frac{2 \pi f_c}{f_s}$$

The ideal cut off frequency, f_c , is at the midpoint between the pass band and stop band edge frequencies set in equation 2.22:

$$f_c = \frac{(f_{\text{pass}} + f_{\text{stop}})}{2} \tag{2.22}$$

The transition width is defined as:

$$\Delta f = f_{\text{stop}} - f_{\text{pass}} \tag{2.23}$$

Since the role of f_{pass} and f_{stop} are interchanged in order to design high pass filter. The ideal high pass impulse response is obtained from the inverse fourier transform of the ideal high pass frequency response. It is specified by equation 2.24:

$$d(k) = \left(\delta(k) - \frac{\sin(w_c \cdot k)}{\pi k} \right) \quad (2.24)$$

The windowed filter impulse response is:

$$h(n) = w(n) \cdot \left[\delta(n - M) - \frac{\sin[(n - M) \cdot w_c]}{(n - M) \pi} \right] \quad (2.25)$$

$$h(n) = \delta(n - M) - w(n) \cdot \frac{\sin[(n - M) \cdot w_c]}{(n - M) \pi}$$

2.3 IIR Filter Design

An IIR filter is one whose impulse response theoretically continues for ever because the recursive terms feed back energy into the filter input and keep it as specified in the following equation:

$$y(n) = \left[\sum_{k=1}^N a(k) \cdot y(n-k) + \sum_{k=0}^M b(k) \cdot x(n-k) \right]$$

$$H(z) = \frac{\sum_{k=0}^M b(k) \cdot z^{-k}}{\sum_{k=0}^N a(k) \cdot z^{-k}} \quad (2.26)$$

The theory of Butterworth function is explained here but, the order of the filter should be high and implementing a filter of that order is not easy to perform. In addition to this difficulty, solving these high order equations is not straightforward.

2.3.1 Butterworth Function

The magnitude squared function of the Butterworth approximation is

$$(|H(w)|)^2 = \frac{1}{1 + w^{2 \cdot n} \cdot c} \quad (2.27)$$

for an n'th order filter. The constant c determines at which frequency, w, the transition of the pass band to stop band occurs. The order of the required Butterworth filter is calculated by:

$$n \geq \frac{\ln(M)}{\ln(\Omega)}$$

$$\Omega = \frac{w_s}{w_p} \quad (2.28)$$

$$M = \sqrt{\frac{10^{0.1 K_s} - 1}{10^{0.1 K_p} - 1}}$$

K_s , K_p are ripples in stop-band and pass-band respectively and in decibels (dB) [14].

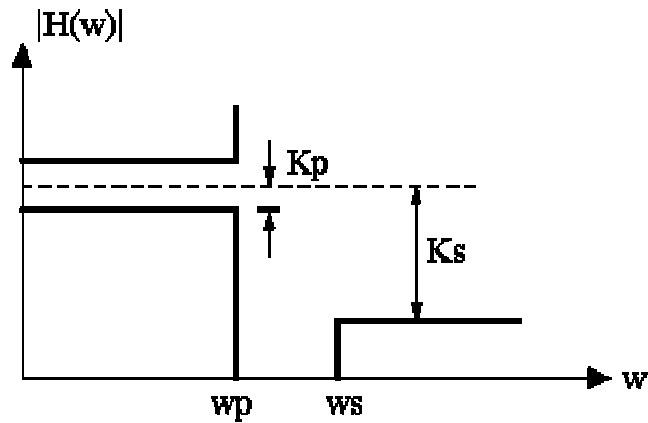


Figure 2.7: Butterworth filter design parameters. The ripples, pass-band and stop-band region and the boundaries of the frequency selective filter are illustrated.

2.3.2 IIR Filters from Analog Filters

Analog filters are designed by using approximation methods. The bilinear transformation converts the analog filter into a digital IIR filter. Bilinear transformation is a frequency domain method of converting the analog filter transfer function $H(s)$ into a digital form, $H(z)$. The transformation is performed by changing the variables:

$$s = \left(\frac{2}{T} \right) \cdot \frac{z - 1}{z + 1} \quad (2.29)$$

where T is the sampling period.

It is called bilinear since both the numerator and denominator of these transformation equations are linear. This transformation is reversible in that $H(s)$ can be obtained from $H(z)$ by the following substitution [14]:

$$z = \frac{\left(\frac{2}{T}\right) + s}{\left(\frac{2}{T}\right) - s} \quad (2.30)$$

2.3.3 Bidirectional IIR Filtering

High pass IIR filters are recursive filters that offer the advantage of fewer computations than the FIR filters. But IIR filters have a phase distortion that is caused by nonlinear phase response of IIR filters. A solution to phase distortion problem is to apply the IIR filter to the ECG signal in both directions. This is referred to as the “zero phase IIR filter”. Filtering in forward direction distorts the ECG signal. The reverse direction filtering corrects the distortion of the ECG signal. The algorithm of the bidirectional filtering is shown in Figure 2.8. And the algorithm is represented with a filter $h'(n)$ which is given in Figure 2.9.

2.3.4 Non Causal Zero-phase IIR Filtering

The phase response of causal IIR filter is non linear. However, if the IIR filter is implemented as a non causal operator, its phase response can be made exactly zero or linear. The recursive difference row is implemented as causal systems and it executes in forward, starting at $n=0$ than $n=1, 2, 3...$ When the difference equation is applied at $n=0$, then $n=-1, -2...$ In this case the impulse response of the system is left sided and system is anti-causal. The bilateral z-transform describes anti causal systems [30, 31]. If a causal system has a rational z-transform:

$$H_c(z) = \frac{B(z)}{A(z)} \quad (2.31)$$

ROC is given as:
 $|z| > R_{\max}$

the related anti-causal system is:

$$H_a(z) = \frac{B\left(\frac{1}{z}\right)}{A\left(\frac{1}{z}\right)} \quad (2.32)$$

ROC is given as:

$$|z| < \frac{1}{R_{\max}}$$

Also the radius of the largest root of $A(z)$ satisfies $R_{\max} < 1$ and both of these systems are stable. The region of convergence (ROC) determines whether the impulse response is right sided or left sided.

$$h_a(n) = h_c(-n) \quad (2.33)$$

$$H_a(z) = H_c\left(\frac{1}{z}\right)$$

The two impulse responses are related with a time flip (time reversal).

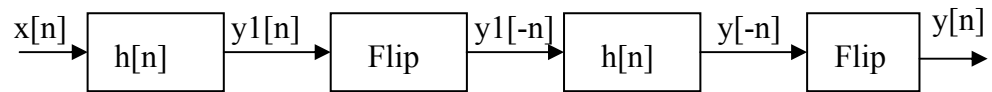


Figure 2.8: Block diagram of a bidirectional filter. The $h[n]$ is the order 5 Butterworth IIR filter and flip is the time reversal of the signal in time domain.

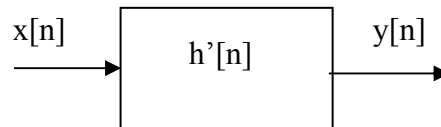


Figure 2.9: The $h'(n)$ is a bidirectional zero-phase filter. It is a zero phase filter to simply show the group of block diagrams specified in Figure 2.8.

2.4 ECG QRS Detection and Spline Filtering

One of the most common technique for baseline wander removal is spline interpolation where the QRS waves are detected and interpolation techniques are employed in order to determine the smoothest curve joining several QRS point. Then, filtering of the ECG baseline wander can be performed by subtracting the curve representing the baseline wander estimated by the cubic spline technique from the ECG signal [32, 33]. In this approach, first, R peaks are detected, than the Q and S peaks and iso-electric lines are distinguished. The baseline curve is constructed and subtracted from the noisy data. The steps are divided into QRS detection and spline interpolation parts and each part is examined in the following subsections.

2.4.1 QRS Detection Algorithm

The block diagrams shown in Figure 2.10 are applied serially and each block is explained in detail in this subsection. The block diagrams in Figure 2.10 are applied in order to find the QRS points.

Pre-filtering: A low pass and a high pass filter are employed serially for a better result on the output of the differentiator to smooth the input data before derivation. Smoothing filters defined by equations 2.34 are used for low pass and high pass filtering.

For low pass filtering:

$$y(n) = \frac{x(n) + 2 \cdot x(n-1) + x(n-2)}{4} \quad (2.34)$$

For high pass filtering:

$$y(n) = -x(n) + 3 \cdot x(n-1) - x(n-2)$$

Derivative operator: The derivative procedure suppresses the low frequency components of P and T waves, and provides a large gain to the high frequency components arising from the high slopes of the QRS complexes [34]. The derivative operation for the algorithm is specified as:

$$y(n) = \frac{2 \cdot x(n) + x(n-1) - x(n-3) - 2 \cdot x(n-4)}{8} \quad (2.35)$$

Squaring: The squaring operation makes the result positive and emphasizes large differences resulting from QRS complexes. The small differences arising from P and T waves are suppressed, and the high frequency components in the signal related to the QRS complexes are further enhanced.

Integration: The output of a derivative based operation will exhibit multiple peaks within the duration of a single QRS complex. The algorithm performs smoothing of the output of the preceding operations through a moving window integration filter to yield a single peak for the detection of a single QRS complex using equation 2.36 [35].

$$y(n) = \frac{x(n - (N - 1)) + x(n - (N - 2)) + \dots + x(n)}{N} \quad (2.36)$$



Figure 2.10: The algorithm to find the QRS waves. In our thesis, it is executed to identify the R peaks. The block diagrams are carried out in cascade.

At the end of the above procedures, R points are detected. An interpolation curve is fitted passing through these points [36] and baseline correction is realized by using the created interpolation curve.

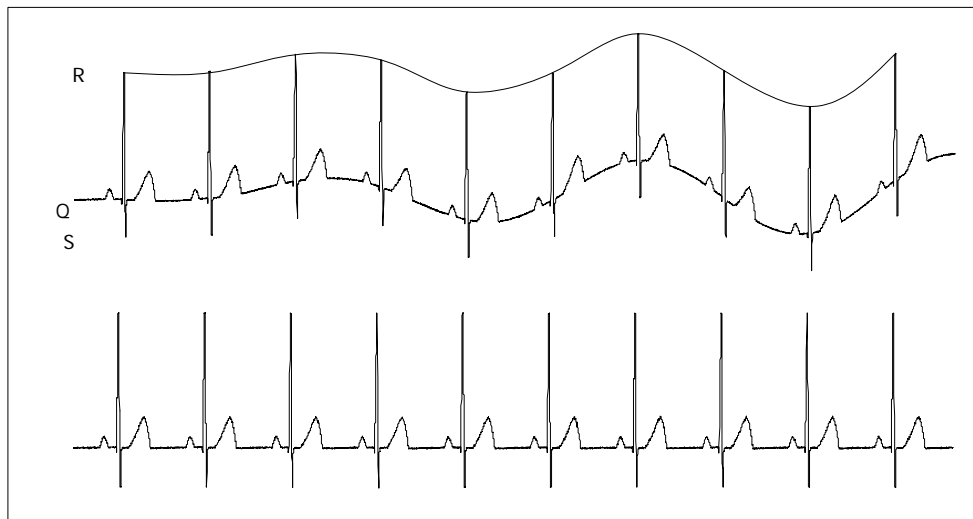


Figure 2.11: Base line correction with respect to R waves. In the first curve, signal has baseline noise and the estimated baseline noise is shown. In the second figure, the signal is corrected by subtracting the estimated baseline noise.

The simplest method of performing spline correction is the linear spline interpolation method. Other methods are quadratic and cubic spline. In these methods, interpolation is executed using curves instead of lines [37]. The following section will present the theory of spline interpolation.

2.4.2 Spline Interpolation

Spline interpolation is a method that fit a polynomial between an interval using points according to the degree of interpolation. After the detection of interpolation points the spline interpolation is performed with these points. In each interval 'i' a spline is constructed according to the degree of polynomial $S_i(x)$ (linear, quadratic or cubic). Spline function $S_i(x)$ in the specified intervals is given as:

$$S_0(x): x \in [x_0, x_1]$$

$$S_1(x): x \in [x_1, x_2]$$

...

$$S_{n-1}(x): x \in [x_{n-1}, x_n]$$

Using $S_i(x)$ polynomial of degree 'n', data set is uniquely interpolated.

2.4.2.1 Linear Spline Interpolation

Linear spline interpolation is the simplest form of spline interpolation. The data points are graphically connected by straight lines. The resultant spline is just a polygon. Each $S_i(x)$ is a linear function and it is formulated with equation 2.37. The linear spline interpolation is illustrated in Figure 2.12.

$$S_i(x) = y_i + \frac{(y_{i+1} - y_i) \cdot (x - x_i)}{x_{i+1} - x_i} \quad (2.37)$$

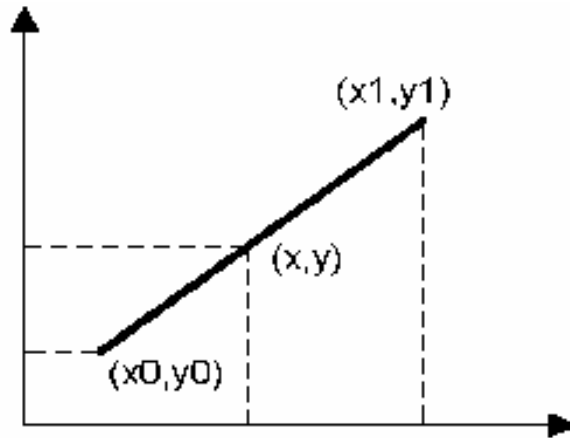


Figure 2.12: Spline interpolation curve (linear). The present and the neighbor points used in the iteration to find the spline curve.

2.4.2.2 Cubic Spline Interpolation

For a data set, x_i , using 'n+1' points, we can build a cubic spline curve with 'n' piecewise cubic polynomials between these data points. Cubic polynomial $S_i(x)$ is such that:

$$S_0(x): x \in [x_0, x_1]$$

$$S_1(x): x \in [x_1, x_2]$$

...

$$S_{n-1}(x): x \in [x_{n-1}, x_n]$$

Interpolation polynomial to build cubic spline curve is defined in equation 2.38 and z_i is the second derivative of $S_i(x_i)$.

$$S_i(x) = \frac{\left[z_{i+1} (x - x_i)^3 + z_i (x_{i+1} - x)^3 \right]}{6h_i} + \left(\frac{y_{i+1}}{h_i} - \frac{h_i}{6} z_{i+1} \right) (x - x_i) + \left(\frac{y_i}{h_i} - \frac{h_i}{6} z_i \right) (x_{i+1} - x) \quad (2.38)$$

$$h_i = x_{i+1} - x_i \quad (2.39)$$

2.5 Adaptive Filters

Adaptive filters are used when the noise is not stationary and the noise is uncorrelated with the signal. When no information is available about the spectral characteristics of the signal and noise, a second source or recording site is available to obtain a reference signal that is strongly correlated with the noise but uncorrelated with the signal. Adaptive filter acts as a fixed filter when the signal and noise are stationary [17]. Least mean square and normalized least mean square algorithms are explained in the following subsections.

2.5.1 Least Mean Square (LMS) Algorithm

The objective of the algorithm is to adapt the coefficients of FIR filter, W , to match as closely as possible to the response of unknown system, H . The adaptive filter, W , is adapted using the least mean square algorithm, which is the most widely used adaptive filtering algorithm. As shown in Figure 2.13 $d(n)$ is the desired signal and $y(n)$ is the output of filter. The error signal $e(n)$, is computed as: $e(n) = d(n) - y(n)$ which measures the difference between the output of the adaptive filter and the output of the unknown system. On the basis of this measure, the adaptive filter will change its coefficients in an attempt to reduce the error [38]. In equation 2.40 the filter adaptation equation is given as:

$$w_{n+1}(k) = w_n(k) + \mu \cdot E(e(n) \cdot x(n)) \quad (2.40)$$

In this equation, μ is a constant that represents the step size and it controls the gradient information used to update each coefficient. After adjusting each coefficient according to the gradient of the error, the adaptive filter should converge; that is, the difference between the unknown and adaptive systems should get small. The adaptation of the equation is:

$$w_{n+1}(k) = w_n(k) + \mu \cdot e(n) \cdot x(n-k) \quad (2.41)$$

When $x(n)$ is a complex number, complex conjugate of $x(n)$ is applied in equations 2.40 and 2.41.

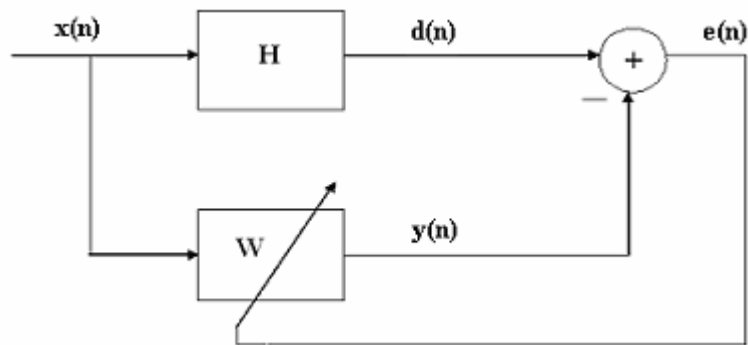


Figure 2.13: Adaptive filtering block diagram using gradient descent adaptation. Here the W is the coefficient matrix, $d(n)$ is the desired signal, $e(n)$ is the error signal, H is the unknown system.

If μ is very small, then the coefficients change only a small amount at each update and the filter converges slowly. On the other hand, when the step-size is too large, the coefficients may change too quickly and the filter will diverge. Suitable step size should be selected by adjusting the step size.

LMS filter may not converge due to suitable step size. Since, it controls the gradient information used to update each coefficient. In normalized least mean square (NLMS) filter gradient step factor is normalized and it converges easily.

2.5.2 Normalized LMS

In ‘normalized’ LMS, the gradient step factor μ is normalized by the energy of the data vector.

$$\mu(n) = \frac{\beta}{x^H(n)x(n) + \varepsilon} \quad (2.42)$$

where β is a normalized step size selected between 0 and 2, and ε is a small number introduced to prevent division by zero if the denominator zero.

$$w_{n+1} = w_n + \mu(n) \cdot x(n) \cdot e(n) \quad (2.43)$$

When $x(n)$ is a complex number in equation 2.43, the complex conjugate of $x(n)$ is applied [39].

CHAPTER 3

SYNTHETIC DATA, NOISE AND THE EVALUATION CRITERIA

In this chapter, the synthetic data recorded from an ECG simulator and the generated noise for modeling baseline wander is presented, and the employed evaluation criteria are specified.

3.1 Reference Synthetic Data

The synthetic data used in this study were recorded from a 12 lead ECG simulator and provided by Oğuz Tanrıseven from Kardiosis. The duration of the recording is 50 seconds and sampling rate is 1 kHz. The resolution of the data is two bytes (16 bits). Lead 'II' is used in the thesis because it has the highest amplitudes in the 12 lead ECG. The magnitudes of the signal at the Q, R, S points of all 12 leads are given in Table 3.1. In Figure 3.1 three consecutive beats are plotted in order to show the data of Lead 'II'. Figure 3.2 shows the entire 50 seconds recording from lead 'II'. The synthetic recording used as the reference data in this thesis is shown in Figure 3.3. In this figure, samples between seconds 10 to 30 are taken from the signal in Figure 3.2 to show the data in detail and also to examine the baseline wandering noise easily.

Table 3.1: Magnitudes of Q, R, S points in 12-lead ECG channels (scaled in millivolts).

	Q	R	S		Q	R	S
I	-0.09	0.92	-0.34	V1	-0.03	0.38	-0.10
II	-0.14	1.50	-0.55	V2	-0.05	0.53	-0.17
III	-0.05	0.58	-0.20	V3	-0.06	0.70	-0.25
AVR	-1.20	0.43	0.08	V4	-0.06	0.70	-0.25
AVL	0	0.18	-0.06	V5	-0.09	1.15	-0.41
AVF	-0.1	1.04	-0.36	V6	-0.08	0.90	-0.30

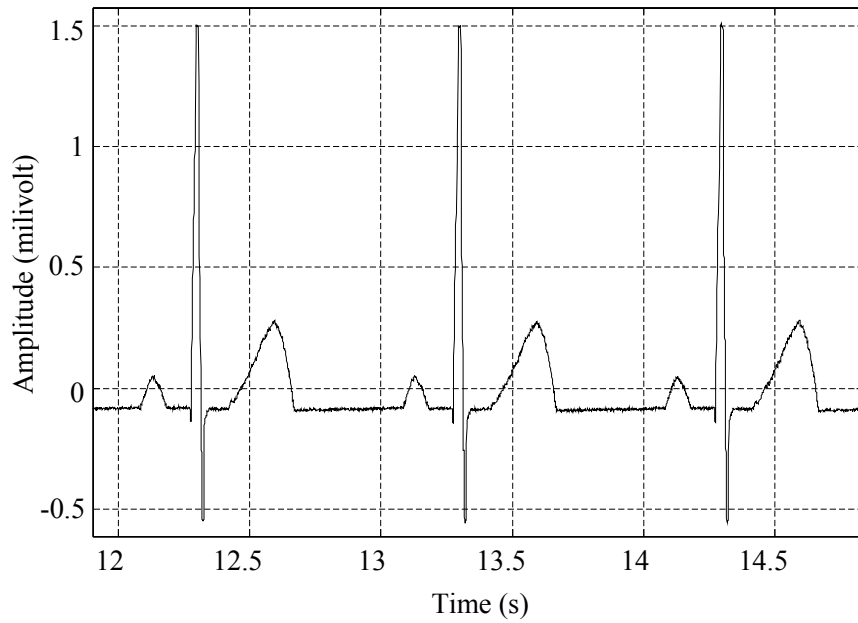


Figure 3.1: Pure ECG signal from Lead ‘II’; 3 consecutive beats taken from synthetic data are plotted in this figure to show the data in detail. It illustrates the Q, R and S points magnitudes given in Table 3.1.

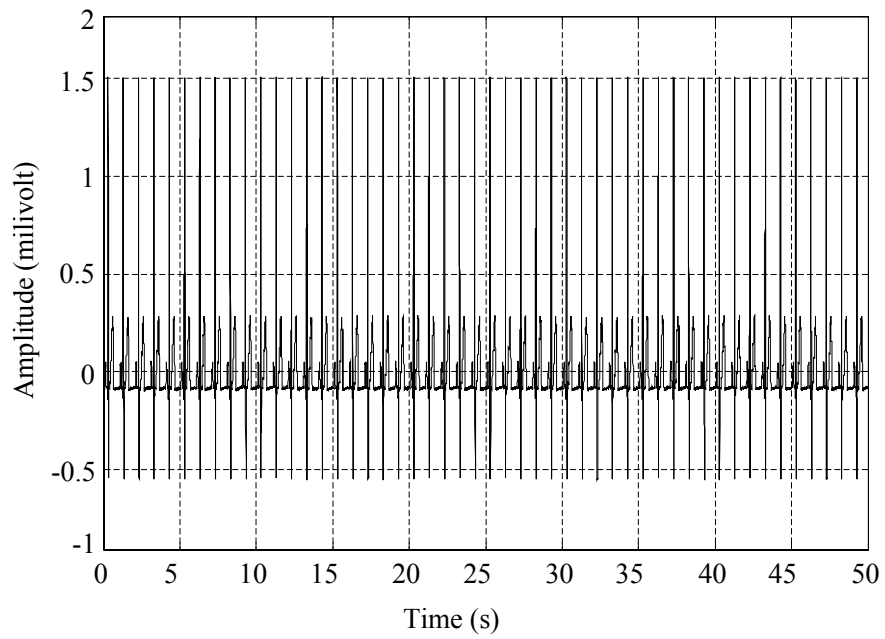


Figure 3.2: Pure (clean) ECG signal. Time axis is scaled in seconds (s), y axis is in millivolts. The amplitude of the data changes between -1 to 2 millivolts.

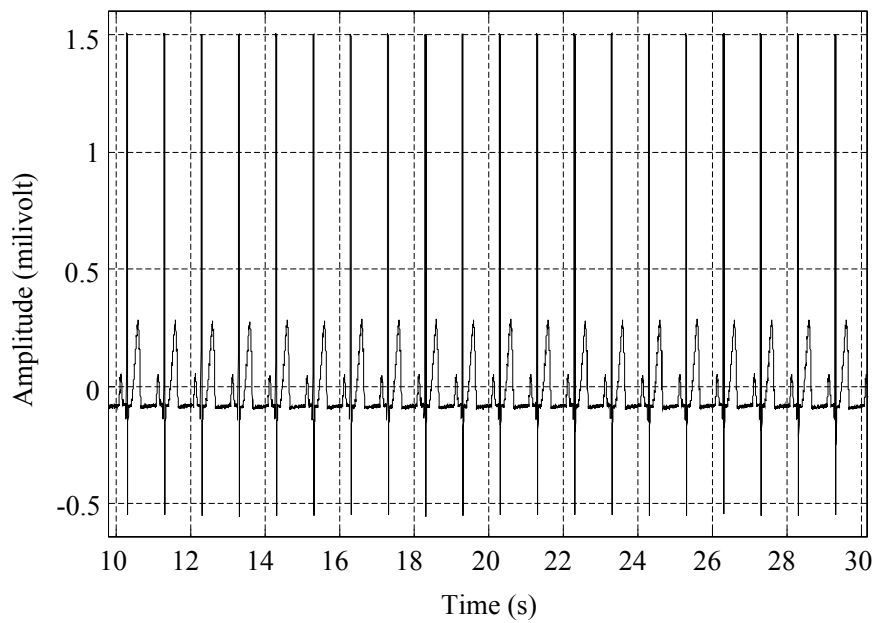


Figure 3.3: Reference data. Samples between 10- 30 seconds are extracted from Figure 3.2.

In Figure 3.4 power spectrum estimation of pure ECG data shown in Figure 3.2 is given. Y-axis is in (power/frequency) unit to understand the spectra easily and the x-axis is the frequency (f) axis with 'Hz' unit. The harmonics of simulator data are given and frequency range is approximately from 1 Hz to 45 Hz. Figure 3.5 is the zoomed version of the Figure 3.4 in order to examine the influenced frequency components by filtering process in detail.

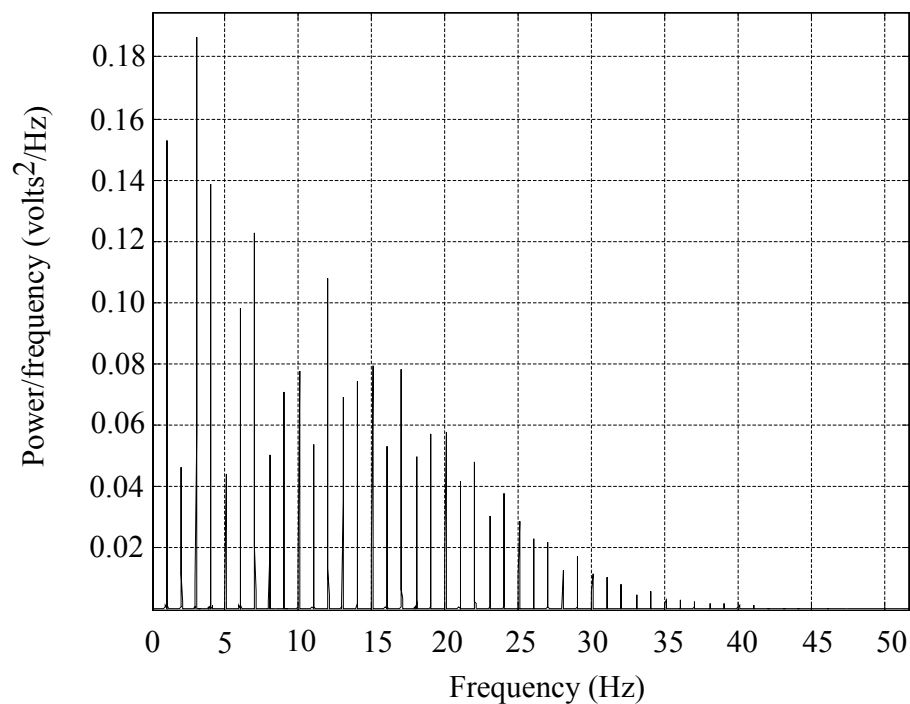


Figure 3.4: Power spectrum density estimation of pure ECG data. The harmonics are given with the frequency. Y axis is formed in power/frequency scale.

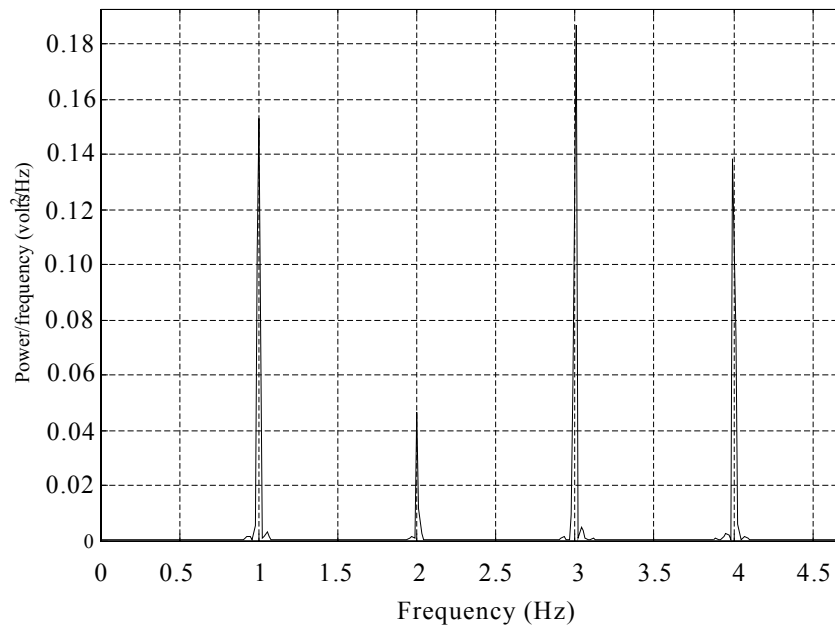


Figure 3.5: Power spectrum density estimation of the pure data. It is specified as a reference. It is scaled up using Figure 3.4 in order to show the spectrum in detail.

3.2 Synthetic Noisy Data

Noise is modeled and added to the pure data to form the noisy data. Pottala's noise model was used in this study [12]. In this model, the noise has two cosine wave components at frequencies 0.25 Hz and 0.3 Hz. These frequencies are the typical respiratory frequencies. The magnitudes of the 0.25 and 0.3 Hz cosine waves have the amplitudes 250 and 200 micro-volts, respectively [12]. Generated noise to simulate baseline wandering noise model is shown in Figure 3.6. The noise in Figure 3.6 is added to the pure data in Figure 3.2 and the noisy data in Figure 3.7 is constructed. In Figure 3.8 samples from second 10 to 30 include one period of noise. Power spectrum density estimation of the noisy data is shown in Figure 3.9 from 0 to 10 Hz. The spectrum is clipped from 4 Hz to compare the noisy data and filtered data in detail. Figure 3.10 is specified as a reference and aim is suppressing the noise and obtaining the PSD of synthetic data given in Figure 3.5.

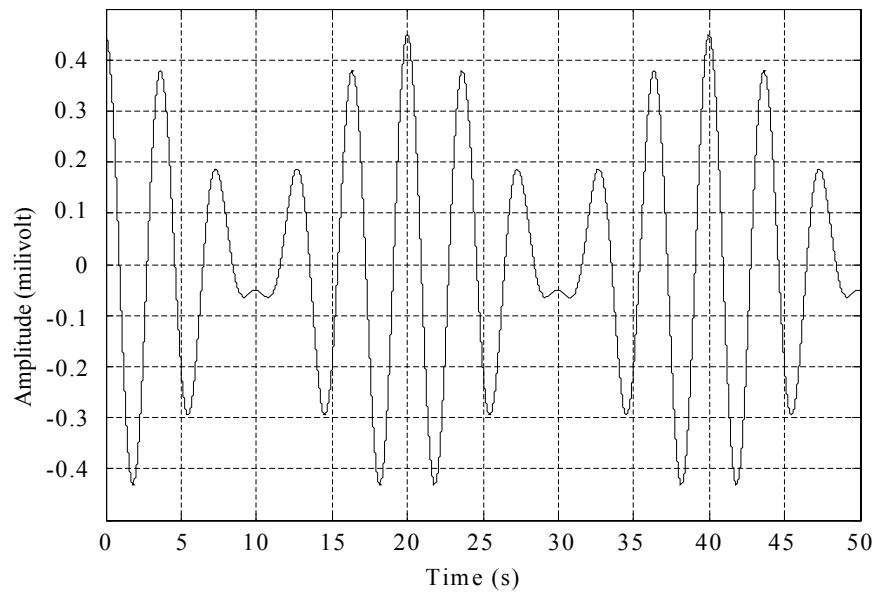


Figure 3.6: Generated noise to form baseline wandering noise model. The noise is added to the pure data using specified cosine waves.

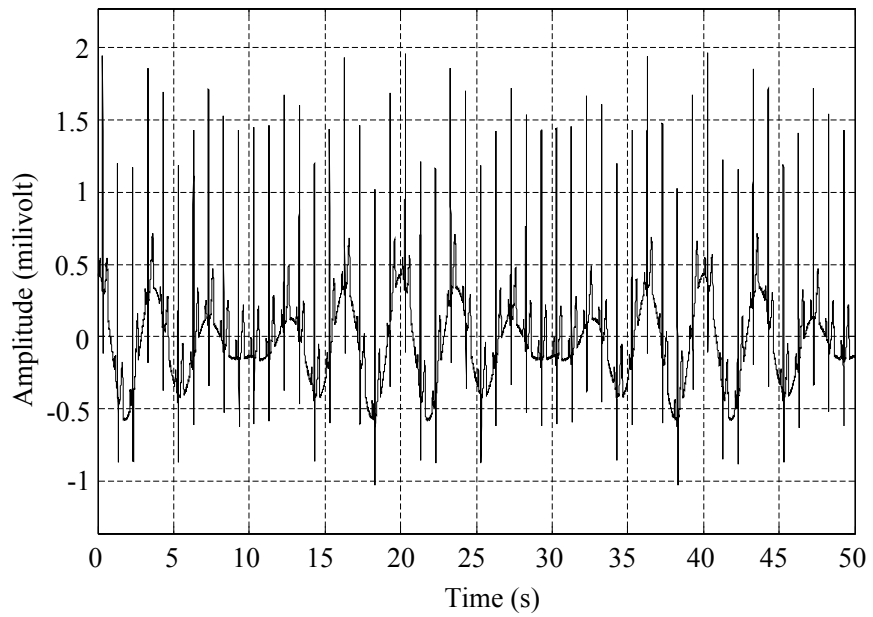


Figure 3.7: Noisy ECG data. The noise in Figure 3.6 is added to the pure data in Figure 3.2.

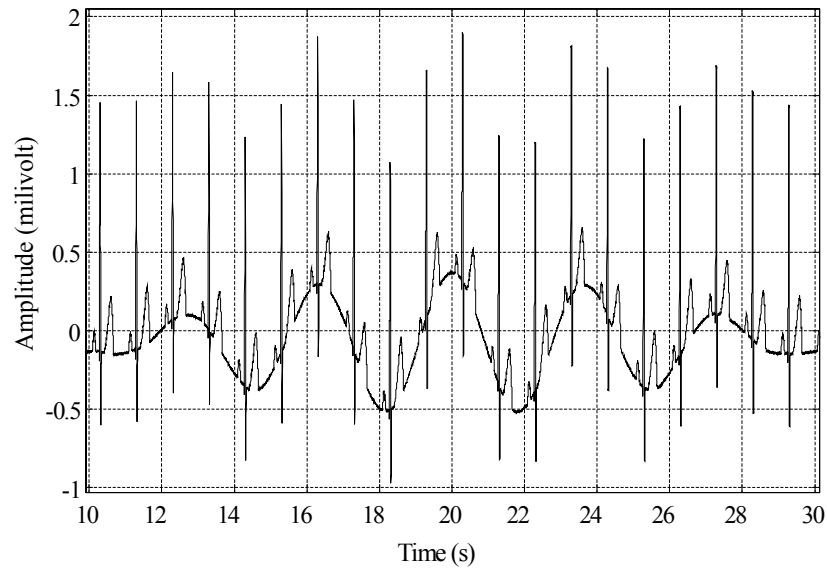


Figure 3.8: Noisy synthetic data. It is focused from Figure 3.7. Samples are from second 10 to 30 including one period of noise.

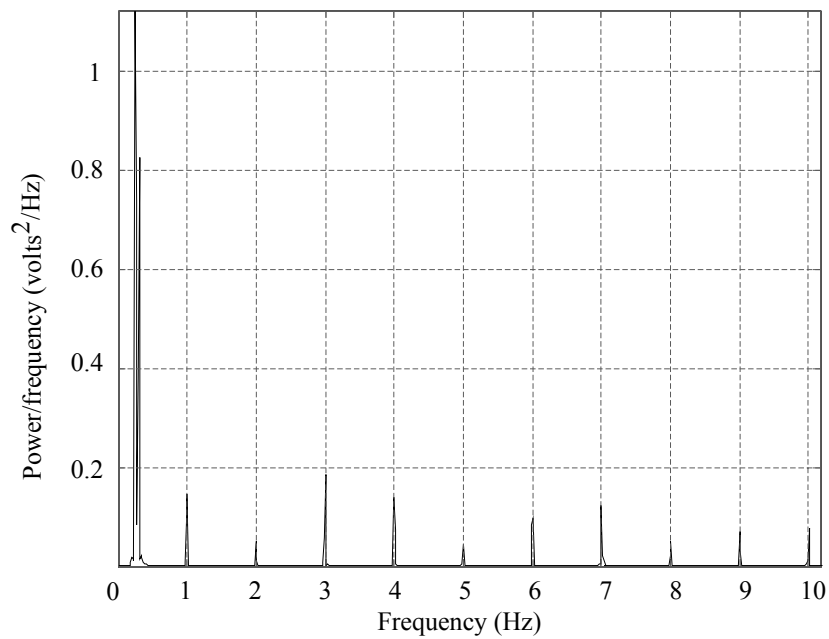


Figure 3.9: Power spectrum density estimation of the noisy data. It is scaled up in order to show the PSD of baseline noisy data in the spectra.

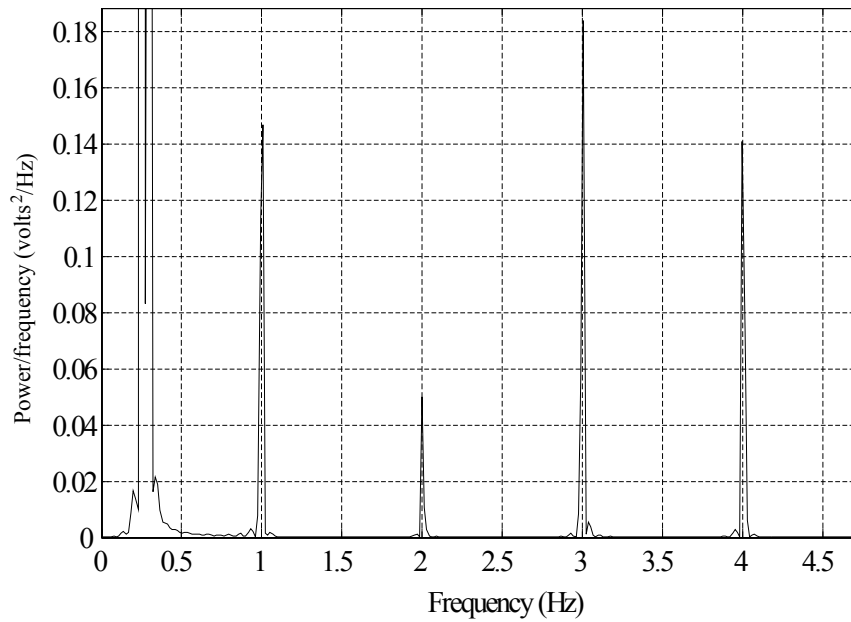


Figure 3.10: Power spectrum density estimation of the noisy data. It is specified as a reference. It is the zoomed version of spectrum in Figure 3.9 in order to show the noisy synthetic data spectra in detail.

3.3 Evaluation Criteria

Root mean square error and root relative square error are the commonly used performance tests. Performance of filter is important because desired filter will be designed according to minimum error criteria in Chapter 4. The filter parameters will be selected suitably in order to perform the filter with minimum RMSE and RRSE.

3.3.1 Root Mean Squared Error

The root mean squared error (RMSE) is one of the most commonly used measures of success for numeric practices. The error is computed by calculating the average of the squared differences between each computed value ‘ c_i ’ and its

corresponding correct value 'a_i'. The root mean squared error is simply the square root of the mean squared error. Here 'n' is the number of samples.

$$\text{RMSE} = \sqrt{\frac{(a_1 - c_1)^2 + (a_2 - c_2)^2 + \dots + (a_n - c_n)^2}{n}} \quad (3.1)$$

3.3.2 Root Relative Squared Error:

Root relative squared error (RRSE) is the total squared error formed with correct and calculated data divided by the error formed with calculated and average data. Here 'a' is the mean value of vector [a₁ a₂ ... a_n]. Similar to the RMSE, the square root of the relative squared error is performed. One can also find the percentage RRSE by multiplying it by 100%. Throughout the thesis, we use the percentage RRSE.

$$\text{RRSE} = \sqrt{\frac{(a_1 - c_1)^2 + (a_2 - c_2)^2 + \dots + (a_n - c_n)^2}{(a_1 - a)^2 + (a_2 - a)^2 + \dots + (a_n - a)^2}} \quad (3.2)$$

CHAPTER 4

RESULTS WITH SYNTHETIC DATA

In this chapter, various baseline wander removal filters will be applied to synthetic noisy ECG data, and the performances of these filters will be studied. In the following sections, frequency response of filters, frequency spectrum of filtered ECG data, the result of filtered ECG data and deviation from noise-free data (difference) will be given. The RMSE and the RRSE values will be determined for each filter.

In the first part of this chapter, offline filters are applied to the noisy ECG data shown in Figure 3.7 and suppression performances are compared in detail. In the second part, successful offline filters will be used in online filtering of the same simulated data, and the suppression performances of the filters are compared. In section 4.7 the effects of the cut-off frequency using a bidirectional IIR filter on an ST segment depressed-baseline noisy ECG signal is demonstrated.

4.1 Offline FIR Filters

In this section, computer based iterative FIR filter, windowing FIR filters with Hamming, Hanning and Blackman functions are performed. The performance characteristics of these filters will be given in the following subsections.

4.1.1 Computer Based Iterative FIR Filter

As we have discussed in Chapter 2, basic filter design parameters are pass-band ripple, stop-band ripple and cut-off frequencies. The filter design process that was given in section 2.1 is applied step by step; in this design, pass-band ripple (rp) is 0.01 dB, stop-band ripple (rs) is 30 dB and the desired cut-off frequency is 0.67 Hz. With these design parameters and using equation 2.4, the order of the filter was found to be 7412 and it is quite high. Computer based iterative FIR filter was designed using mini-max criterion of difference, between designed filter and desired filter, given in equation 2.6. The designed filter has a small ripple in the pass band (0.1 dB) and cut-off frequency of 0.89 Hz which is shown in Figure 4.1. The transition band of this filter is narrow and approximately 0.1 Hz (from 0.89 Hz to 1 Hz). Throughout the design process given in section 2.1, the selected filter has the smallest RRSE and RMSE among the computer-based iterative FIR filters.

When this filter was applied to the synthetic ECG signal with the baseline noise shown in Figure 3.7, this filter introduced 3706 ms of group delay in the filtered signal. After compensation of the group delay, the filtered output signal shown in Figure 4.2 (a) is obtained. The error signal, which is the difference between the pure data (without any noise component) shown in Figure 3.3 and the filtered data shown in Figure 4.2 (a), is less than 5 micro-volts and this deviation represents a satisfactory performance of this filter, especially when compared to 1.5 mV values at R peaks. The RMSE and the RRSE are calculated as 1.55 micro-volts (μV) and 0.7 %, respectively. Performances of filters which have RRSE less than 1 % are quite good and this filter can be implemented due to its successful suppression performances.

Finally, the power spectrum density estimate of the filtered signal is presented in Figure 4.3. When we compare this estimate with the power spectrum density estimate of the pure data shown in Figure 3.5, we observe that the filtering performance of this filter is acceptable and the signal's frequency components are

not disturbed. There is not too much difference between the pure and the filtered data in the spectrum as shown in Table 4.1.

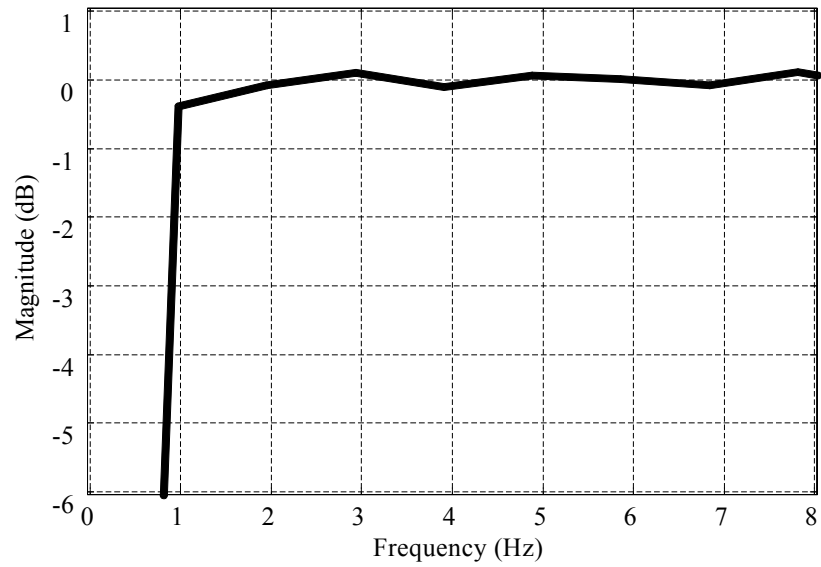
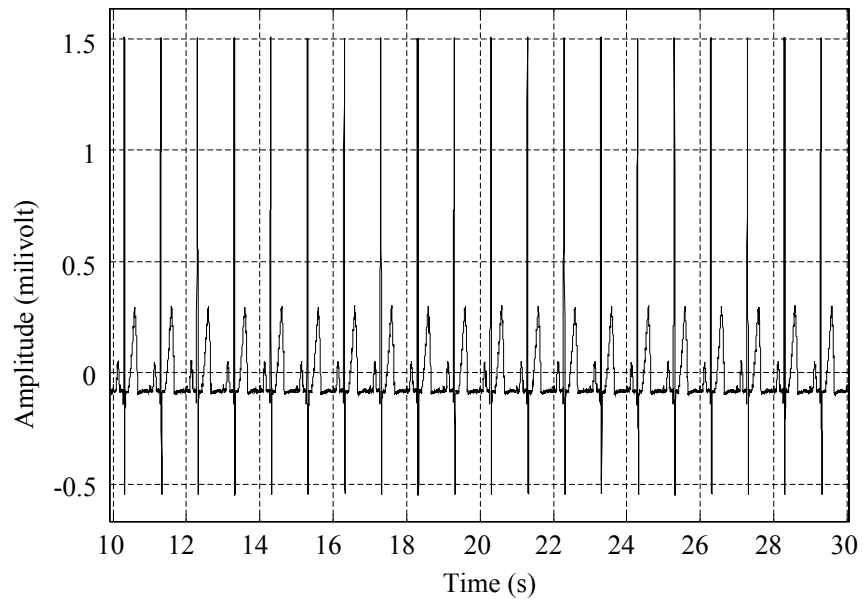
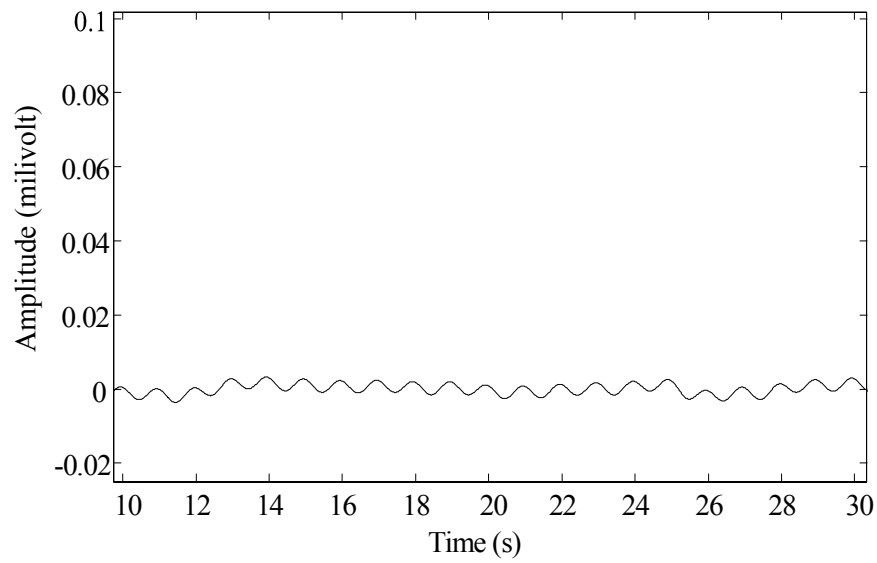


Figure 4.1: Optimal FIR filter's frequency response. Magnitude is given in dB.



(a)



(b)

Figure 4.2: (a) Optimal FIR filtered data. The group delay is compensated, thus, there is no group delay. (b) The difference between the pure and the filtered data.

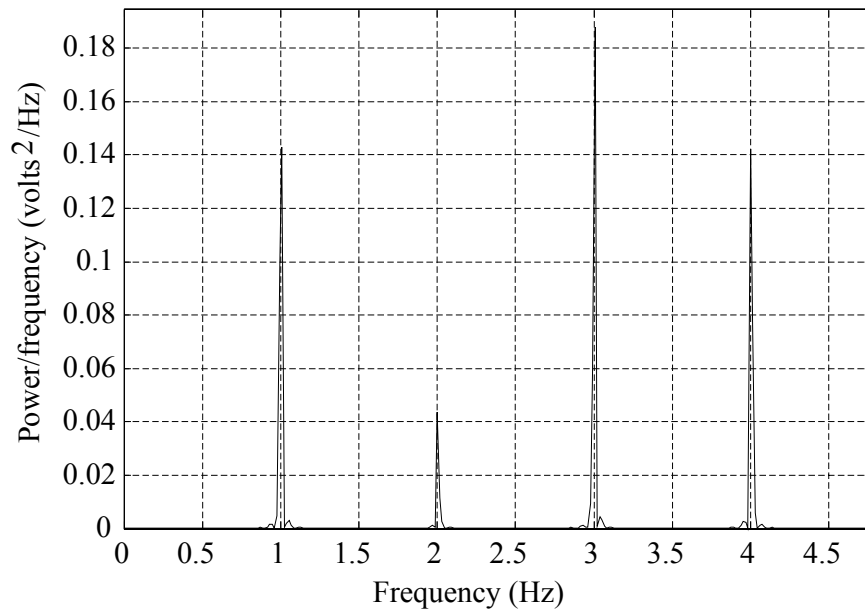


Figure 4.3: Power spectrum density estimation of iterative FIR filtered signal.

4.1.2 FIR Filtering with Windowing Methods

The Hamming, Hanning and Blackman windowing methods are implemented in this subsection and performances of these filters are examined.

4.1.2.1 Hamming Window Filtered Data

Filter design parameters are the same in every FIR filters performed in the thesis study and the parameters are shown in section 4.1.1. Since the order of all windowing functions is calculated as 7412, the group delays of all FIR filters are the same. As shown in the frequency response of the filter, there is no ripple in the pass band (Figure 4.4). Cut-off frequency at the 3 dB point is 0.85 Hz (this filter is designed according to minimum RRSE criteria). The transition band is narrow (approximately 0.1 Hz). The window length is 7413 which is selected according to filter order 7412 (window length is order plus one).

The group delay effect is corrected by using the following steps; apply zero padding to data, then, filter it, and, finally, shift the resultant signal to the left. The result of this filter is given in Figure 4.5 (a). Figure 4.5 (b) displays the error signal, which is the difference between the pure data shown in Figure 3.3 and the filtered data shown in Figure 4.5 (a). The RMSE and the RRSE are calculated as 1.09 microvolts (μV) and 0.49 %, respectively. Since filters with RRSE less than 1 % are accepted to be good filters, this filter can be considered a good filter.

Finally, the power spectrum density estimate of the filtered signal is presented in Figure 4.6. It is observed that the filtering performance of the filter is acceptable and the signal's frequency components are not disturbed. There is not too much difference between the pure and the filtered data in the spectrum as shown in Table 4.1. The filtering time of windowing filter (mathematical complexity of filter) is shorter than the computer based iterative filter due to iterative algorithm of computer based iterative filters.

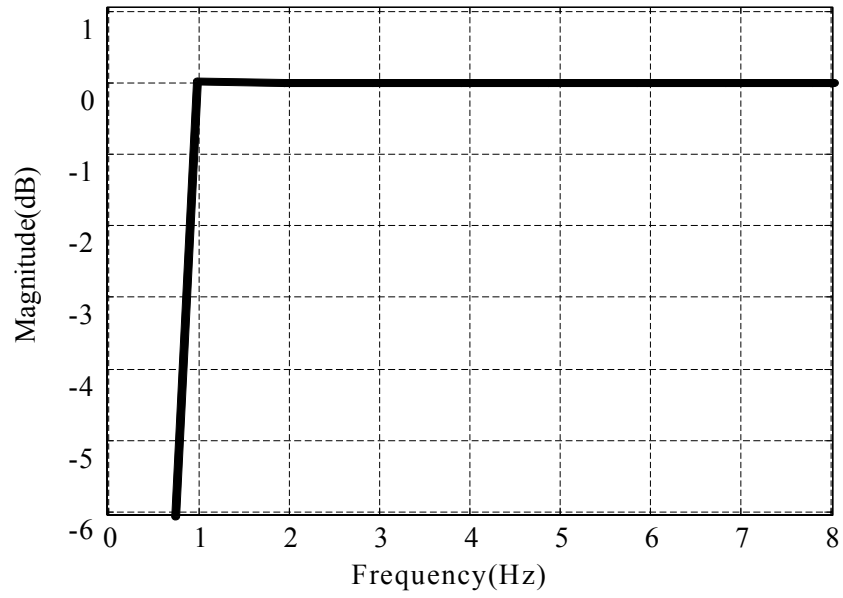
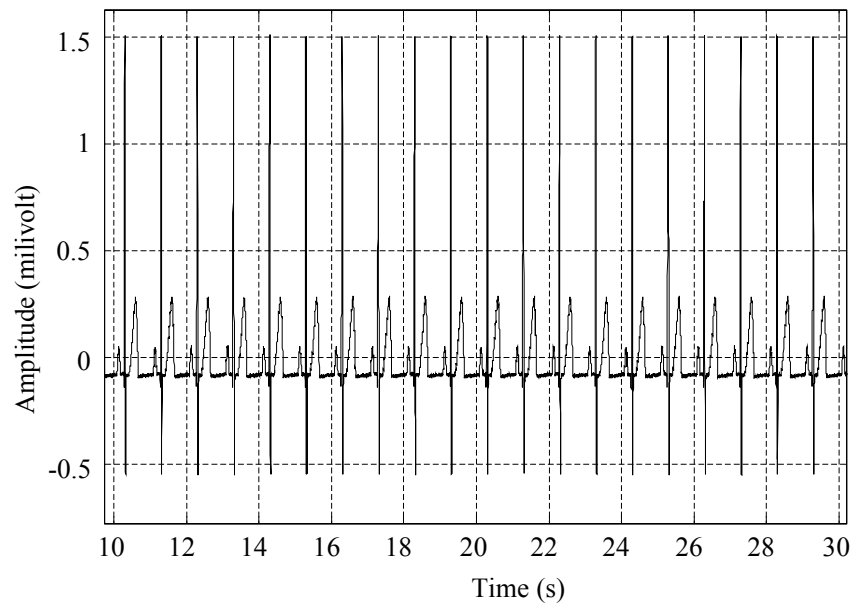
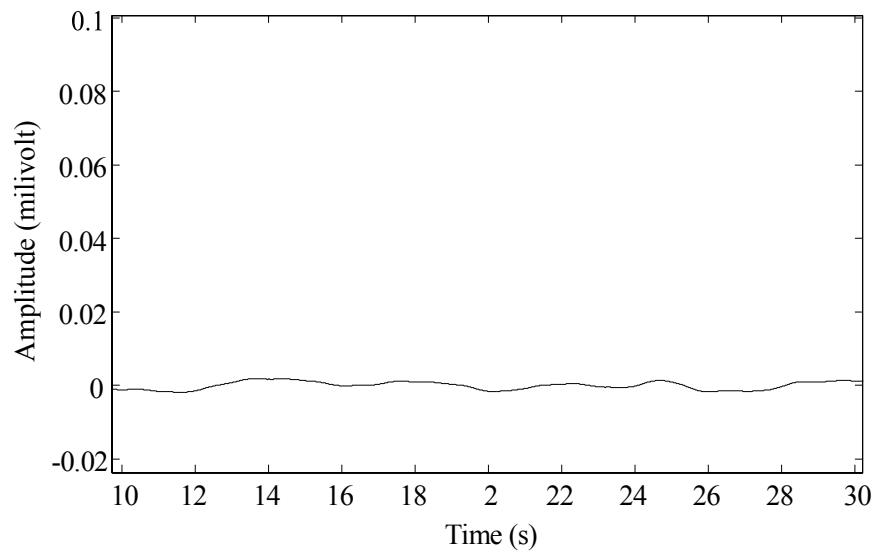


Figure 4.4: Hamming window FIR filter's frequency response.



(a)



(b)

Figure 4.5: Hamming window FIR filter results. (a) filtered data, (b) the difference between the filtered data and the pure signal.

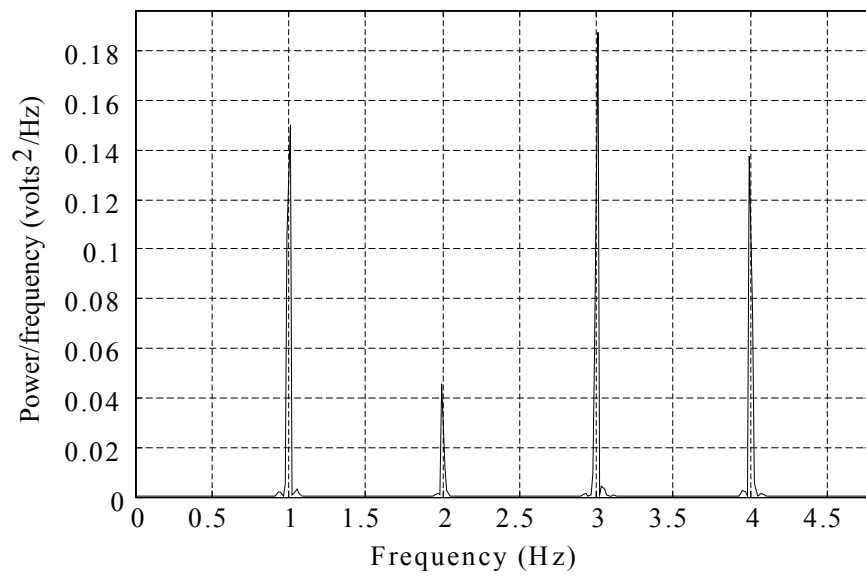


Figure 4.6: Power spectrum density estimation of hamming window filtered signal.

4.1.2.2 Hanning Window Filtered Data

Filter design parameters are the same in every FIR filters performed in the thesis study and the parameters are shown in section 4.1.1. Since the order of all windowing functions is calculated as 7412, the group delays of all FIR filters are the same. As shown in the frequency response of the filter, there is no ripple in the pass band (Figure 4.7). Cut-off frequency at the 3 dB point is 0.85 Hz (this filter is designed according to minimum RRSE criteria). The transition band is narrow (approximately 0.1 Hz).

The result of this filter is given in the Figure 4.8 (a). The error signal, which is the difference between the pure data (without any noise component) shown in Figure 3.3 and the filtered data is shown in Figure 4.8 (b). The RMSE and the RRSE are calculated as 1.05 micro-volts (μV) and 0.48 %, respectively. Performances of filters which have RRSE less than 1 % are quite well.

Finally, the power spectrum density estimate of the filtered signal is presented in Figure 4.9. When we compare this estimate with the power spectrum density estimate of the pure data shown in Figure 3.5, we observe that the filtering performance of the filter is acceptable and the signal's frequency components are not disturbed. The windowing methods are quite similar. Only the window function is changed.

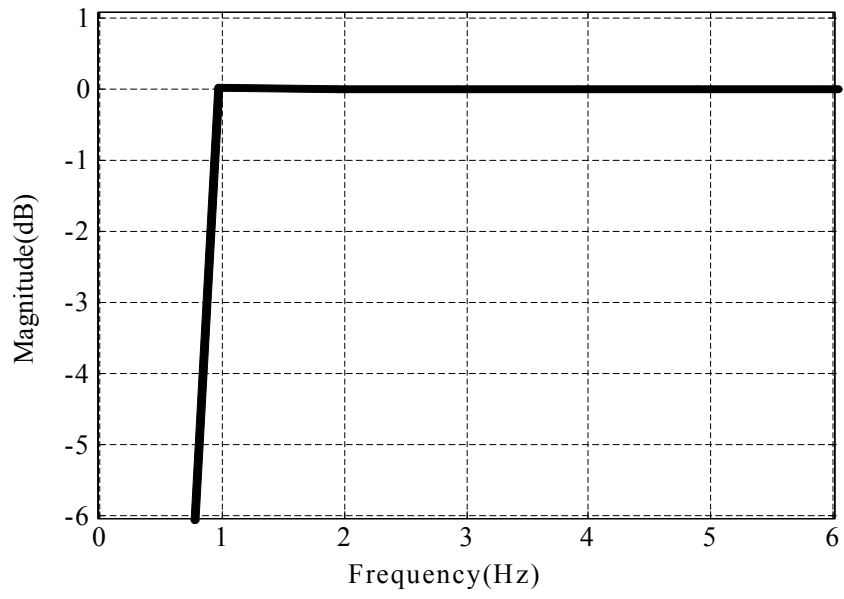
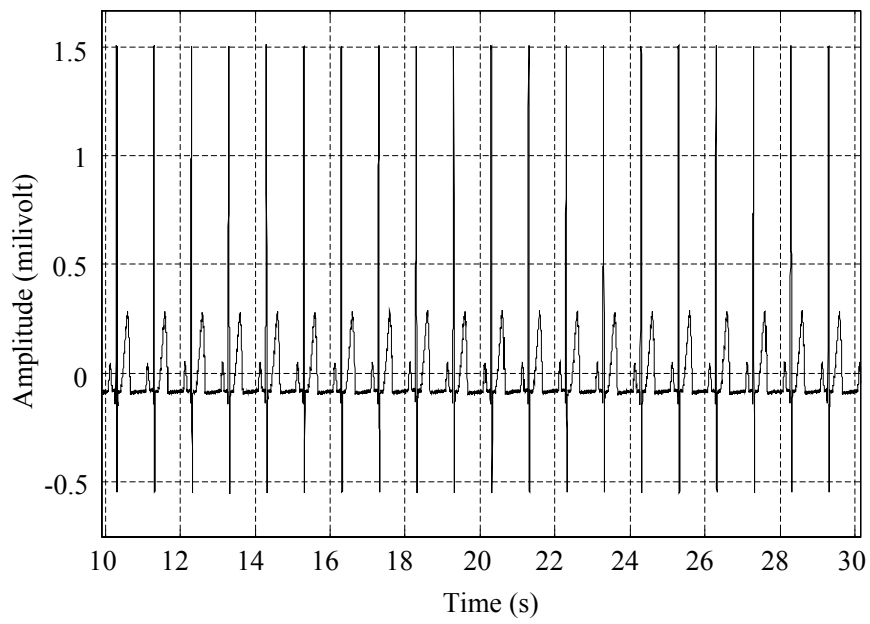
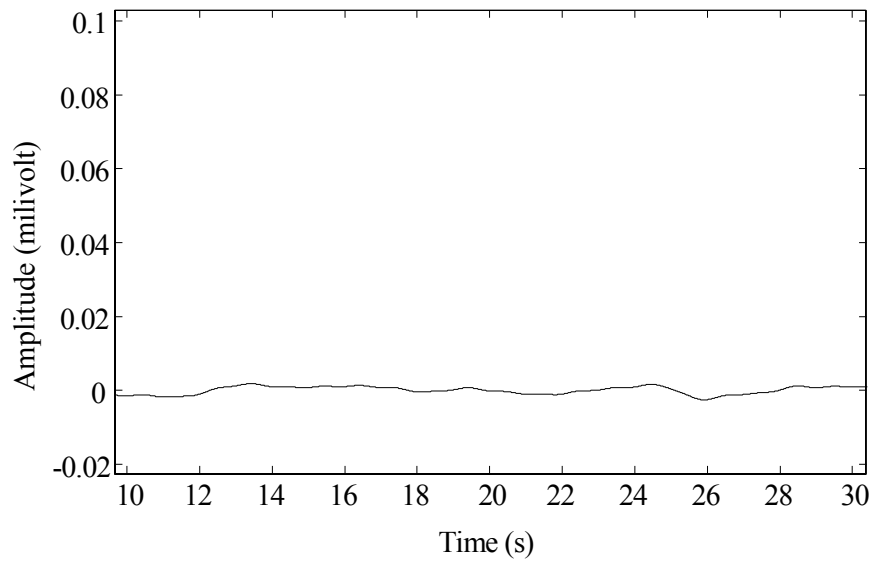


Figure 4.7: Hanning window FIR filter's frequency response.



(a)



(b)

Figure 4.8: Hanning window FIR filter results. (a) filtered data, (b) the difference between the filtered data and the pure signal.

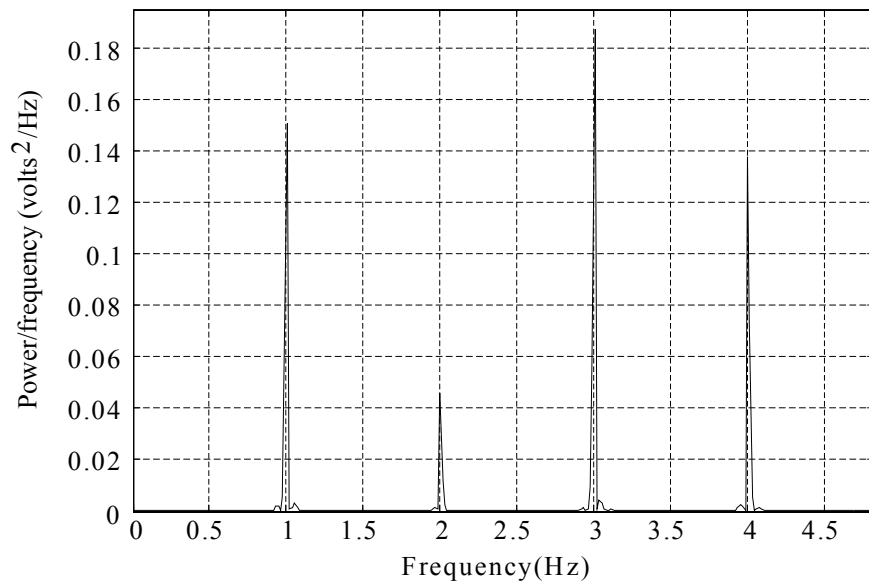


Figure 4.9: Power spectrum density estimation of Hanning window filtered signal.

4.1.2.3 Blackman Window Filtered Data

Filter design parameters are the same in every FIR filters performed in the thesis study and the parameters are shown in section 4.1.1. As shown in the frequency response of the filter, there is no ripple in the pass band (Figure 4.10). Cut-off frequency at the 3 dB point is 0.8 Hz (this filter is designed according to minimum RRSE criteria). The transition band is narrow (approximately 0.1 Hz). The transition band is narrower than both in the Hamming and Hanning windows. There is no ripple in the pass band.

The result of this filter is given in the Figure 4.11 (a). The error signal, which is the difference between the pure data (without any noise component) shown in Figure 3.3 and the filtered data is shown in Figure 4.11 (b). The RMSE and the RRSE are calculated as 1 micro-volt (μV) and 0.45 %, respectively. This filter has the smallest RRSE and RRSE among all filters examined during this thesis study. Thus, suppression performance of this filter is the most successful among all filters.

Finally, the power spectrum density estimate of the filtered signal is presented in Figure 4.12. When we compare this estimate with the power spectrum density estimate of the pure data shown in Figure 3.5, we observe that the filtering performance of the filter is acceptable and the signal's frequency components are not disturbed as shown in Table 4.1.

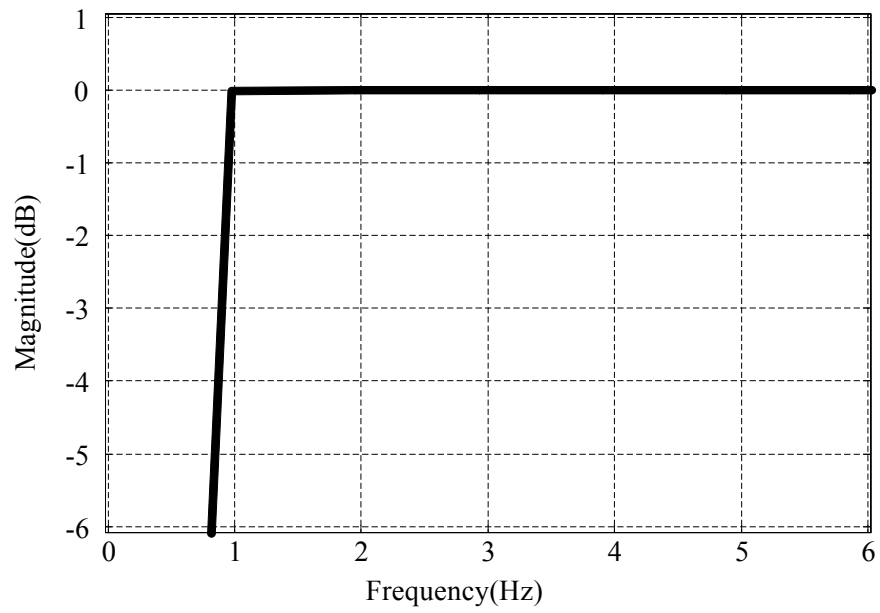
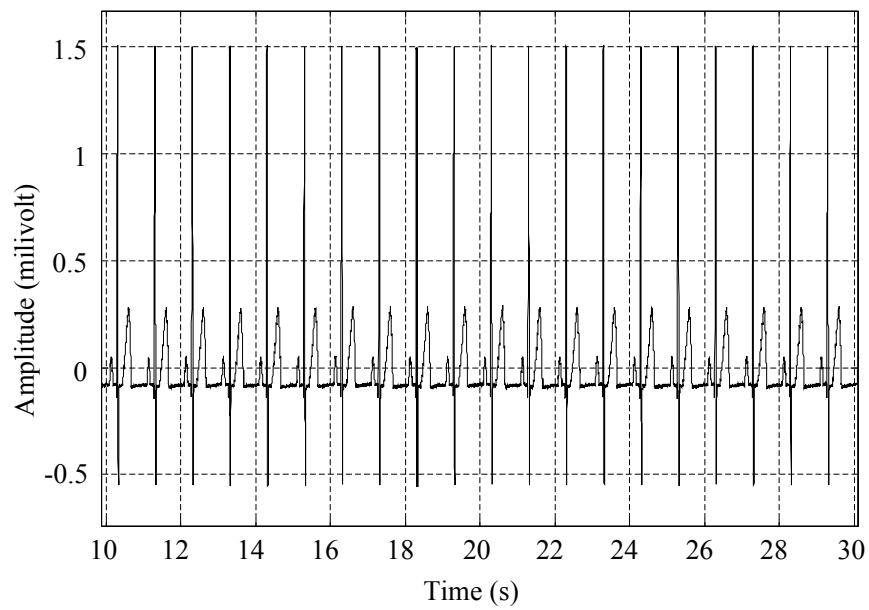
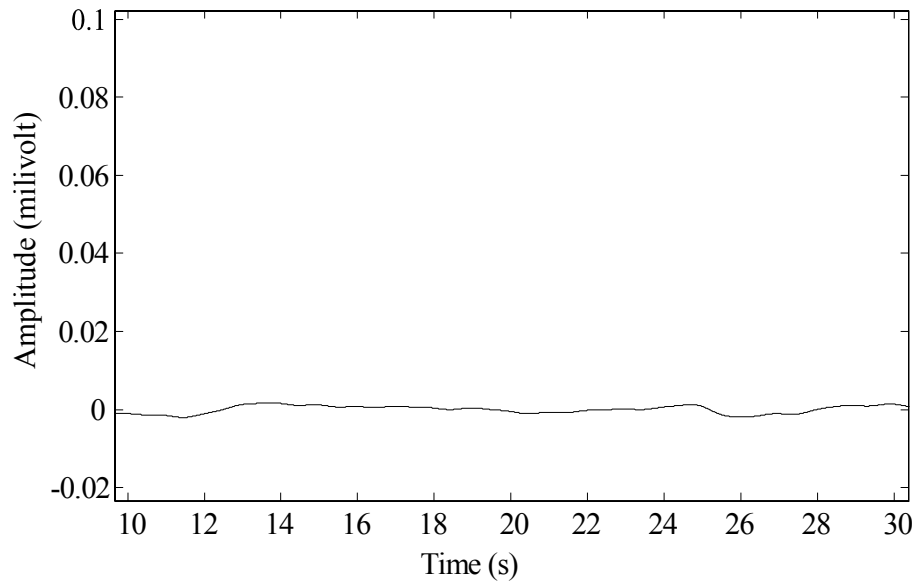


Figure 4.10: Blackman window FIR filter's frequency response.



(a)



(b)

Figure 4.11: Blackman window FIR filter results. (a) filtered data, (b) the difference between the filtered data and the pure signal.

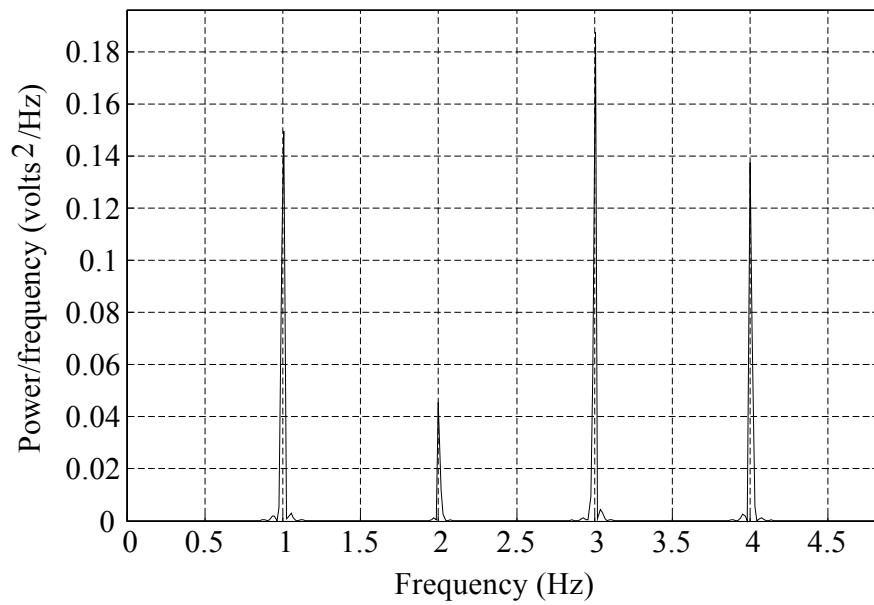


Figure 4.12: Power spectrum density estimation of Blackman window filtered signal.

4.2 Offline IIR Filter Results

Butterworth IIR filter is one of the commonly used IIR filters. In this study, it is used to filter the noisy ECG data both in one-directional and zero-phase (bidirectional) filtering cases. One-directional filter changes the original signal. Because of the frequency components of the original signal, the filters, which have wide transition band (one-directional filter has a wide transition band as shown in Figure 4.13) distorts the original signal. Especially 1 Hz and 3 Hz components in the frequency spectrum are important (Because the magnitude of the energy is high at 1Hz and 3 Hz). Since, these frequency components are distorted and the original signal will be changed. Also we know that IIR filter has non-linear phase responses and the filter changes the signal considerably. But there is a solution of removing this non-linearity of phase in the zero phase IIR filtering section. The results of both filters are given in the following subsections.

4.2.1 Butterworth IIR Filtered Data

The Butterworth IIR filter has a quite wide transition band compared to the other filters as shown in Figure 4.13. The order of the filter is selected 5 according to equation 2.28. The coefficients of this filter are:

$$a = [1 \quad -4.9864 \quad 9.9454 \quad -9.9185 \quad 4.9458 \quad -0.9865]$$

$$b = [0.9932 \quad -4.9661 \quad 9.9321 \quad -9.9321 \quad 4.9661 \quad -0.9932]$$

The output of this filter is given in Figure 4.14 (a). The error signal, which is the difference between the pure data shown in Figure 3.3 and the filtered data is shown in Figure 4.14 (b). The RMSE and the RRSE are calculated as 141.34 micro-volt (μV) and 64.66 %, respectively. This filter has the highest RMSE and RRSE

among all filters examined during this thesis study. Thus, suppression performance of this filter is not satisfactory.

The power spectrum density estimate of the filtered signal is presented in Figure 4.15. When we compare this estimate with the power spectrum density estimate of the pure data shown in Figure 3.5, we observe that the filtering performance of the filter is not acceptable and the signal's frequency components are disturbed. We know that IIR filter has a non-linear phase response and the filter changes the signal considerably. The solution to remove this non-linearity of phase is to use bidirectional zero phase IIR filtering.

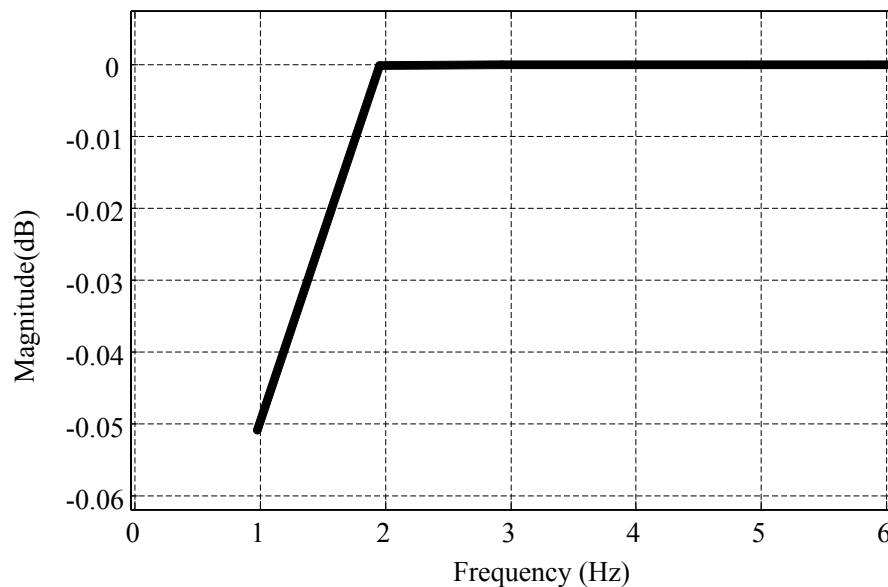
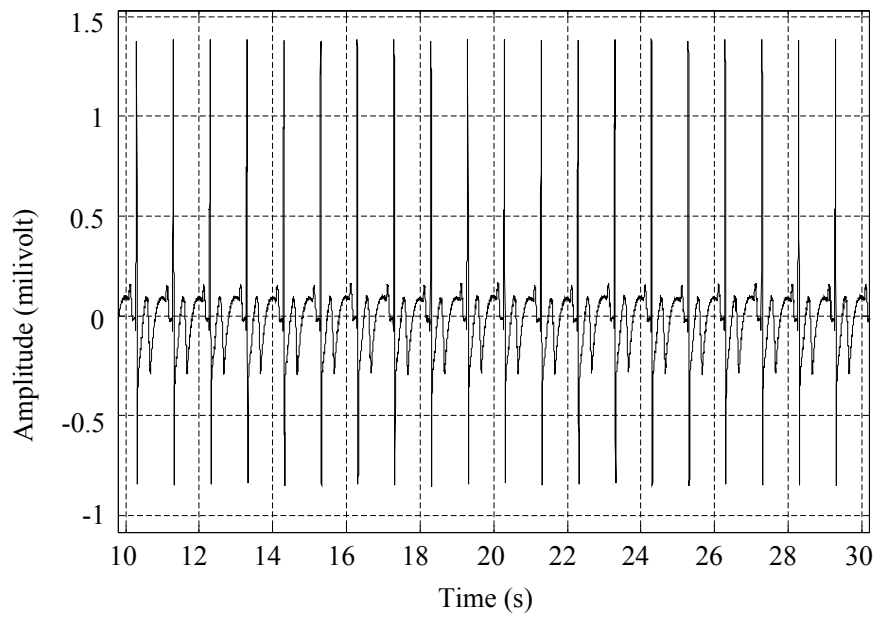
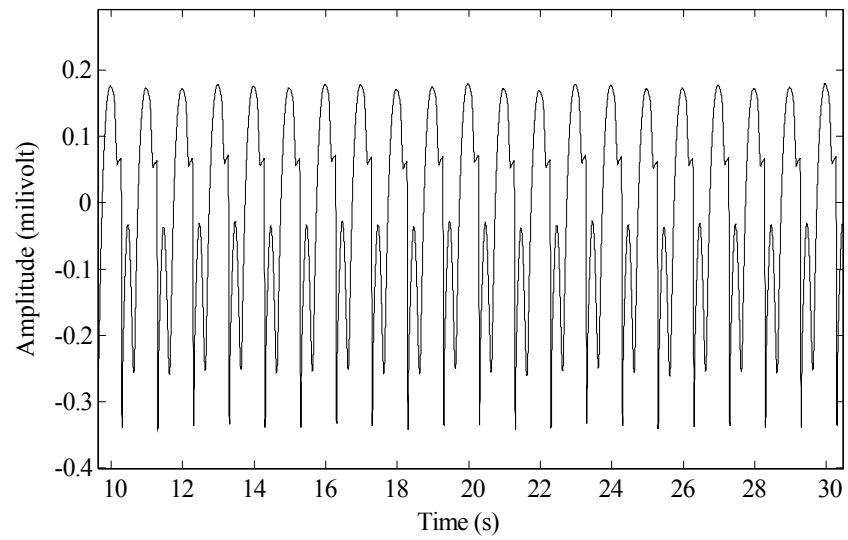


Figure 4.13: Butterworth IIR filter's frequency response.



(a)



(b)

Figure 4.14: IIR filtered data results. (a) filtered data, (b) the difference between the filtered data and the pure signal.

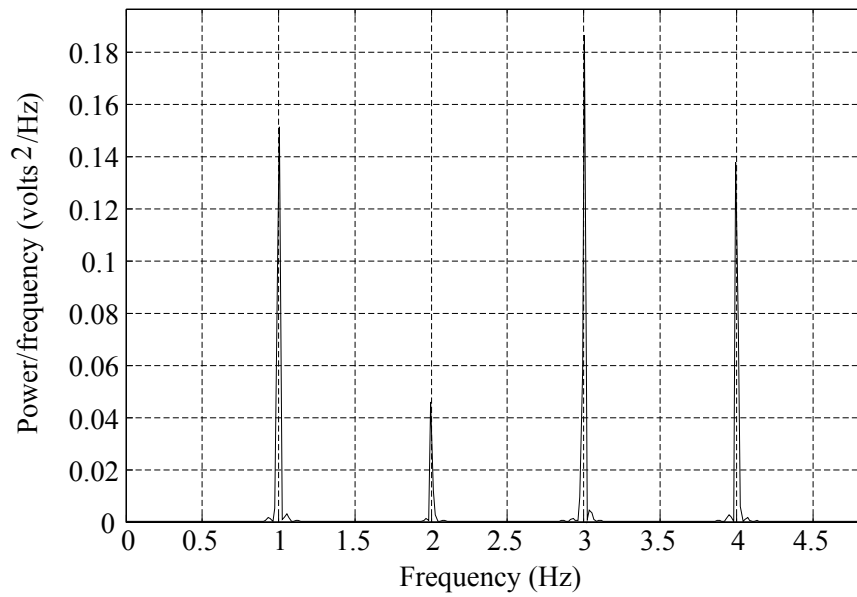


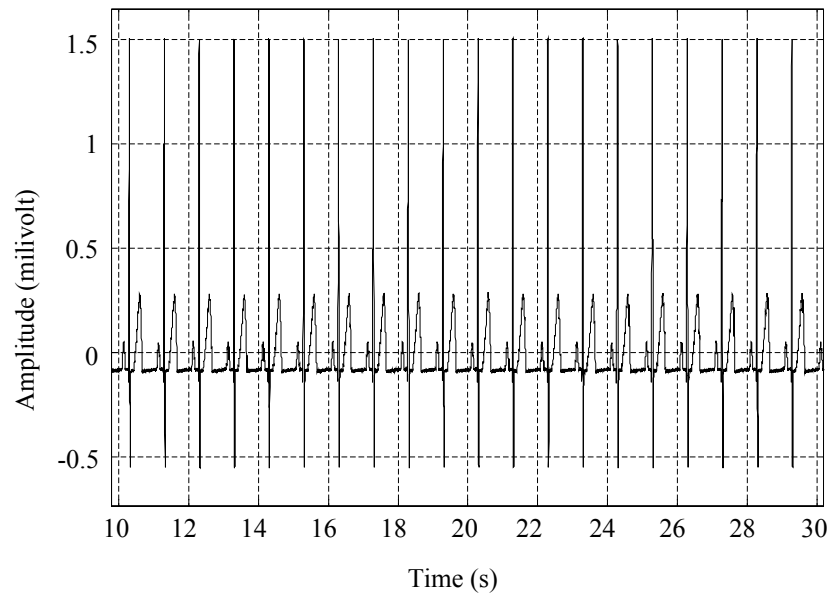
Figure 4.15: Power spectrum density estimation of Butterworth IIR filtered signal.

4.2.2 Butterworth Bidirectional IIR Filter

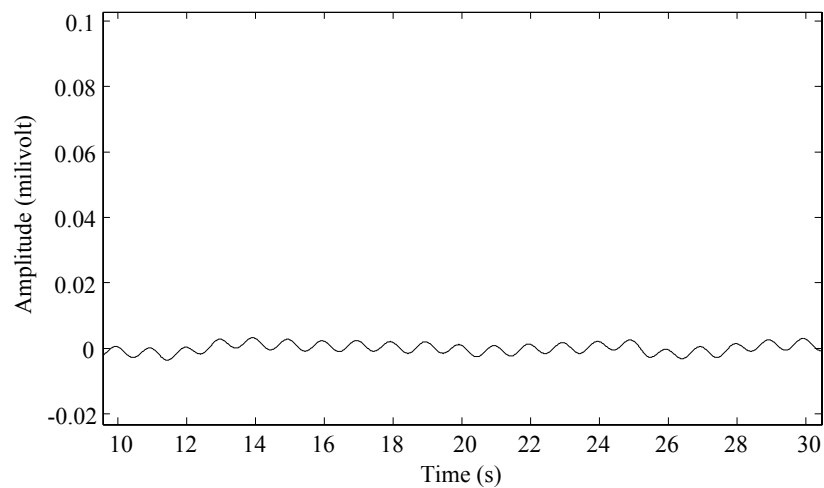
The Butterworth IIR filter studied in section 4.2.1 (the frequency response of the filter is given in Figure 4.13) is applied in both forward and backward directions to suppress the nonlinear phase distortion. The result of this filter is given in Figure 4.16 (a). The error signal, which is the difference between the pure data shown in Figure 3.3 and the filtered data is shown in Figure 4.16 (b). The RMSE and the RRSE are calculated as 1.55 micro-volt (μV) and 0.70 % respectively. Error results are satisfactory and filter has successful suppression performance.

Finally, the power spectrum density estimate of the filtered signal is presented in Figure 4.17. When we compare this estimate with the power spectrum density estimate of the pure data shown in Figure 3.5, we observe that the filtering performance of the filter is acceptable and the signal's frequency components are not disturbed. The frequency spectrum terms are almost the same with the pure data. But there is a small difference in the 1 Hz component as shown in Table 4.1.

Implementing this filter is easy in real life because the signal is filtered in one direction and then reversed signal is passed through the same filter. As a result, the phases of the filters in two directions cancel each other yielding a zero phase filter.



(a)



(b)

Figure 4.16: Butterworth bidirectional IIR filtered data results. (a) filtered data, (b) the difference between the filtered data and the pure signal.

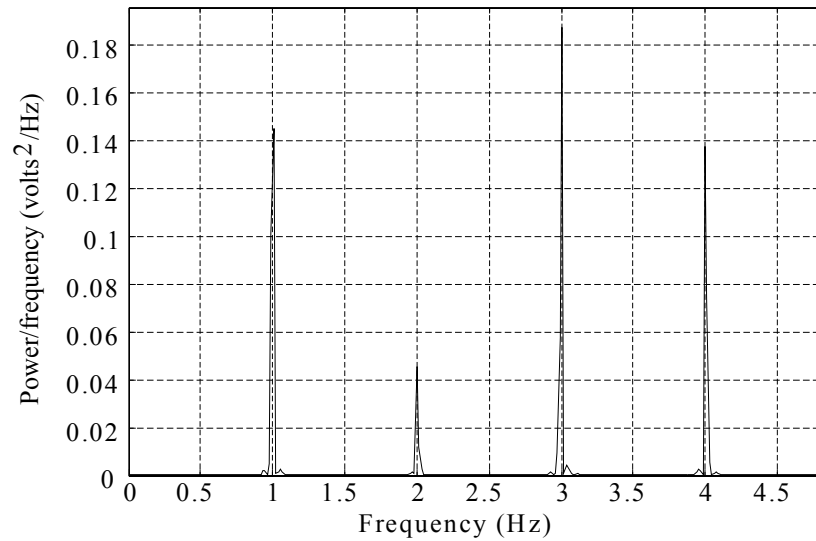


Figure 4.17: PSD estimation of butterworth bidirectional IIR filtered signal.

4.3 Offline Interpolation Filters

In Section 2.4 we have stated that the interpolation of the baseline wander noise can be carried out with respect to different correction points, such as Q, R, S and isoelectric line points. To determine the locations of these correction points (i.e., knots) the QRS detection algorithm introduced in Section 2.4.1 was performed. The cubic spline (interpolation polynomial of order 3) is selected as an interpolation method which is given in section 2.4.2.2, since cubic spline interpolation is widely used as a reference method compared to linear and quadratic interpolation cases.

In the following subsections we present Q, R and S point alignment. Aim of examining Q, R and S point alignment is deciding the best method corresponding to the baseline noise. So, the chief point is the correspondence between the baseline noise and the interpolated noise. The filtering time is quite long for interpolation type filters since the mathematical complexity is high. The performance of interpolation methods is not satisfactory when compared to FIR and bidirectional IIR methods. However, since it does not change the frequency spectrum, this is considered a fundamental study.

4.3.1 Correction with respect to R-Peaks

R point aligning filter requires less time among interpolation filters and this is an advantage compared to other correction points since other points are detected after detection of R peaks. The detected R-peaks are used as knots of the cubic spline curve. The cubic spline curve is created and it is subtracted from the noisy ECG signal. Cubic spline interpolation curve with respect to R-peaks (blue) and synthetic baseline noise (red) are plotted in Figure 4.18. In general, the interpolated noise matches the synthetic noise. However, there is some deviation at the crest points.

The result of this filter is given in the Figure 4.19 (a). The error signal, which is the difference between the pure data shown in Figure 3.3 and the filtered data is shown in Figure 4.19 (b). The RMSE and the RRSE are calculated as 8.58 microvolt (μV) and 3.91 % respectively. The RRSE is high and it is greater than 1 %, which is an expected result considering that the cubic-spline interpolation curve does not correspond to the baseline noise exactly.

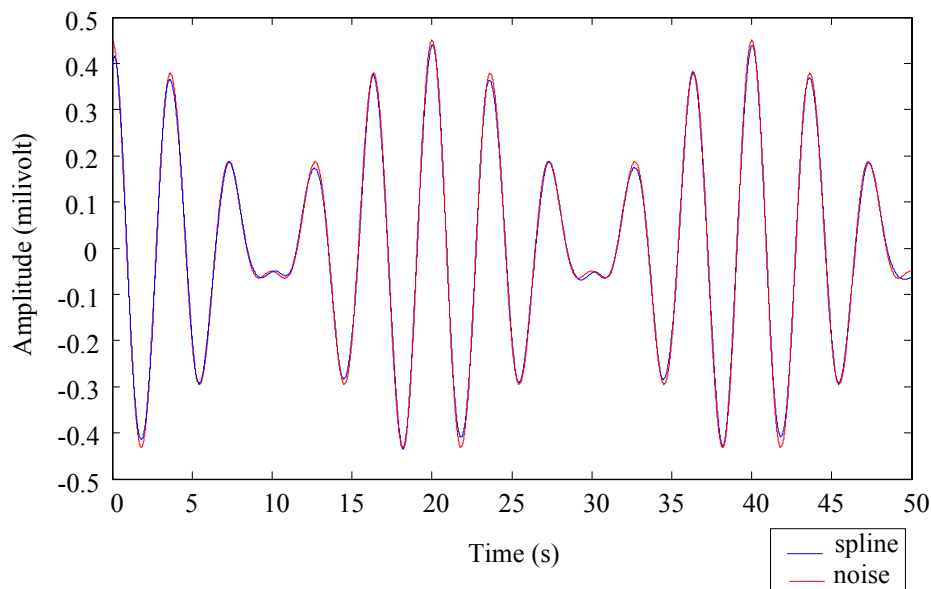
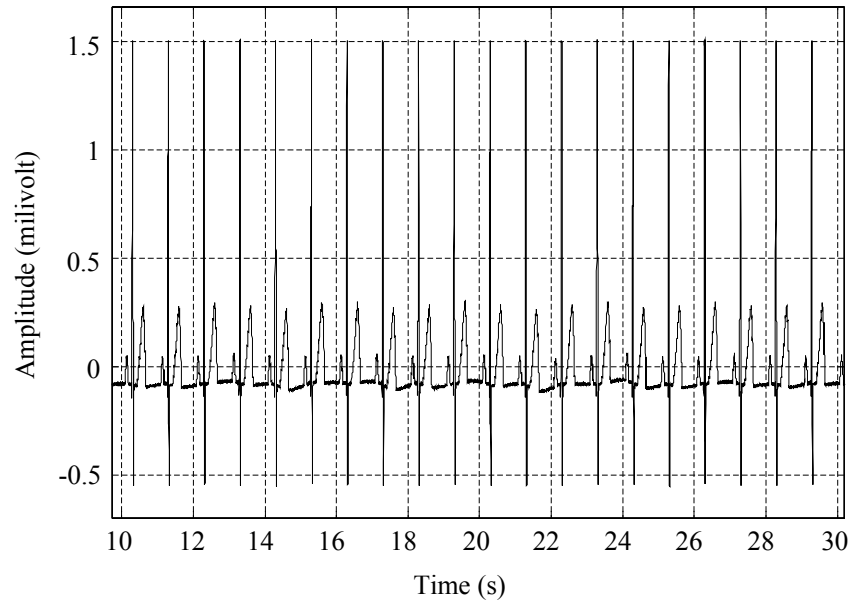
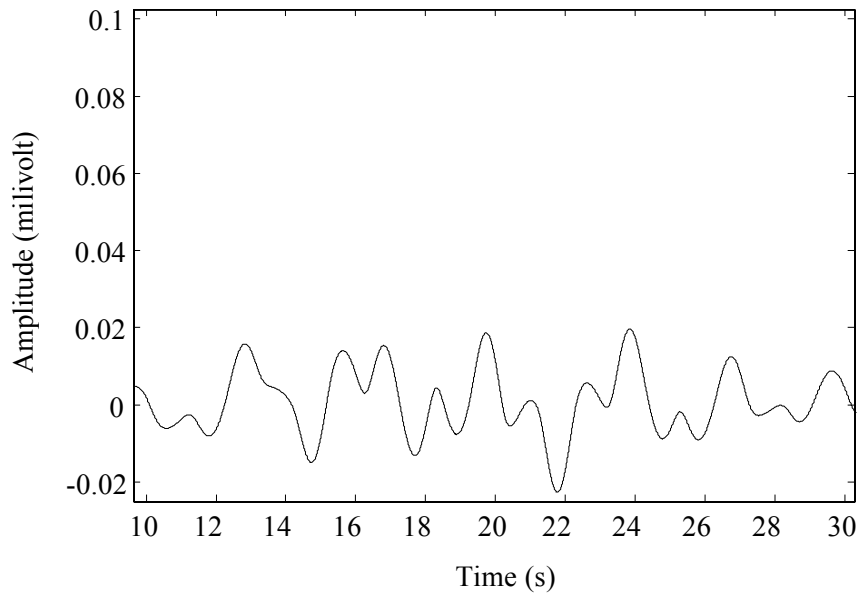


Figure 4.18: Cubic spline interpolation curve with respect to R-peaks (blue) and synthetic baseline noise (red) is plotted in the same figure.



(a)



(b)

Figure 4.19: Cubic spline correction with respect to R peaks. (a) filtered data, (b) the difference between the filtered data and the pure signal.

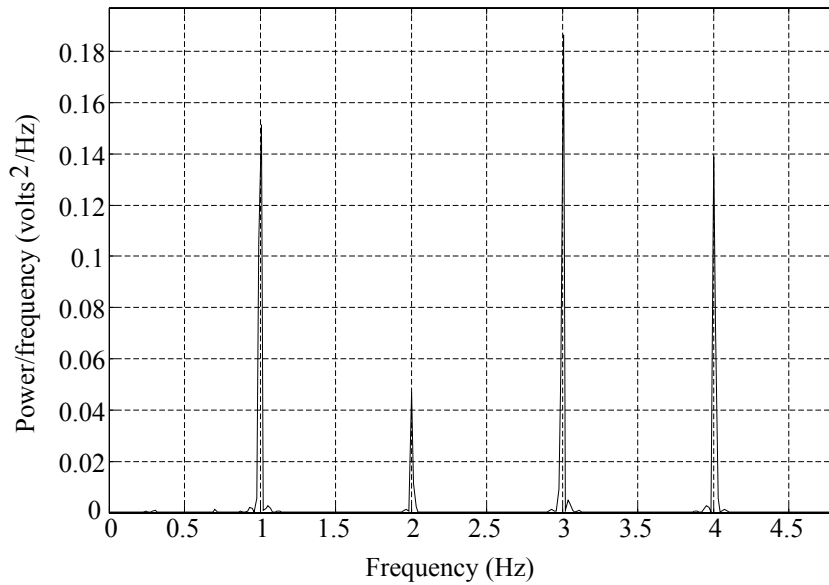


Figure 4.20: Power spectrum density estimation of cubic spline correction with R peaks.

When we compare the spectrum of the filtered signal shown in Figure 4.20 with the spectrum of the pure ECG data in Figure 3.5, we observe that there is some frequency component that is not suppressed below 1 Hz. Frequency components corresponding to larger frequencies, on the other hand, are not distorted since it is not a frequency domain filter. This method has some area of usage when the 2 Hz, 3 Hz frequencies' energies are desired to be very similar to the original signal's energies.

4.3.2 Correction with respect to S Peaks

The S points are detected and a cubic spline is implemented. This method's difference from the correction with respect to the R points is finding and using the S points instead of R points as knots. Cubic spline interpolation curve with respect to S peaks (blue) and synthetic baseline noise (red) is plotted in Figure 4.21 and the

interpolated noise is following the synthetic noise. However, similar to the interpolation with respect to R points, there is some deviation at the crest points. The result of this filter is given in the Figure 4.22 (a). The error signal, which is the difference between the pure data shown in Figure 3.3 and the filtered data is shown in Figure 4.22 (b). The RMSE and the RRSE are calculated as 7.72 micro-volt (μV) and 3.52 % respectively. The RRSE is high and it is greater than 1 %. Correction with respect to S points gives the minimum error results among the other aligning methods. So, S points are most suitable nodes for interpolation.

The power spectrum density estimate of the filtered signal is presented in Figure 4.23. When we compare this estimate with the power spectrum density estimate of the pure data shown in Figure 3.5, we observe that the signal's frequency components are not disturbed but, there is some frequency component that is not suppressed below 1 Hz.

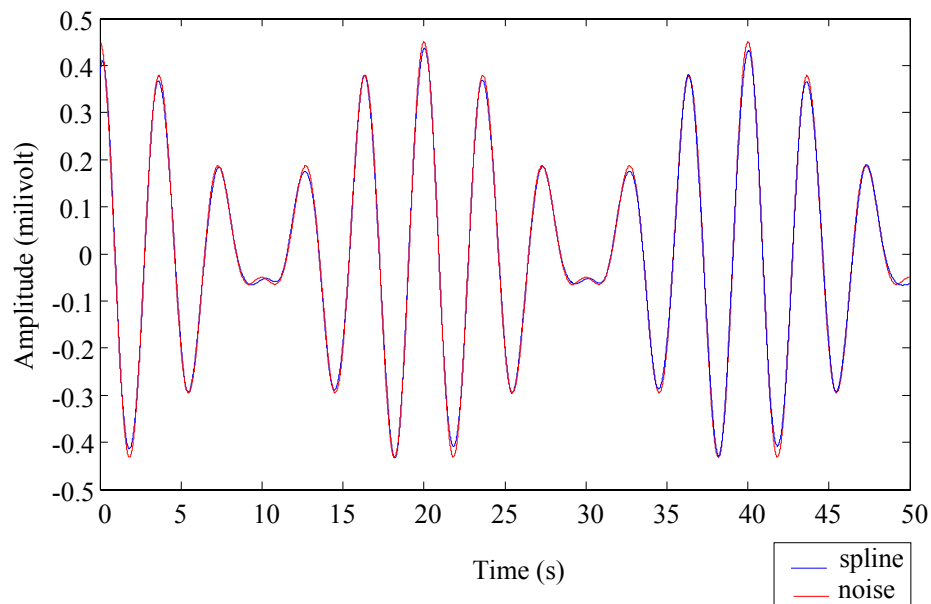
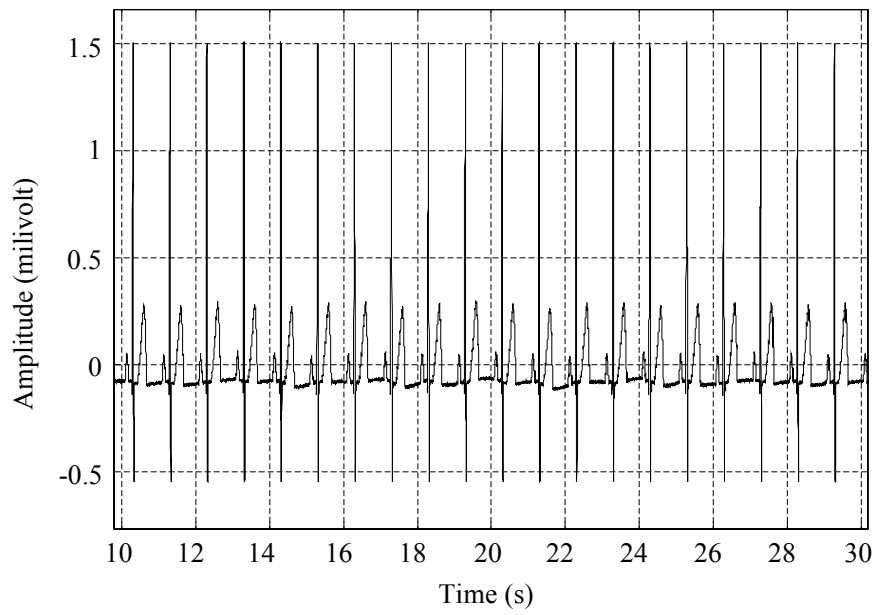
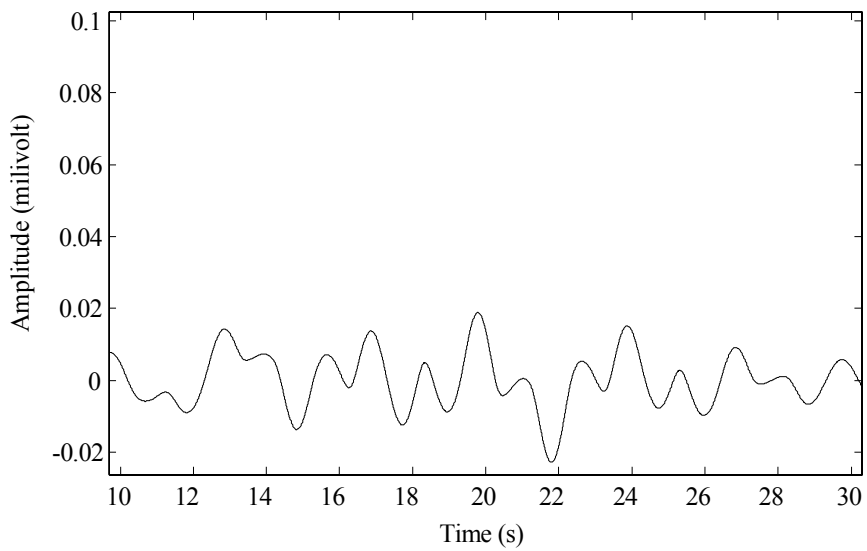


Figure 4.21: Cubic spline interpolation curve with respect to S-peaks (blue) and synthetic baseline noise (red) is plotted in the same figure.



(a)



(b)

Figure 4.22: Cubic spline correction with respect to S peaks. (a) filtered data, (b) the difference between the filtered data and the pure signal.

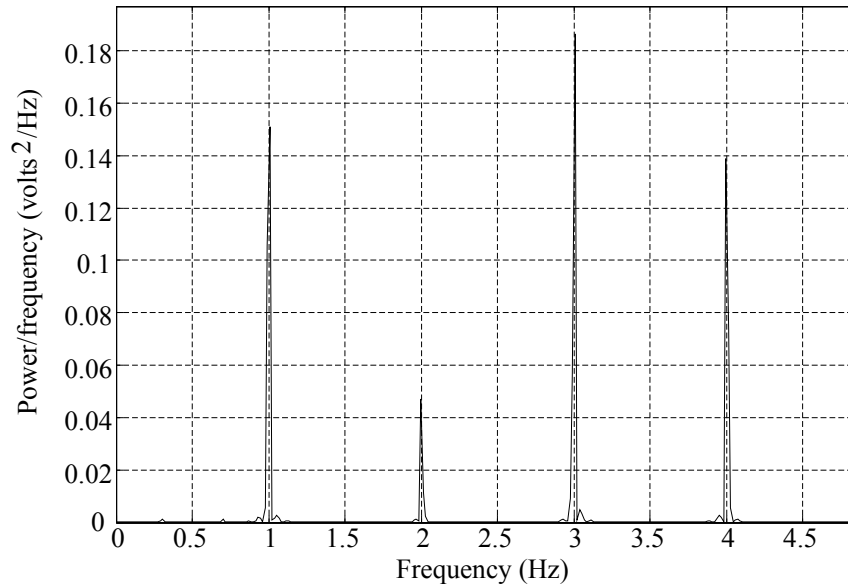


Figure 4.23: PSD estimation of cubic spline correction with S peaks.

4.3.3 Correction with respect to the Isoelectric Line

The isoelectric line points are detected and a cubic spline is implemented. This method's difference from the correction with respect to the R and S points is finding and using the isoelectric points instead of R and S points as knots. Cubic spline interpolation curve with respect to isoelectric line points (blue) and synthetic baseline noise (red) is plotted in Figure 4.24 and the interpolated noise is following the synthetic noise. However, there is some deviation at the crest points and at the beginning of signal since the first interpolation node is far from the beginning of signal. The result of this filter is given in the Figure 4.25 (a). The error signal, which is the difference between the pure data shown in Figure 3.3 and the filtered data, is shown in Figure 4.25 (b). The RMSE is 15.99 micro-volt (μV) and RRSE is 7.28 % thus, error is maximum among the other interpolation methods. The result of power spectrum density estimation is shown in Figure 4.26. There is some frequency component that is not suppressed below 1 Hz since, the baseline wander noise estimation using isoelectric points does not match the true baseline noise.

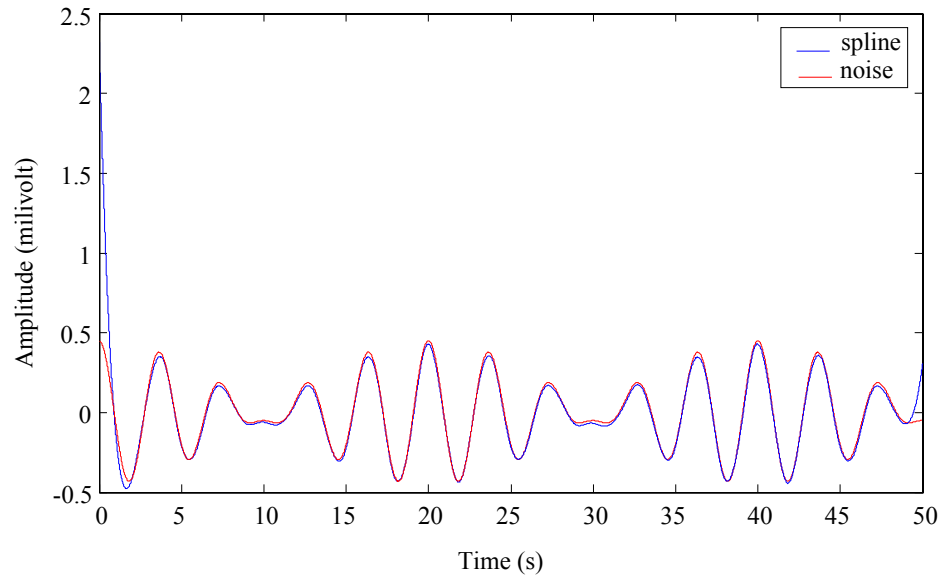
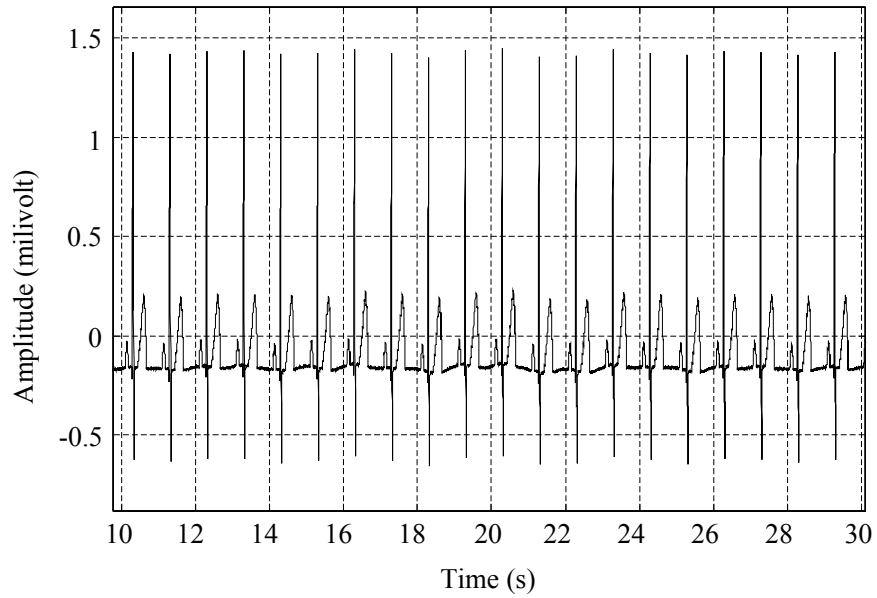
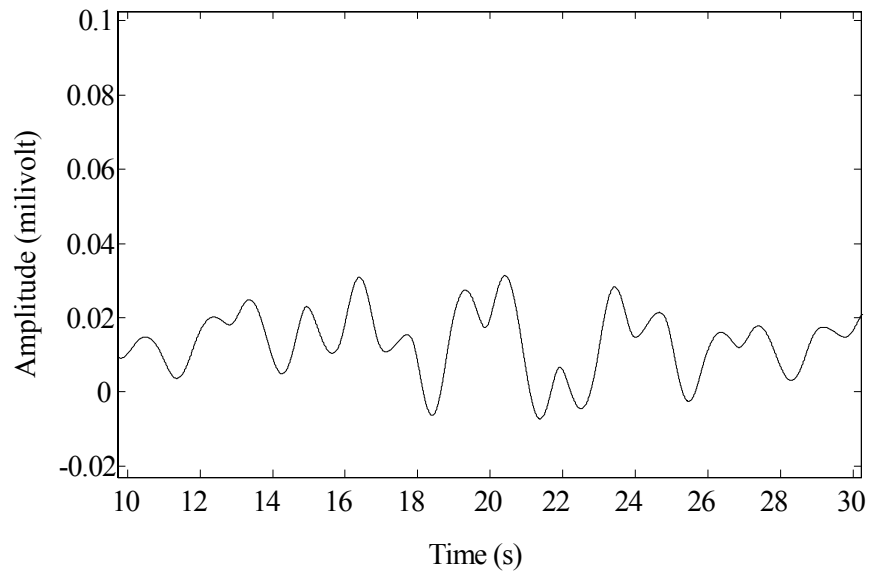


Figure 4.24: Cubic spline interpolation curve with respect to isoelectric line points (blue) and synthetic baseline noise (red) is plotted in the same figure.



(a)



(b)

Figure 4.25: Cubic spline correction with respect to isoelectric line. (a) filtered data, (b) the difference between the filtered data and the pure signal.

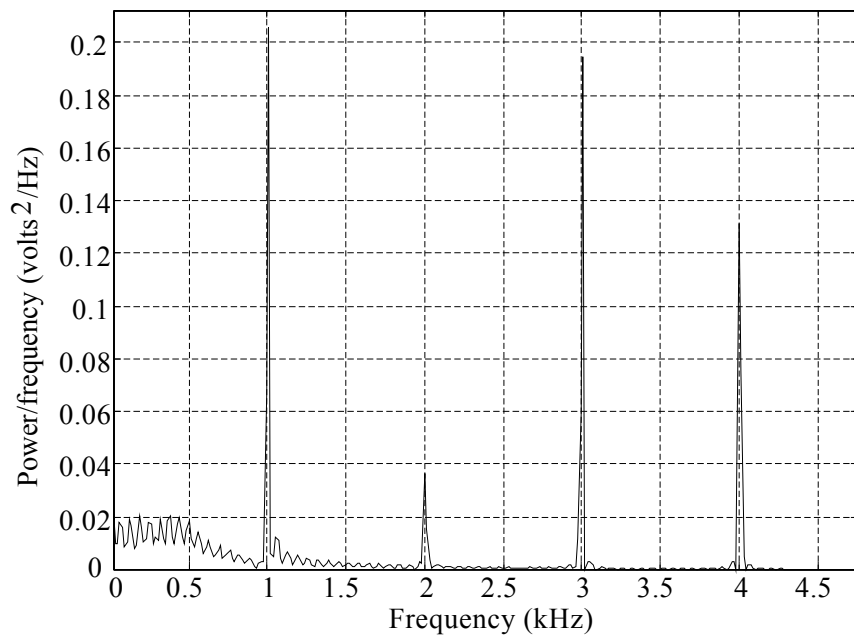


Figure 4.26: Power spectrum density estimation of cubic spline correction with isoelectric line points.

4.3.4 Correction with respect to Q Peaks

This method's difference from the correction with respect to the other points is finding and using the Q points instead other points as knots. Cubic spline interpolation curve with respect to Q-peaks (blue) and synthetic baseline noise (red) is plotted in Figure 4.27 and the interpolated noise is following the synthetic noise. However, there is some deviation at the crest points. The result of this filter is given in Figure 4.28 (a). The error signal, which is the difference between the pure data shown in Figure 3.3 and the filtered data, is shown in Figure 4.28 (b). The RMSE is 7.99 micro-volt (μV) and RRSE is 3.64 %. Power spectrum density estimation is shown in Figure 4.29 and it is quite similar to those of interpolation with respect to Q and R points methods.

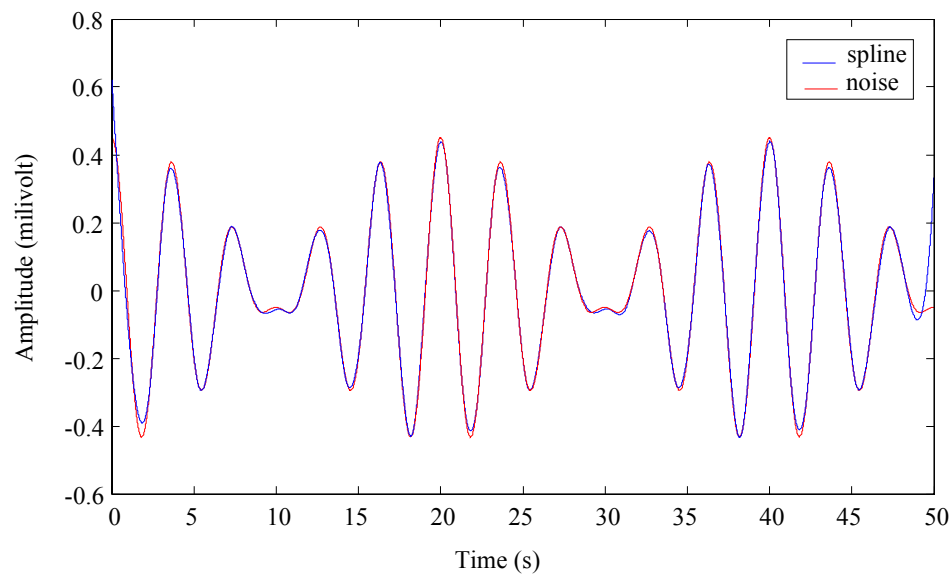
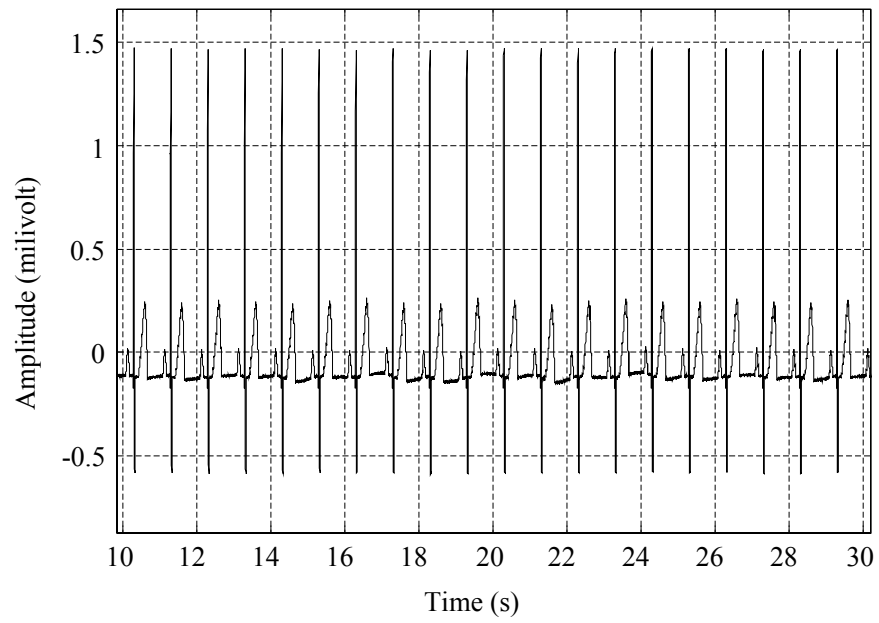
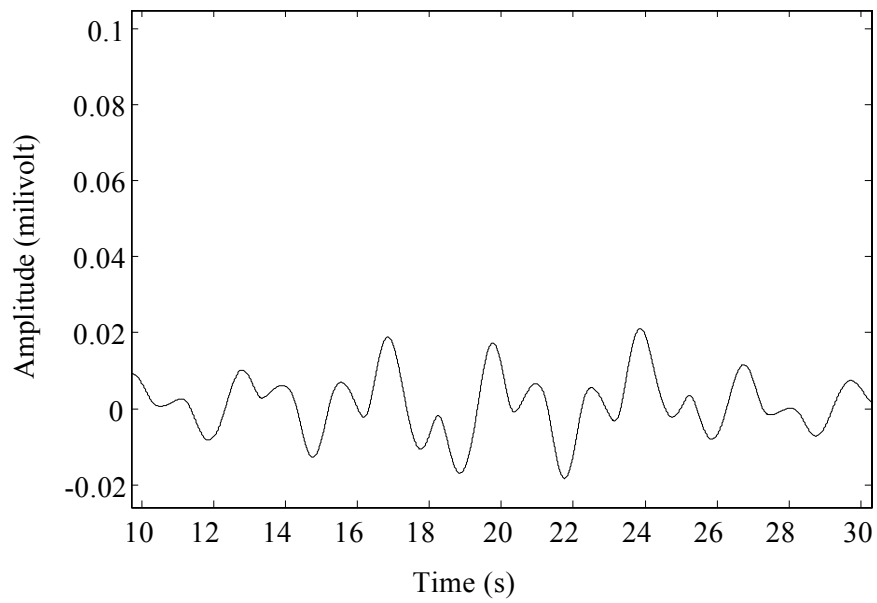


Figure 4.27: Cubic spline interpolation curve with respect to Q-peaks (blue) and synthetic baseline noise (red) is plotted in the same figure.



(a)



(b)

Figure 4.28: Cubic spline correction with respect to Q peaks. (a) filtered data, (b) the difference between the filtered data and the pure signal.

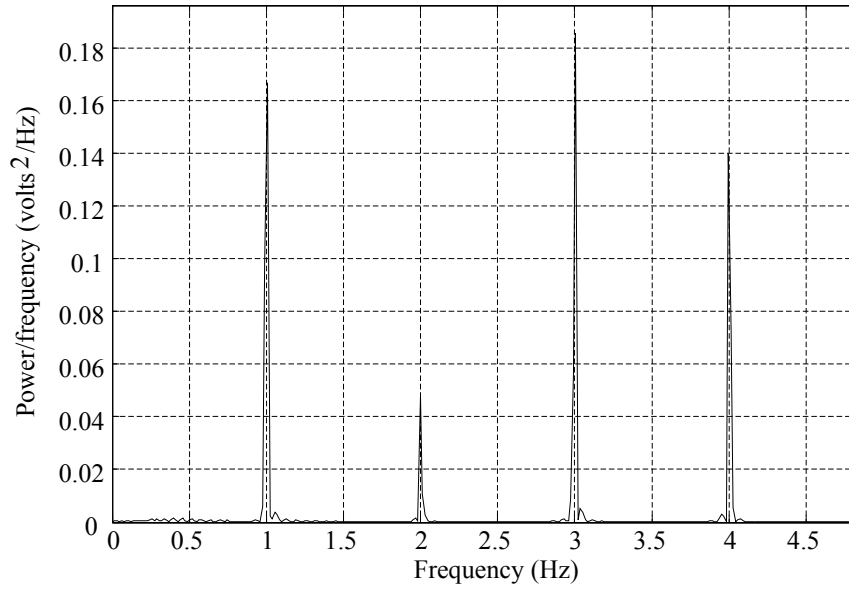


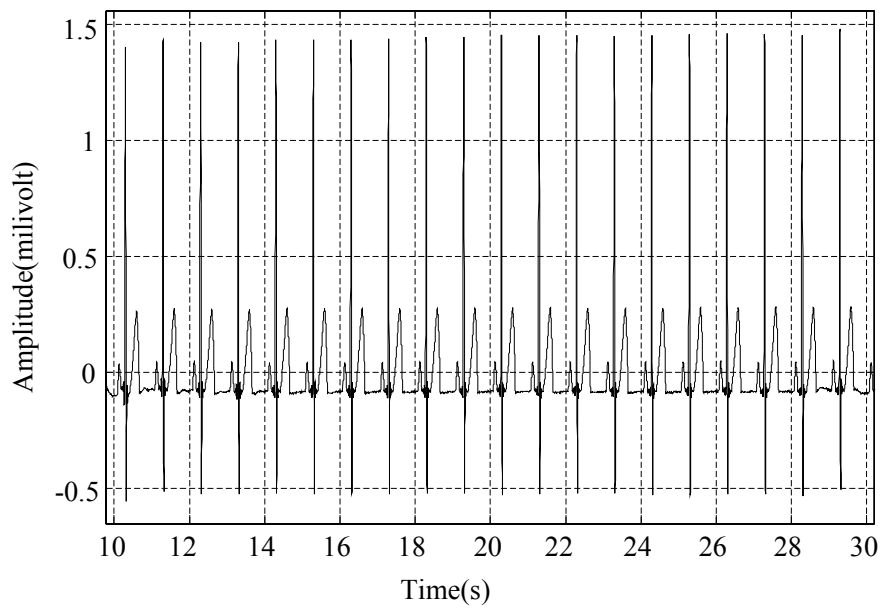
Figure 4.29: Power spectrum density estimation of the correction with Q peaks.

4.4 Offline Adaptive Filtering

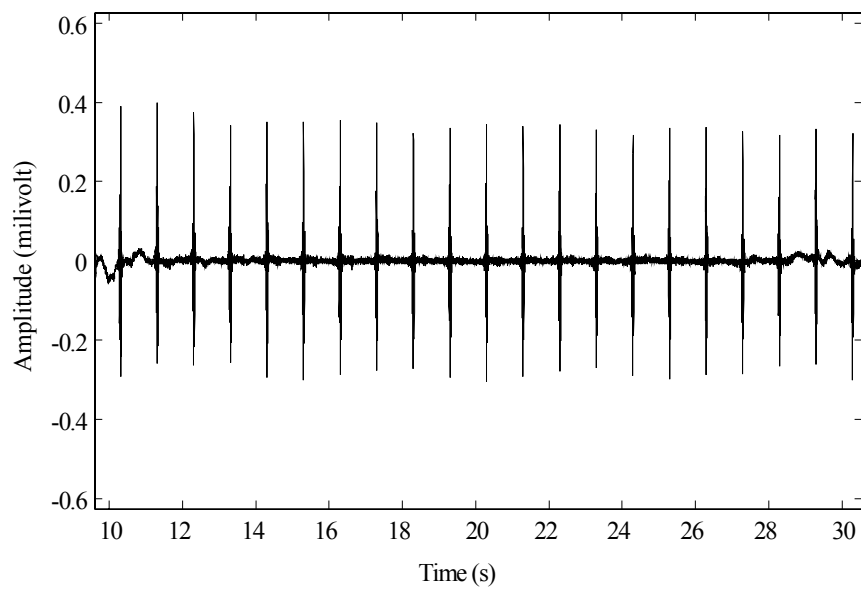
The normalized LMS filter is used as an adaptive filter since it converges easily.

4.4.1 NLMS Filtering

Different values are tried in order to minimize the RRSE and RMSE. As a result of the design process the following values are selected as filter parameter: the normalized step size ' β ' is 0.1 and NLMS offset ' ϵ ' is 0.0001. Length of the filter is 1024. The result of this filter is given in the Figure 4.30 (a). The error signal, which is the difference between the pure data shown in Figure 3.3 and the filtered data, is shown in Figure 4.30 (b). The magnitude of the peaks in signal is changed as shown in Figure 4.30 (b) because of that reason, the difference is high and the periodic pulses are seen in that figure. RMSE is 30.26 micro-volt (μV) and RRSE is 14.01 %. The result of power spectrum density estimation is shown in Figure 4.31. The performance of filter is not satisfactory; RMSE and RRSE values are quite high.



(a)



(b)

Figure 4.30: Adaptive NLMS filtering result (a) filtered data, (b) the difference between the filtered data and the pure signal.

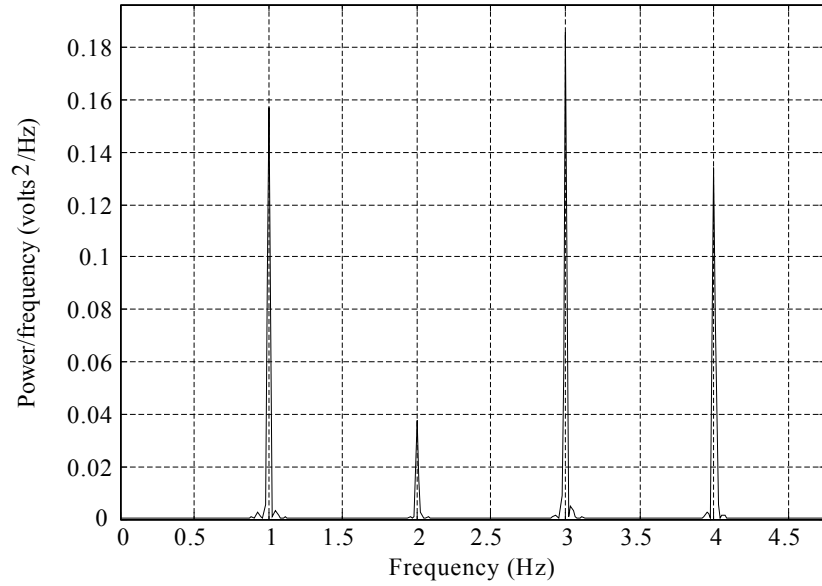


Figure 4.31: Power spectrum density estimation of adaptive NLMS filtered signal.

4.5 Summary of Offline Filtering Results

In this section the results of offline filters are summarized in Table 4.1, Table 4.2 and Table 4.3. The PSD of pure data is the reference (shown in Figure 3.5) and the performances of the filters on the spectra (normalized form) can be seen for the frequencies of 1, 2, 3 and 4 Hz in Table 4.1. Calculated RRSE and RMSE values are given in Table 4.2 and Table 4.3 in order to examine the error performances for whole ECG data and one period noise included ECG data. Also the graphical projections of these Tables are shown in Figure 4.32, Figure 4.33 and Figure 4.34.

The performed cut-off frequency for FIR optimal filter is 0.89 Hz, the pass band ripple is 0.1 dB and the order of filter is 7412, the group delay is 3706 milliseconds. The group delay of the windowing FIR filter is again 3706 milliseconds and the window length is 7413. Also, performed cut-off frequency for both Hamming and the Hanning window filters is 0.85 Hz and there is no ripple in the pass band. Performed cut-off frequency of the Blackman window is 0.8 Hz. When RRSE and RMSE values are compared, Blackman window FIR filter has the best

suppression performance among the all filters. The error of IIR filter is the highest compared to the other filters as shown in Tables 4.2 and Table 4.3. Graphical form of the percentage RRSE of the filters are shown in Figure 4.34. The interpolation filters use the knots and the most proper method as knots is the R peaks. When PSD estimate of filters are compared interpolation filters give the smallest deviation from the PSD estimate of original signal. But the error terms of interpolation filters are high as shown in Figure 4.32 and Figure 4.33. The IIR and bidirectional IIR filters are quite sufficient both for time and complexity because of their small order. When RRSE and RMSE values are compared the most successful filters are Blackman window FIR filter and bidirectional IIR filters. These two filters are examined for online case in this chapter and they are performed to filter real noisy signals in Chapter 5 due to their successful suppression performances.

Table 4.1: The power spectrum density estimation normalized with respect to the pure data.

	1Hz	2Hz	3 Hz	4 Hz
Pure data	1	1	1	1
FIR optimal filter	0.93	0.93	1.01	1.03
FIR Hamming window filter	0.98	0.98	1.01	0.99
FIR Hanning window filter	0.98	0.98	1.01	0.99
FIR Blackman window filter	0.98	0.98	1	0.99
IIR Butterworth filter	0.94	0.97	1.01	0.99
Bidirectional Butterworth IIR filter	0.98	1	1	0.99
Q peak aligning interpolation filter	1.01	1.03	0.99	1
R peak aligning interpolation filter	0.99	1	1	1
S peak aligning interpolation filter	0.99	1	1	1
Isoelectric line aligning interpolation filter	1.30	0.81	1.04	0.95
NLMS Adaptive filter	1.03	0.82	0.99	0.97

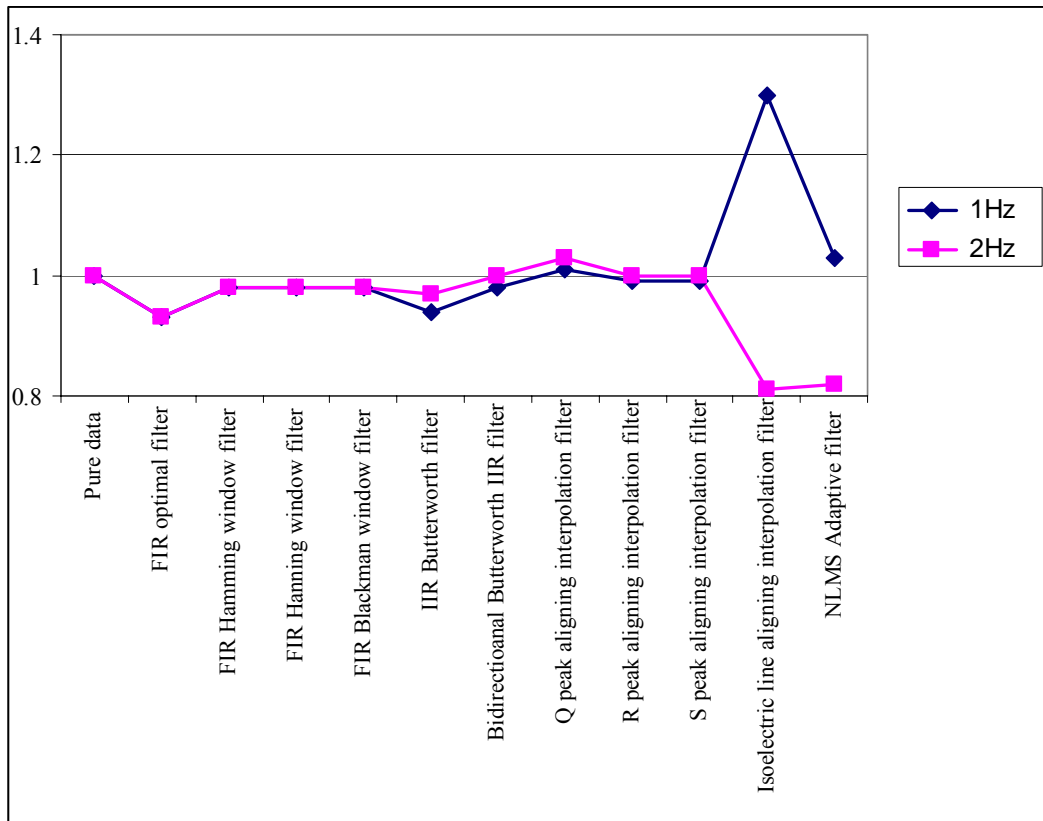


Figure 4.32: The normalized deviations from the pure data for 1 Hz and 2 Hz. It is the graphical projection of Table 4.1.

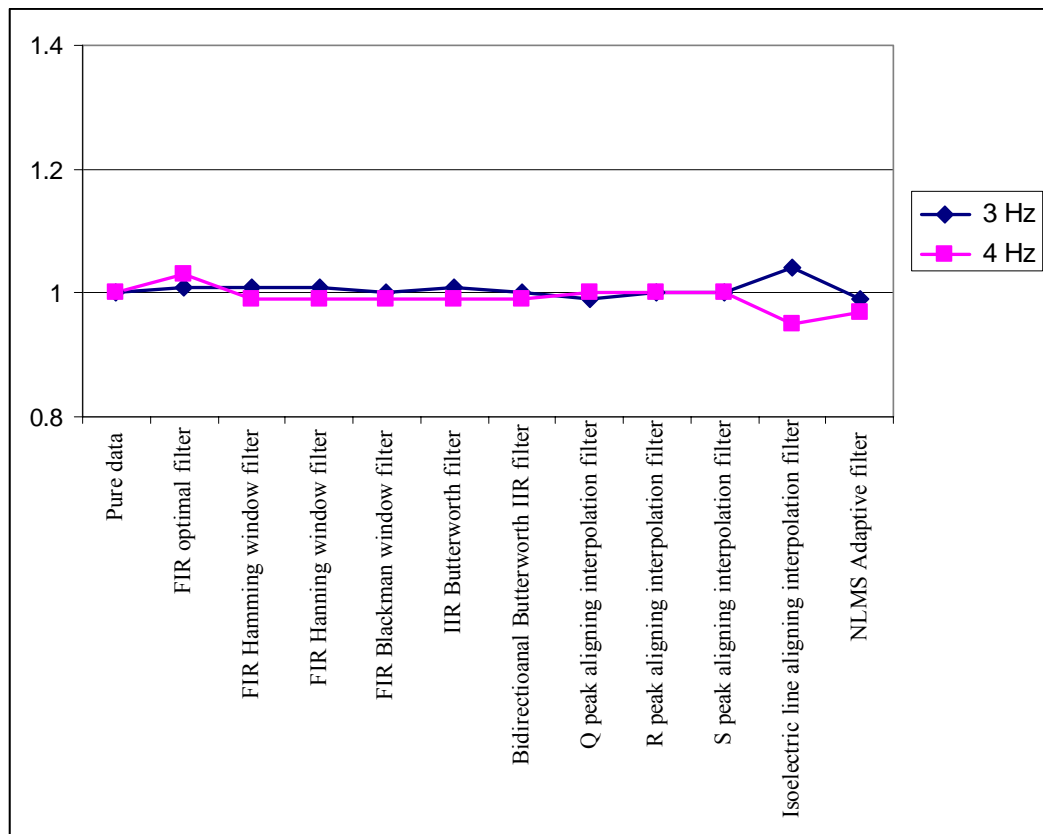


Figure 4.33: The normalized deviations from the pure data for 3 Hz and 4 Hz. It is the graphical projection of Table 4.1.

Table 4.2: The RMSE and percentage RRSE of the filters.

(calculated from second 10 to 30)	RMSE (μV)	RRSE %
Pure data	0	0
FIR optimal filter	1.55	0.70
FIR Hamming window filter	1.09	0.49
FIR Hanning window filter	1.05	0.48
FIR Blackman window filter	1.00	0.45
IIR Butterworth filter	141.34	64.46
Bidirectional Butterworth IIR filter	1.55	0.70
Q peak aligning interpolation filter	7.99	3.64
R peak aligning interpolation filter	8.58	3.91
S peak aligning interpolation filter	7.72	3.52
Isoelectric line aligning interpolation filter	15.99	7.28
NLMS Adaptive filter	30.26	14.01

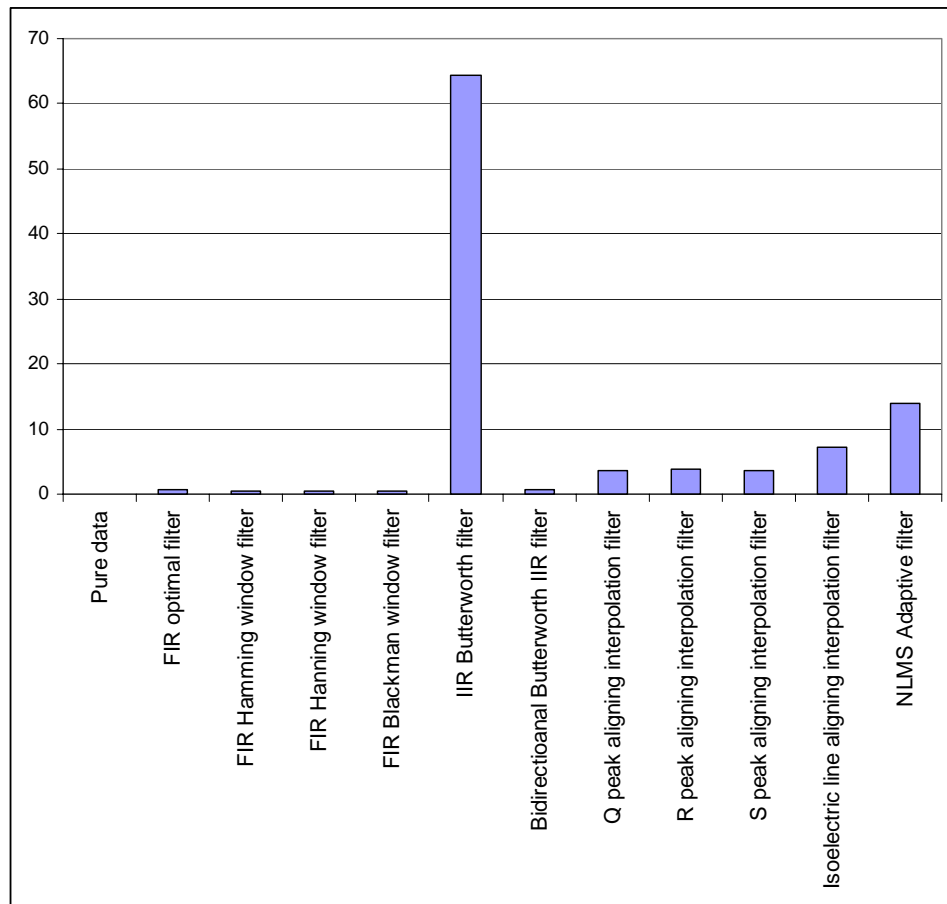


Figure 4.34: The percentage RRSE of the filters. It is the graphical projection of Table 4.2. Error term is calculated for the time interval from 10 to 30 seconds which contains a period of synthetic noise.

Table 4.3: The RMSE and percentage RRSE of the filters.

(calculated from second 0 to 50)	RMSE(μ V)	RRSE %
Pure data	0	0
FIR optimal filter	7.21	3.29
FIR Hamming window filter	7.05	3.21
FIR Hanning window filter	6.97	3.18
FIR Blackman window filter	7.08	3.23
IIR Butterworth filter	141.19	64.39
Bidirectional Butterworth IIR filter	7.21	3.29
Q peak aligning interpolation filter	26.01	11.74
R peak aligning interpolation filter	8.56	3.89
S peak aligning interpolation filter	8.53	3.88
Isoelectric line aligning interpolation filter	120.07	47.93
NLMS Adaptive filter	38.99	18.14

4.6 Online Filtering

Online filtering is the case when real time processing and visualization are required and the signal is simultaneously filtered and monitored. In our model, whole signal is divided into windows of length 'w1' as shown in Figure 4.35. In real applications signal is loaded from ECG device to the memory and the loaded window of length 'w1' is filtered and monitored. Online filters need extra efforts in order not to deteriorate the original signal at the edges of the w1 windows, since there are deterioration 'transients' at the beginning and the end of the w1 windows.

First, signal length is divided into number of 'w1' windows in order to perform equal size 'w1' windows. Second, in order to suppress the deterioration due to transients of the filter, a symmetric data is padded at the beginning of the first and at the end of the last window. As each w1-length window is received, a filtering window of length $w1+2.w2$ is formed that consists an w2-length window at the beginning, the w1-length window of interest and an w2-length window at the end. After the signal in this filtering window is filtered, w2-length windows at the beginning and at the end are discarded, since we are only interested in filtering the w1-length window in the middle. The transients are thrown out with the two w2-length windows, and we are left with a filtered w1-length window that is almost free of the transient deteriorations. This procedure is repeated for every w1-length window in the ECG recording. If the whole filtered signal is needed, for analysis or for display purposes, it is formed by combining all filtered w1-length windows. This procedure is illustrated in Figure 4.35.

We have observed that Blackman window FIR filter and bidirectional IIR filters have the minimum RRSE and RRSE among the all offline filters. Therefore, these filters are used for online filtering in the following subsections.

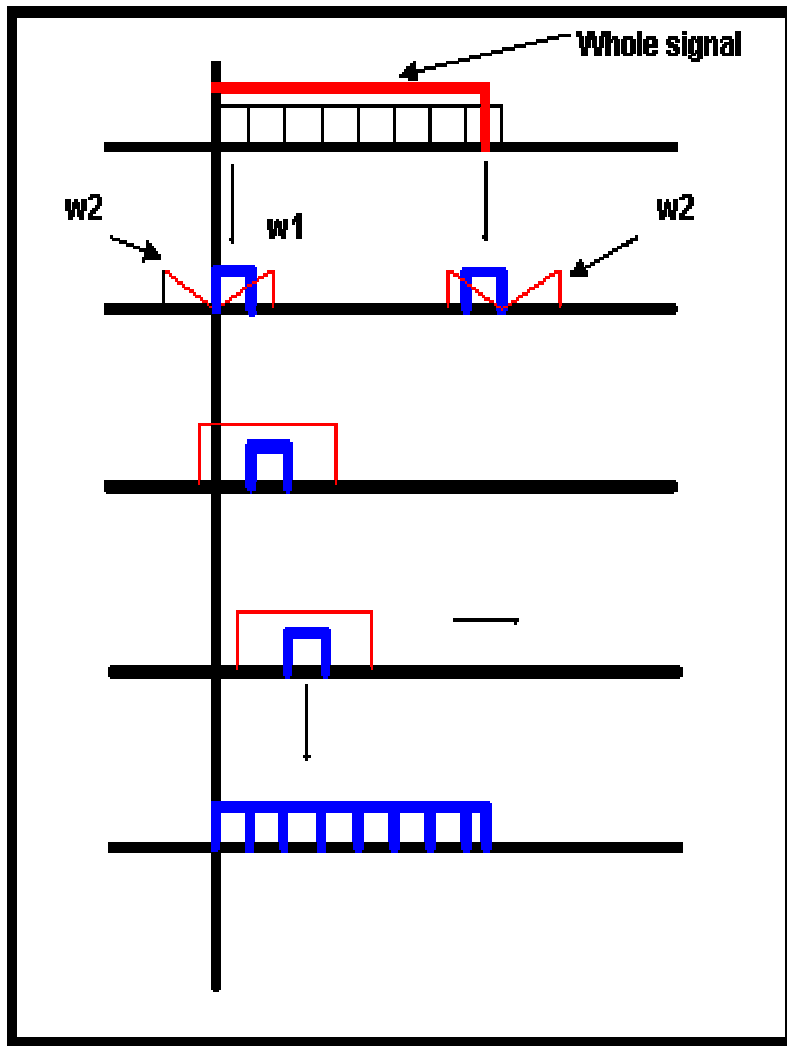


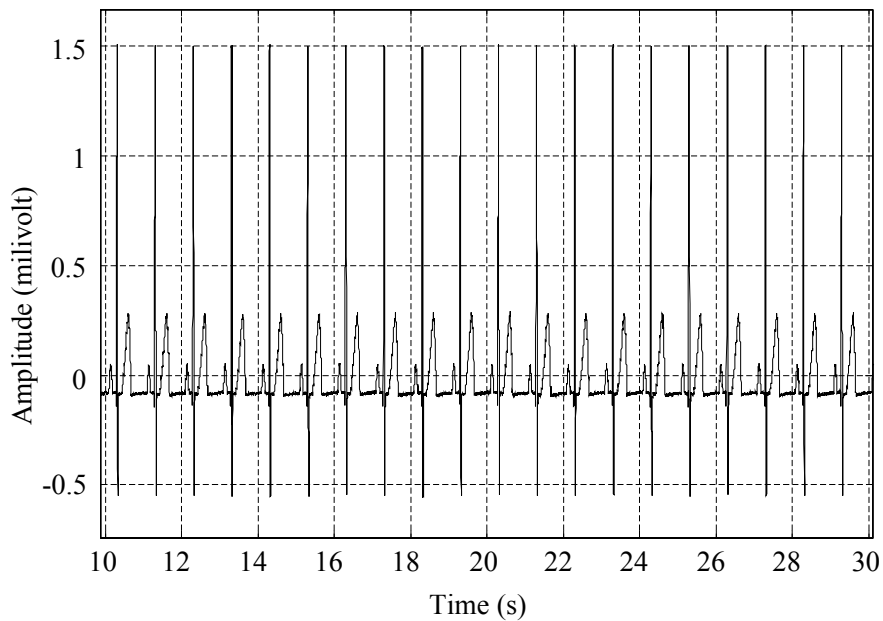
Figure 4.35: Graphical diagram of online filtering algorithm.

4.6.1 Blackman Window FIR Online Filter

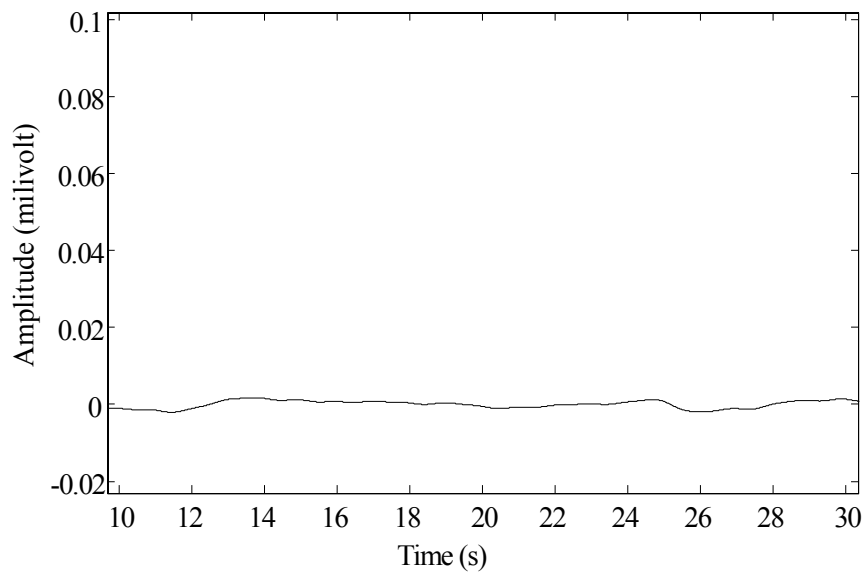
The offline Blackman window FIR filter is performed for online filtering. The result of offline Blackman window FIR filter was given in the Figure 4.11 (a), and the RMSE and the RRSE were calculated as 1 micro-volt (μV) and 0.45 %, respectively for the offline case. This offline filter had the smallest RRSE and RRSE values among all filters examined during this thesis study. Therefore, we chose it as one of the online filtering methods that we implement in this study.

In this study, 'w1' is selected as 2000. The value of w2 should be at least 3706 milliseconds for this filter, which is the length of group delay, therefore 'w2' is selected as 4000. The group delay effect is suppressed for each w1-length window.

The result of online Blackman window FIR filter is given in the Figure 4.36 (a). The error signal, which is the difference between the pure data shown in Figure 3.3 and the filtered data, is shown in Figure 4.36 (b). The RMSE and the RRSE are calculated as 1 micro-volt (μV) and 0.45 %, respectively for the online case. This means that the online Blackman window FIR filter has the same error as the offline case. Also the results of other windowing methods are shown in Table 4.4, Table 4.5 and Table 4.6. The power spectrum density estimate of the online filtered signal is presented in Figure 4.37. When we compare this estimate with the power spectrum density estimate of the pure data shown in Figure 3.5, we observe that the signal's frequency components are not disturbed.



(a)



(b)

Figure 4.36: Blackman window online FIR filter results. (a) filtered data, (b) the difference between the filtered data and the pure signal.

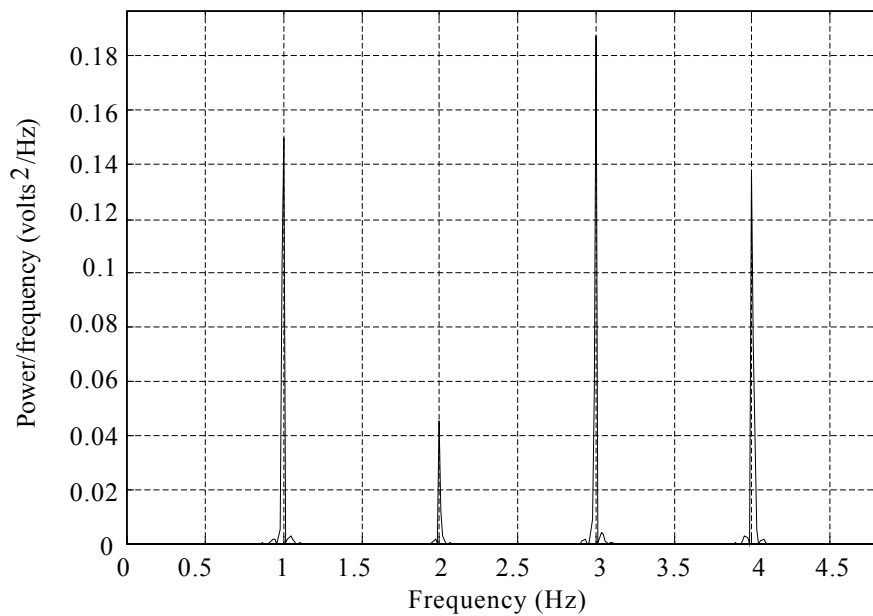


Figure 4.37: Power spectrum density estimation of online Blackman window filtered signal.

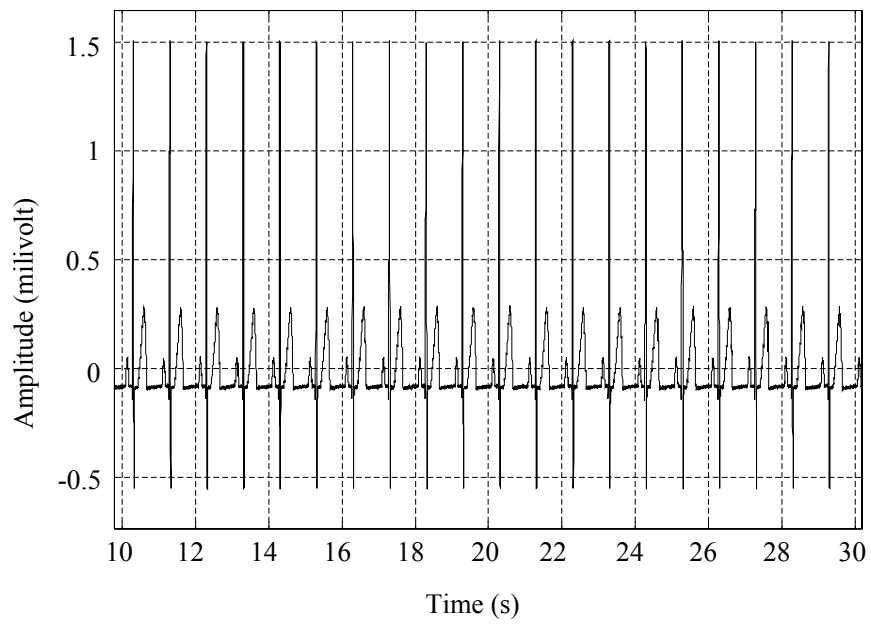
4.6.2 Bidirectional IIR Online Filter

The offline bidirectional IIR filter is performed for online filtering. The result of offline filter was given in Figure 4.16 (a). The error signal, which is the difference between the pure data shown in Figure 3.3 and the filtered data, was shown in Figure 4.16 (b). The RMSE and the RRSE were calculated as 1.55 micro-volt (μV) and % 0.70 respectively for the offline case. So, suppression performance of offline filter is quite well and it is applied for the online case.

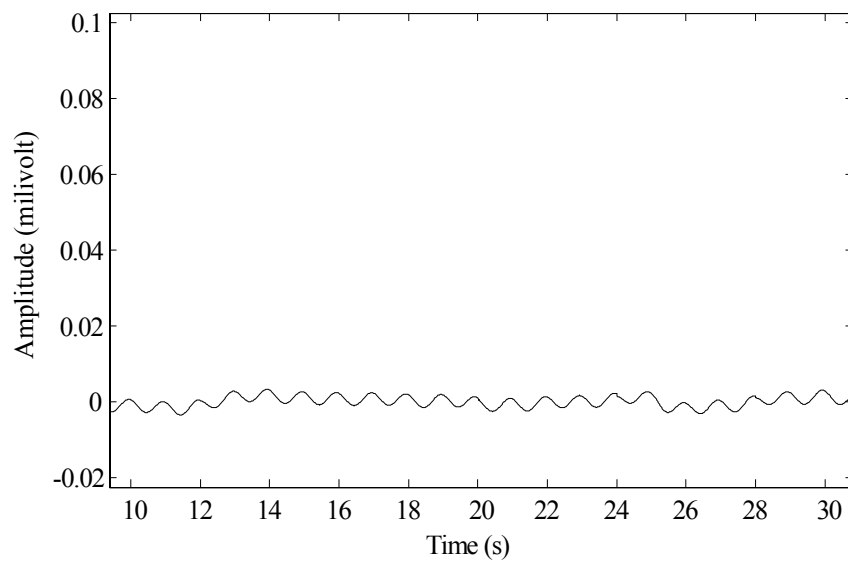
In this study, similar to the Blackman window online FIR filtering case, 'w1' and 'w2' are selected as 2000 and 4000, respectively.

The result of online bidirectional IIR filter is given in Figure 4.38 (a). The error signal is shown in Figure 4.38 (b). Again, this online filter has the same error as the offline case; the RMSE and the percentage RRSE values are 1.54 micro-volt (μV) and 0.70 % respectively.

The power spectrum density estimate of the online filtered signal is presented in Figure 4.39. When we compare this estimate with the power spectrum density estimate of the pure data shown in Figure 3.5, we observe that the signal's frequency components are not disturbed. The results are summarized in Table 4.4, Table 4.5 and Table 4.6.



(a)



(b)

Figure 4.38: Bidirectional IIR online filtered data results (a) filtered data, (b) the difference between the filtered data and the pure signal.

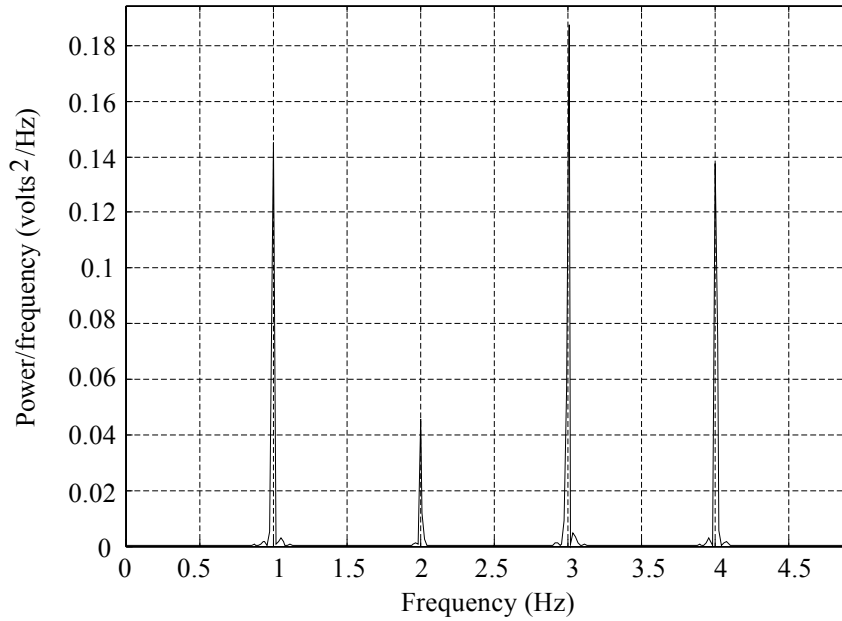


Figure 4.39: Power spectrum density estimation of online bidirectional IIR filtered signal.

4.6.3 Summary of Online Filtering Results

The table of the normalized PSD values for the frequencies of 1, 2, 3 and 4 Hz are given in Table 4.4. We compare these normalized PSD values with the power spectrum density estimate of the pure data of Figure 3.5, and the offline filtering results. As a result, the online filter normalized PSD values (in Table 4.4) are quite similar to the offline filter results (in Table 4.1). The length of selected window ‘w2’ is 4 seconds for the performed online filters. The length of window ‘w1’ is selected as 2 seconds and 4 seconds for each filter. We observed that the performance of window length of 4 seconds is better than that of window length of 2 seconds (for the data from 0 to 50 seconds given in Table 4.6), since, the transient effect is a problem at the beginning and at the end of the signal. The algorithm described in Figure 4.35 suppressed the deterioration ‘transients’ at both edges of window ‘w1’. So, the results of online filtering are quite similar to the results of offline filtering given in

Table 4.2 and Table 4.5 (for the signal from second 10 to 30). The result of length 2 seconds is satisfactory, which is given in Table 4.5 and Table 4.6, since, online filters need short window length and short filtering time due to real time monitoring and filtering applications.

Table 4.4: The power spectrum density estimation normalized with respect to the pure data.

	1Hz	2Hz	3 Hz	4 Hz
Pure data	1	1	1	1
FIR Hamming window filter (w1=2000)	0.98	0.98	1	0.99
FIR Hamming window filter (w1=4000)	0.99	0.99	1	1
FIR Hanning window filter (w1=2000)	0.98	0.98	1	0.99
FIR Hanning window filter (w1=4000)	0.99	1	1	1
FIR Blackman window filter (w1=2000)	0.98	0.98	1	0.99
FIR Blackman window filter (w1=4000)	0.99	1	1	1
Bidirectional Butterworth IIR filter (w1=2000)	0.95	0.98	1	1
Bidirectional Butterworth IIR filter (w1=4000)	0.96	0.99	1	1

Table 4.5: The RMSE and percentage RRSE of the filters from 10 s to 30 s of the original ECG signal

(from second 10 to 30)	RMSE (μV)	RRSE %
Pure data	0	0
FIR Hamming window filter (w1=2000)	1.09	0.49
FIR Hamming window filter (w1=4000)	1.09	0.49
FIR Hanning window filter (w1=2000)	1.05	0.48
FIR Hanning window filter (w1=4000)	1.05	0.48
FIR Blackman window filter (w1=2000)	1.00	0.45
FIR Blackman window filter (w1=4000)	1.00	0.45
Bidirectional Butterworth IIR filter (w1=2000)	1.54	0.70
Bidirectional Butterworth IIR filter (w1=4000)	1.54	0.70

Table 4.6: The RMSE and percentage RRSE of the filters from second 0 to 50 of the original ECG signal.

(from second 0 to 50)	RMSE(μ V)	RRSE %
Pure data	0	0
FIR Hamming window filter (w1=2000)	7.07	3.22
FIR Hamming window filter (w1=4000)	3.04	1.38
FIR Hanning window filter (w1=2000)	7.00	3.19
FIR Hanning window filter (w1=4000)	2.88	1.31
FIR Blackman window filter (w1=2000)	7.11	3.24
FIR Blackman window filter(w1=4000)	2.78	1.27
Bidirectional Butterworth IIR filter (w1=2000)	7.24	3.30
Bidirectional Butterworth IIR filter (w1=4000)	3.15	1.43

4.7 The Effect of Cut-off Frequency on the ST Segment Depressed Data

We have stated in Section 1.4 that when heart rate and respiration frequency changes, the cut-off frequency of the baseline wander filters should also change to reflect these changes. In this section, we demonstrate the effects of the cut-off frequency using a bidirectional IIR filter on an ST segment depressed-baseline noisy ECG signal by time domain observations.

ST segment depression is an indicator of myocardial infarction. When ST segment depressed ECG data including baseline noise is filtered, some important information is lost. Therefore, it is important to select an appropriate cut-off frequency for the baseline wander removal filters in order to keep important features of the ST segment depressed ECG signal.

In this study, we used a simulated ECG recording shown in Figure 4.40, which has ST segment depression and baseline noise, obtained from Kardiosis. The duration of the recording is 10 seconds and sampling rate is 1 kHz as shown in Figure 4.40. The resolution of the data is two bytes (16 bits). We used Channel II of a 12-lead ECG recording. PSD estimation of noisy data is shown in Figure 4.41.

Only offline bidirectional IIR filter is implemented due to its successful suppression performance and easy implementation advantage. Four different cut-off frequencies, (0.4 Hz, 0.67 Hz, 0.85 Hz and 1.2 Hz), are used in order to observe the effects of the cut-off frequency. The effect of cut-off frequencies are examined by observing the time domain results and PSD estimate of the filtered signals.

When we apply the filter with a cut-off frequency of 0.4 Hz, we obtain the result shown in Figure 4.42. PSD estimate of this filtered data is shown in Figure 4.43. With this choice of filter cut-off frequency, suppression of baseline wander noise is not satisfactory. When we choose the cut-off frequency as 0.67 Hz, we obtain the result shown in Figure 4.44 with PSD estimate as shown in Figure 4.45. The suppression performance is satisfactory. Result of using the cut-off frequency of 0.85 Hz is shown in Figure 4.46. The PSD estimate of the filtered data is shown in Figure 4.47. With this choice of the cut-off frequency, suppression performance is more satisfactory than 0.67 Hz when the time domain result and PSD estimate are examined carefully. Finally, Figure 4.48 shows the filtered signal when the cut-off frequency is equal to 1.2 Hz, and its PSD estimate is shown in Figure 4.49. This filter distorts the frequency components at 1.2 Hz and the original signal is changed.

When the frequency components between 0 and 1.2 Hz are filtered, the ST segment interval is changed and some vital ECG frequency components are suppressed. Also as can be seen from Figure 4.48, the slope of ST segment depression is altered. When only the frequency range between 0 to 0.4 Hz is suppressed, the suppression performance of baseline filter is not acceptable. The aim of successful baseline suppression is not to change the original data while suppressing the noise more effectively. Cut-off frequency varies from 0.6 Hz to 0.9 Hz corresponding to the heart rate and baseline noise spectra. The desired cutoff frequency of 0.67 Hz was adequate for the simulated noisy ECG signal used in the previous sections, however, when the heart rate varies, the spectrum of the signal should be examined for satisfactory selection of cut-off frequency. When baseline spectrum moves right as shown in Figure 4.41, a more proper cut-off frequency,

which lies between 0.8-0.9 Hz for this ECG example, should be selected in order to suppress the baseline noise adequately.

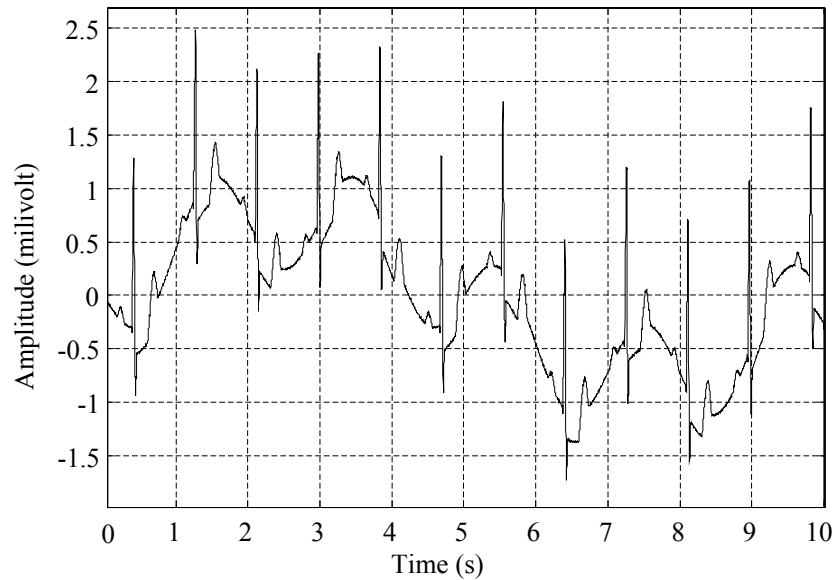


Figure 4.40: ST segment depressed baseline noisy data. Sampling frequency is 1 kHz and it is recorded from an ECG simulator.

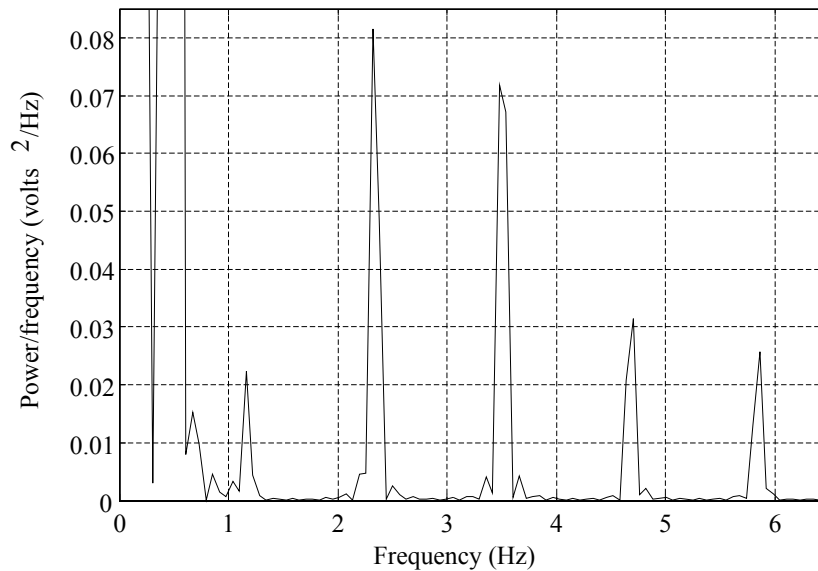


Figure 4.41: Power spectrum density estimation of baseline noisy data which has ST segment depression. Frequency range is from 0 to 6 Hz

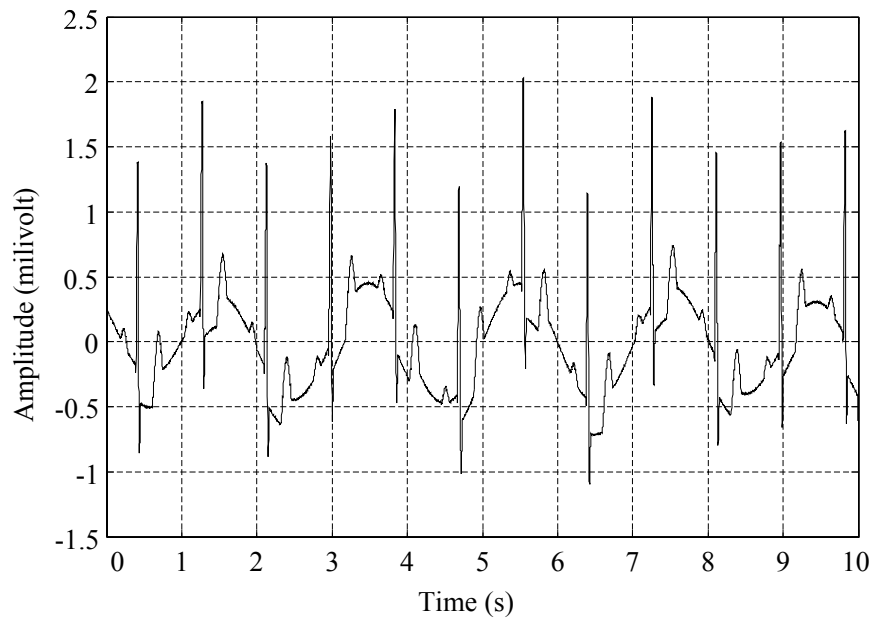


Figure 4.42: Offline bidirectional IIR filtered data. The performed cut-off frequency is 0.4 Hz.

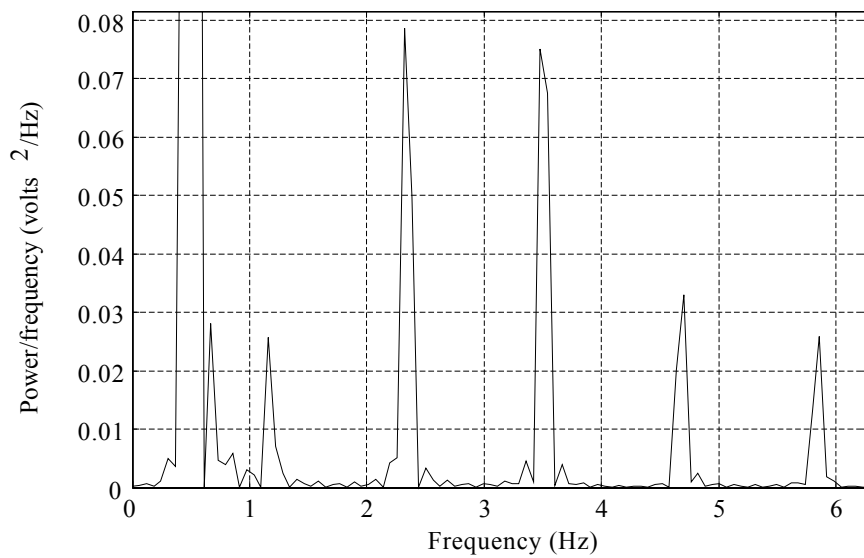


Figure 4.43: PSD estimate of offline bidirectional IIR filtered data. The performed cut-off frequency is 0.4 Hz.

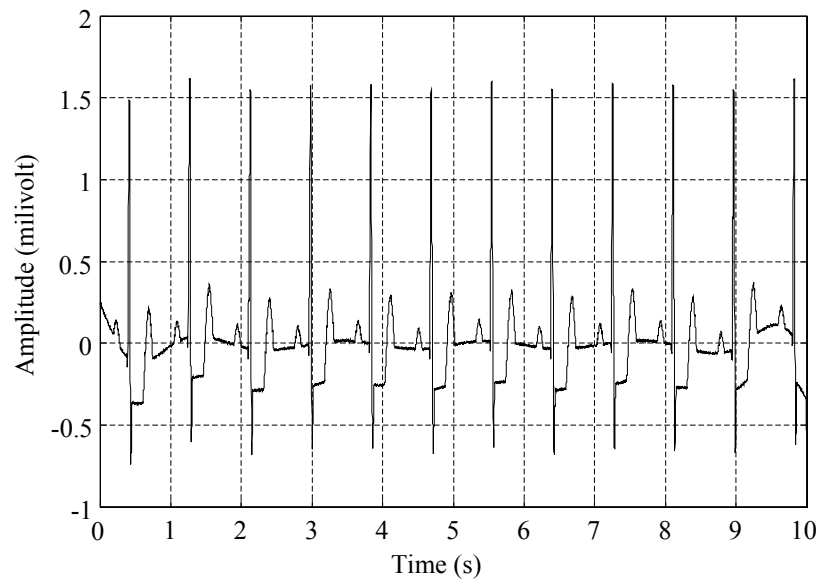


Figure 4.44: Offline bidirectional IIR filtered data. The performed cut-off frequency is 0.67 Hz.

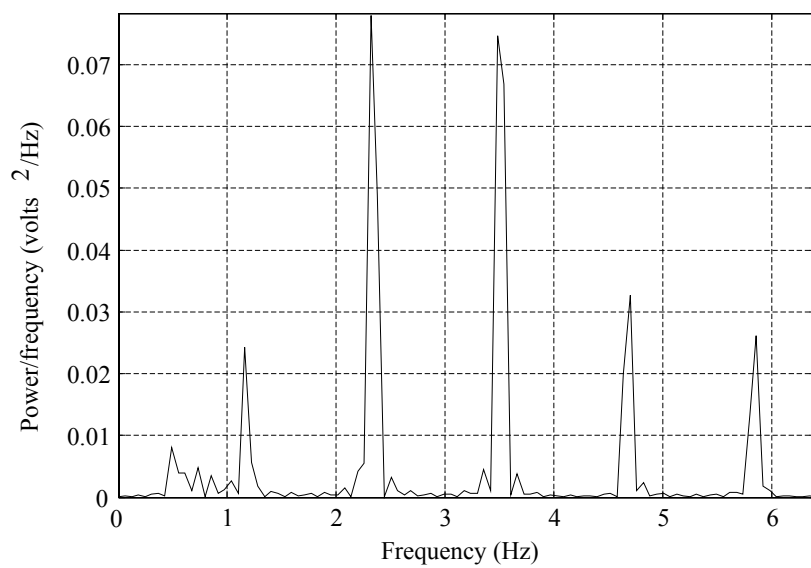


Figure 4.45: PSD estimate of offline bidirectional IIR filtered data. The performed cut-off frequency is 0.67 Hz.

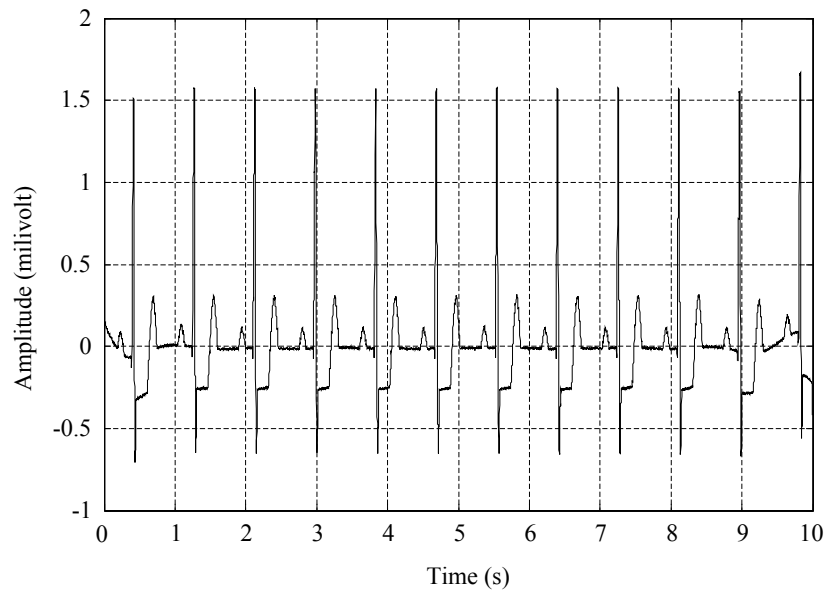


Figure 4.46: Offline bidirectional IIR filtered data. The performed cut-off frequency is 0.85 Hz.

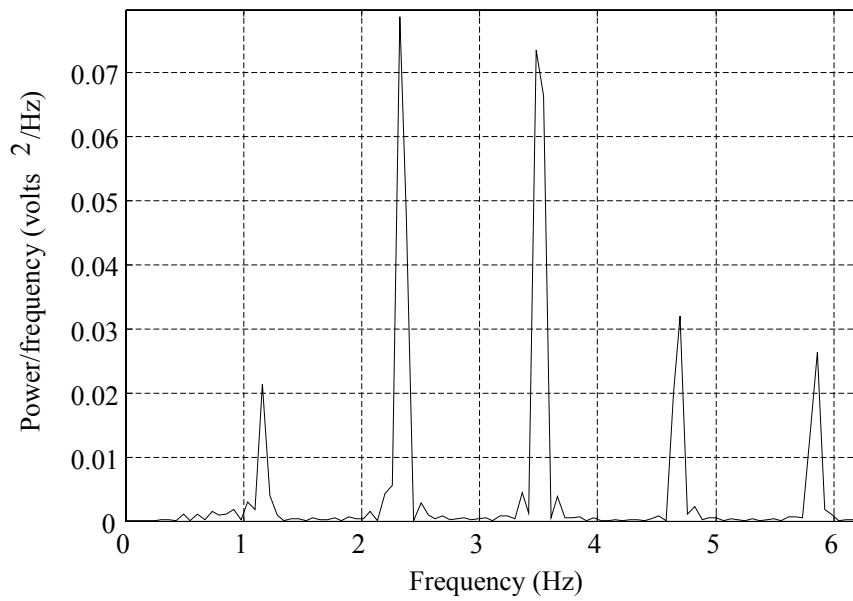


Figure 4.47: PSD estimate of offline bidirectional IIR filtered data. The performed cut-off frequency is 0.85 Hz.

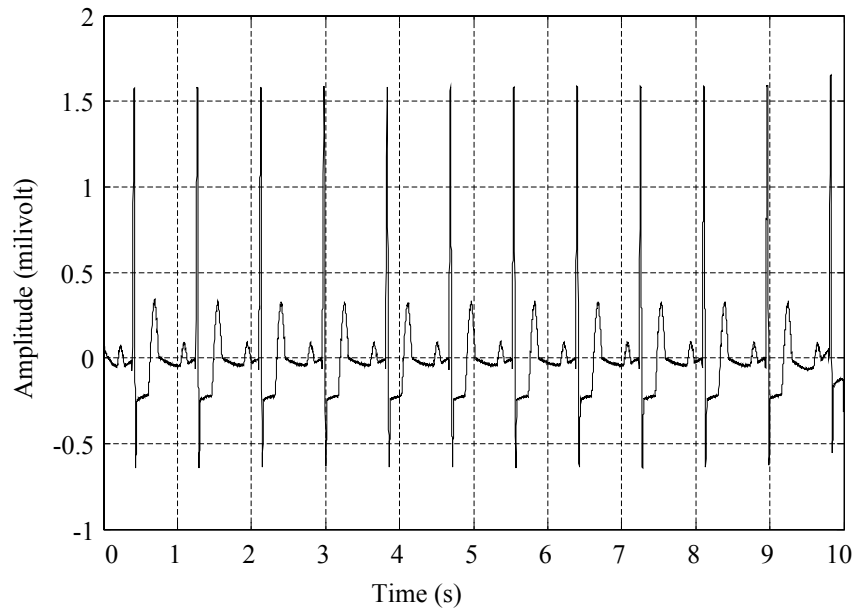


Figure 4.48: Offline bidirectional IIR filtered data. The performed cut-off frequency is 1.2 Hz.

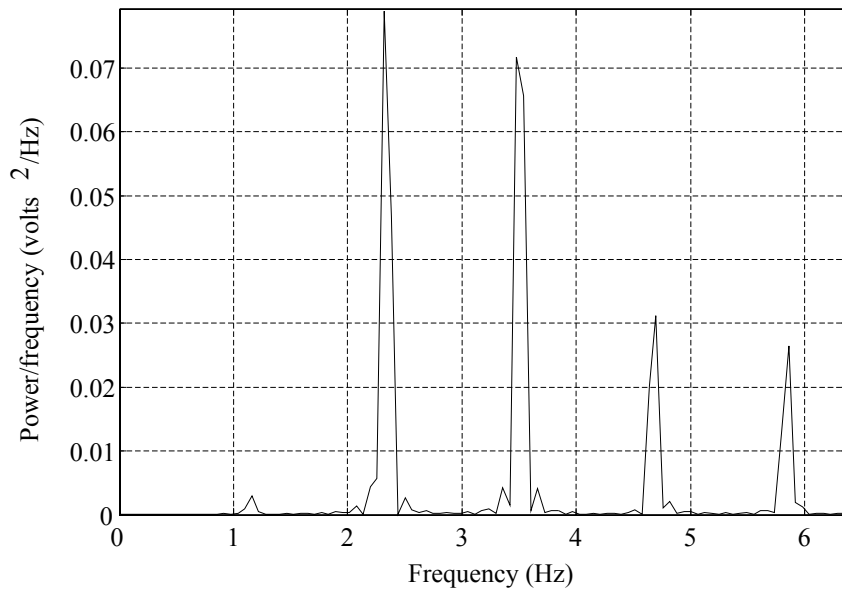


Figure 4.49: PSD estimate of offline bidirectional IIR filtered data. The performed cut-off frequency is 1.2 Hz.

CHAPTER 5

FILTERING REAL ECG DATA WITH BASELINE WANDER

In this chapter, we apply offline and online filtering techniques to real ECG recordings with baseline wandering noise and discuss the effectiveness of these filters in removing this noise. In the previous chapter, we have observed that with simulated noisy ECG data, Blackman window FIR and bidirectional IIR filters removed the baseline wander better than other filters. Therefore, we used only these two filters in this chapter.

5.1 Real ECG Data with Baseline Wander Noise

In this chapter, we applied offline and online Blackman window FIR and bidirectional IIR filters to real ECG data with baseline wander noise. The noisy data were provided by Oğuz Tanrıseven from Kardiosis. The duration of the data is 100 seconds and sampling rate is 1 kHz. The resolution of the data is two bytes (16 bits). We used Channel II of a 12-lead ECG recording, which is shown in Figure 5.1, since it has the highest amplitudes in the 12 lead ECG data. In order to see the details in the signal, we also plot the same ECG signal between 85 and 92 seconds in Figure 5.2 (this interval includes a considerable amount of baseline wander noise). Power spectrum density of the noisy ECG signal is plotted in Figure 5.3 from 0 to 60 Hz. Baseline wander noise appears in the lower frequencies of this spectrum, therefore in order to better observe the effects of the noise components, we show the low frequency components only in Figure 5.4. With real ECG recordings, we do not have access to the noise-free signal, therefore we can not use RMSE or RRSE to evaluate

the filtered outputs. Thus, we compare the suppression performances of the filters by examining the power spectrum density estimate of the filtered signals (cut-off and PSD deviations). Also, we examine the suppression performance visually in time domain.

5.1.1 Offline Filtering Results

In Chapter 4, we observed that Blackman window FIR and bidirectional IIR filters provided the best filtering results with simulated ECG data with baseline wander noise. Therefore, we only apply these two filters to real ECG recordings.

In the first part of this section, Blackman window FIR filter with parameters and characteristics given in section 4.1.2.3 is applied and the resulting ECG signal is plotted in Figure 5.5. In order to better observe the details in this signal, a few consecutive beats are shown in Figure 5.6. This figure plots the signal within the same time interval as in Figure 5.2. When we compare Figure 5.5 with Figure 5.1, and Figure 5.6 with Figure 5.2, we observe that the baseline wander is suppressed and the original signal is not distorted. The power spectrum density estimate of the filtered signal is presented in Figure 5.7. When we compare this estimate with the power spectrum density estimate of the pure data shown in Figure 5.4 (0 to 6 Hz in detail), we observe that the frequencies below 0.6 Hz are suppressed and the signal's frequency components are not disturbed. The frequency spectrum terms are almost the same with the pure data.

In the second part of this section, Bidirectional IIR filter with the parameters and characteristics given in section 4.2.2 is applied and the result is plotted in Figure 5.8. Again, we plot a few consecutive beats from the time interval used in Figure 5.2, in Figure 5.9. We observe that the baseline wander noise is filtered and the original signal is not distorted, when we examine Figure 5.2 and Figure 5.9 carefully. The power spectrum density estimate of the filtered signal is presented in Figure 5.10. When we compare this estimate with the power spectrum density estimate of the pure

data shown in Figure 5.4, we observe that the frequencies below 0.62 Hz are suppressed and the signal's frequency components are not disturbed. The frequency spectrum terms are almost the same with the pure data.

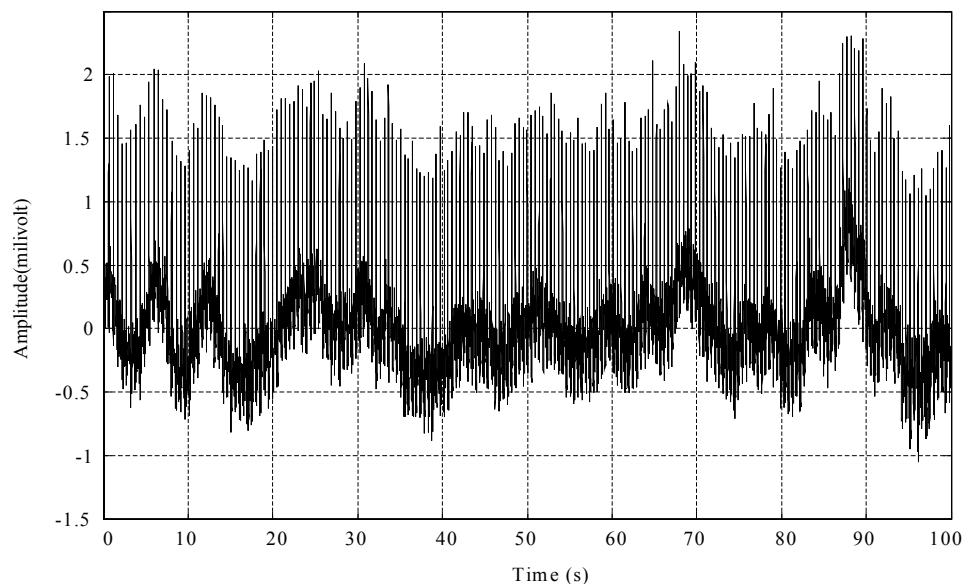


Figure 5.1: Baseline noisy data recorded from Channel II of a 12 channel ECG device.

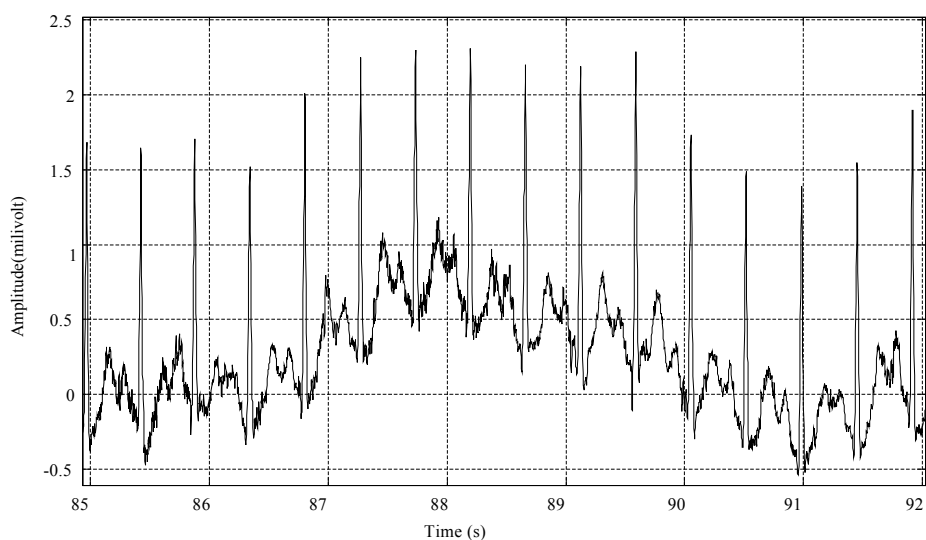


Figure 5.2: Baseline noisy ECG signal. A few consecutive beats taken from real data in Figure 5.1 and are plotted in this figure to show the data in detail.

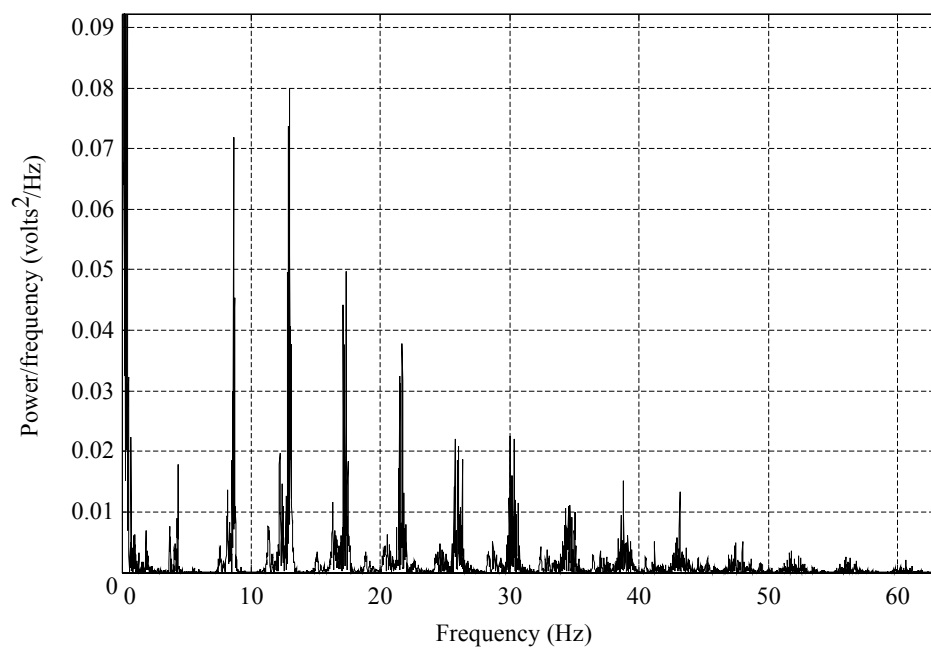


Figure 5.3: Power spectrum density estimation of the baseline noisy data. Frequency range is from 0 to 60 Hz to show the spectra of baseline noise and whole ECG.

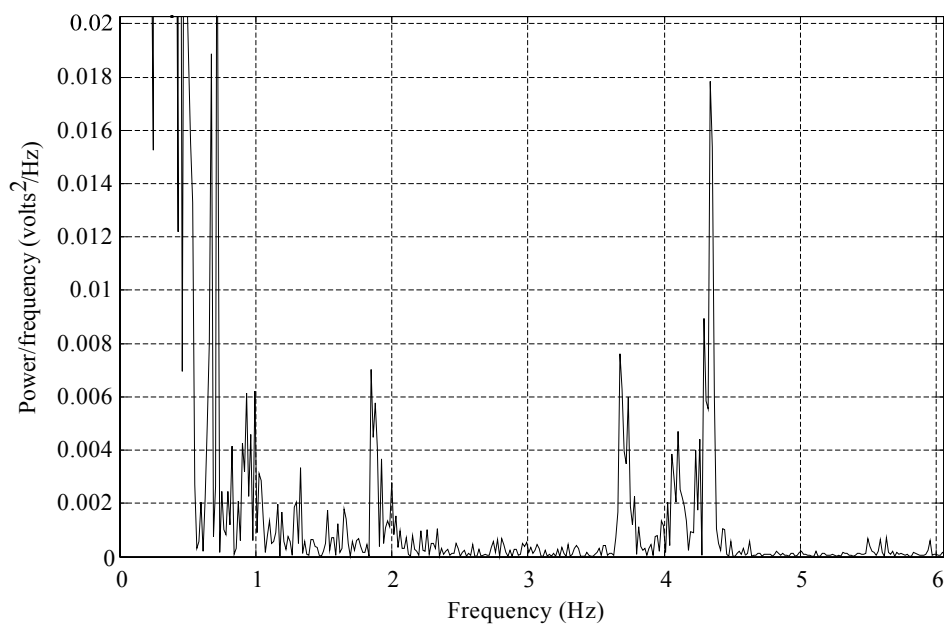


Figure 5.4: Power spectrum density estimation of baseline noisy data. Frequency range is from 0 to 6 Hz to show the baseline noise.

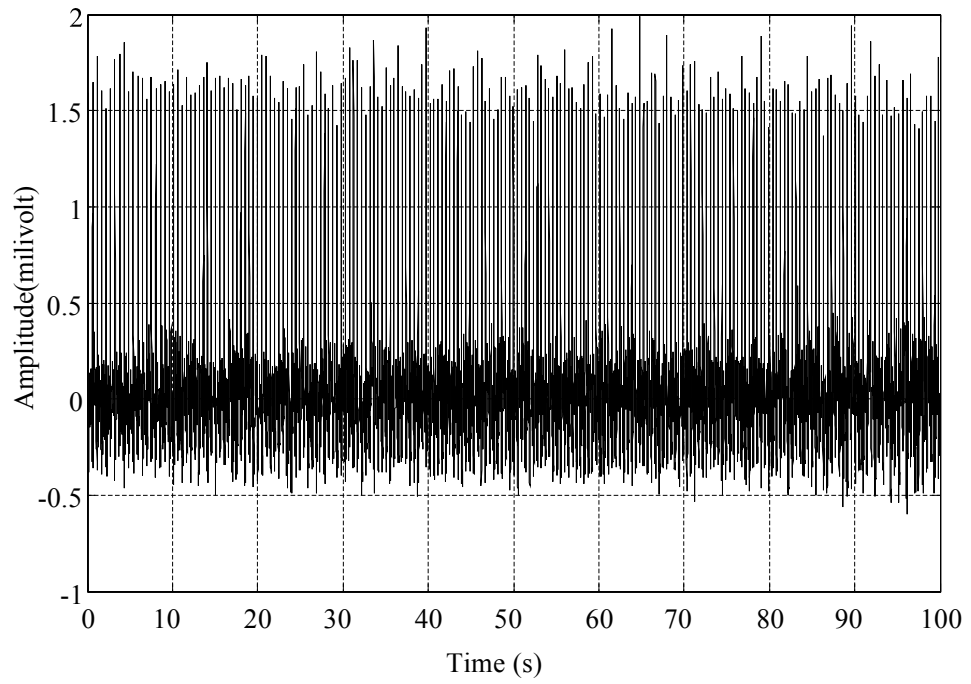


Figure 5.5: Baseline noise is suppressed with Blackman window FIR filter.

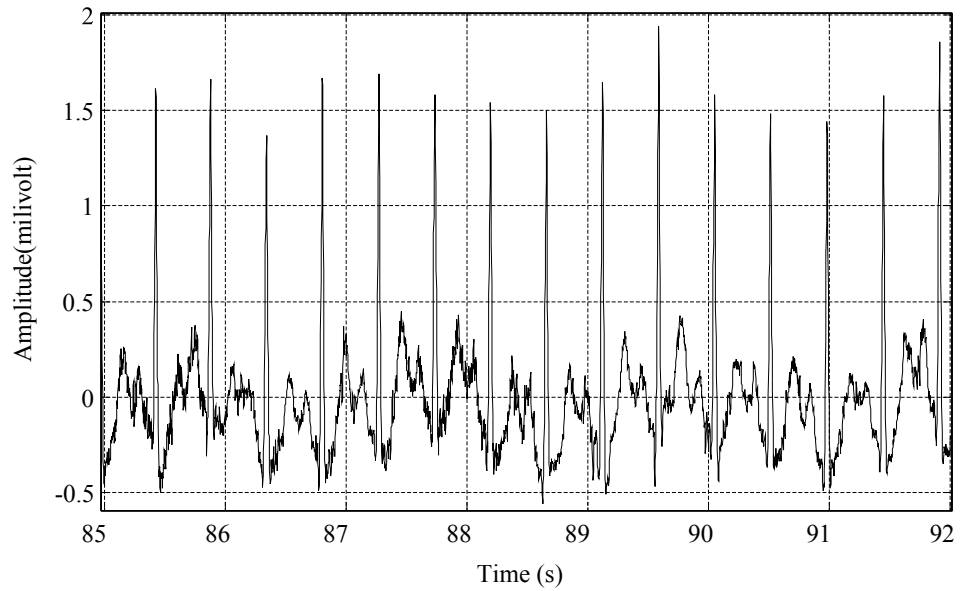


Figure 5.6: Blackman window FIR filtered ECG signal. A few consecutive beats taken from filtered real data in Figure 5.5 and these are plotted in figure to show the data in detail.

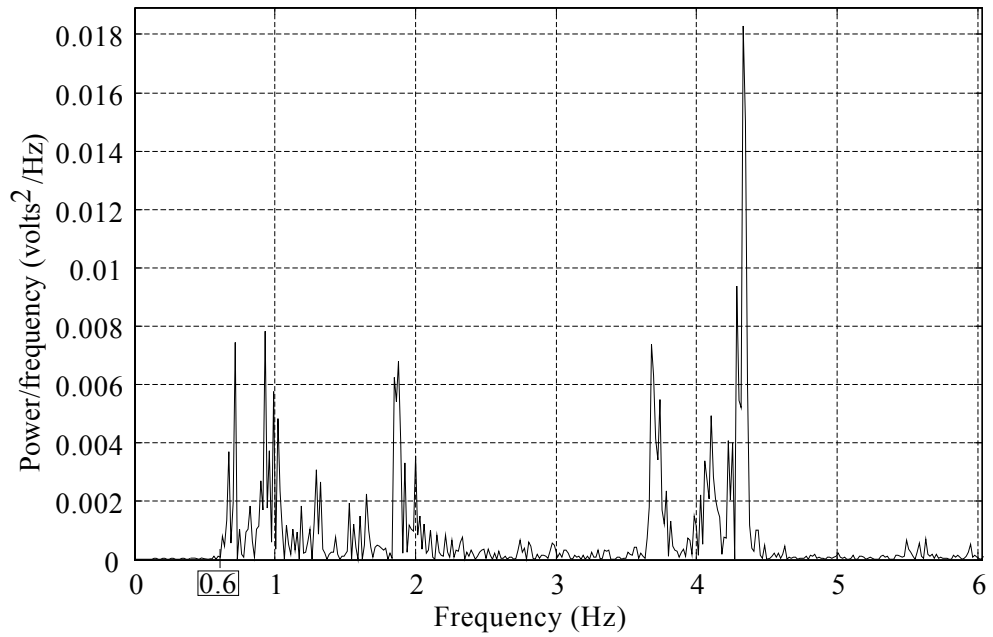


Figure 5.7: Power spectrum density estimation of Blackman window FIR filter. Frequency range is from 0 to 6 Hz to show cut off frequency and suppression of the filter. The performed cut off frequency is 0.6 Hz.

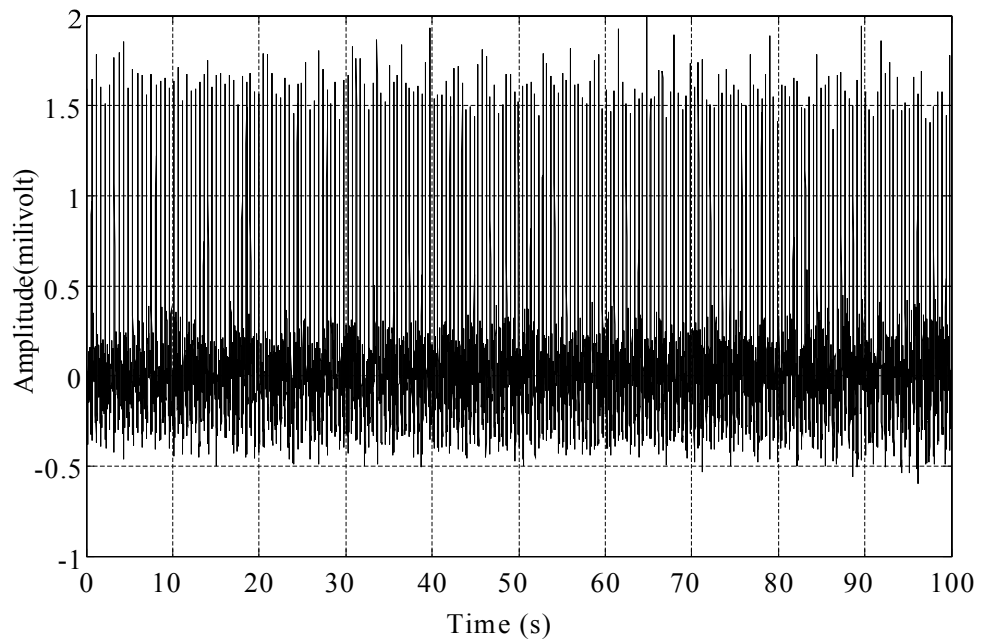


Figure 5.8: Baseline noise is suppressed with Bidirectional IIR filter.

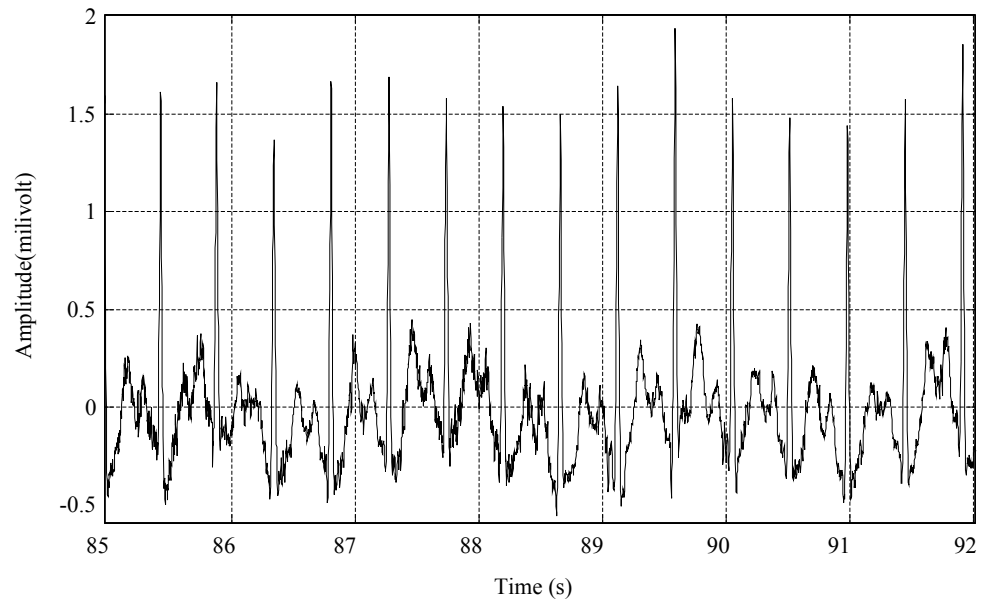


Figure 5.9: Baseline noise is suppressed with Bidirectional IIR filter. A few consecutive beats taken from filtered real data in Figure 5.8 and these are plotted in in order to show the data in detail.

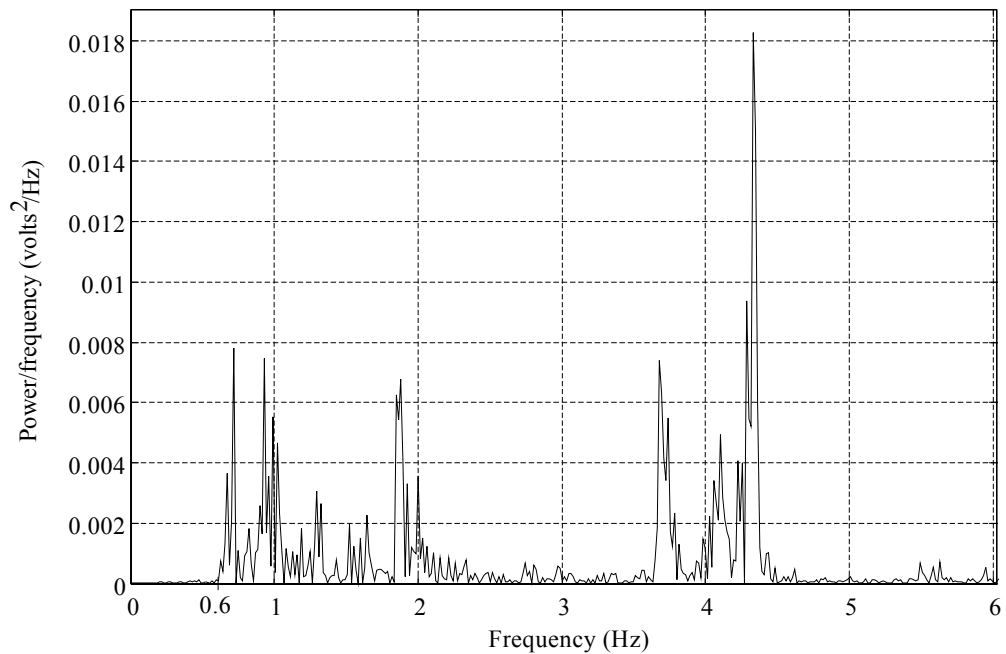


Figure 5.10: Power spectrum density estimation of bidirectional IIR filter. Frequency range is from 0 to 6 Hz to show cut off frequency and suppression of the filter. The performed cut off frequency is 0.62 Hz.

5.1.2 Online Filtering Results

In Chapter 4, we observed that Blackman window FIR and bidirectional IIR filters provided the best filtering results with simulated ECG data with baseline wander noise. Therefore, we only apply these two filters to real ECG recordings.

In the first part of this section, Blackman window FIR filter with parameters and characteristics given in section 4.2.2 is applied and the resulting ECG signal is plotted in Figure 5.11. In order to better observe the details in this signal, a few consecutive beats are shown in Figure 5.12. When we compare Figure 5.12 with Figure 5.2, we observe that the baseline wander is suppressed and the original signal is not distorted. The power spectrum density estimate of the filtered signal is presented in Figure 5.13. When we compare this estimate with the power spectrum density estimate of the pure data shown in Figure 5.4 (0 to 6 Hz in detail), we observe that the frequencies below 0.6 Hz are suppressed and the signal's frequency components are not disturbed. The frequency spectrum terms are almost the same with the pure data.

In the second part of this section, online Bidirectional IIR filter is performed and the result is plotted in Figure 5.14 and a few consecutive beats taken from filtered real data in Figure 5.14 and these are shown in Figure 5.15. The signal is filtered and the original signal is not distorted as Figure 5.2 and Figure 5.15 are examined carefully. The power spectrum density estimate of the filtered signal is presented in Figure 5.16. When we compare this estimate with the power spectrum density estimate of the pure data shown in Figure 5.4, we observe that the frequencies below 0.62 Hz are suppressed similar to the offline case and the signal's frequency components are not disturbed.

The results of the graphs from Figure 5.5 to Figure 5.16 are examined and it is concluded that both the online and the offline type filters used in this chapter provide satisfactory results. And it can be observed that the frequency components do not deviate significantly.

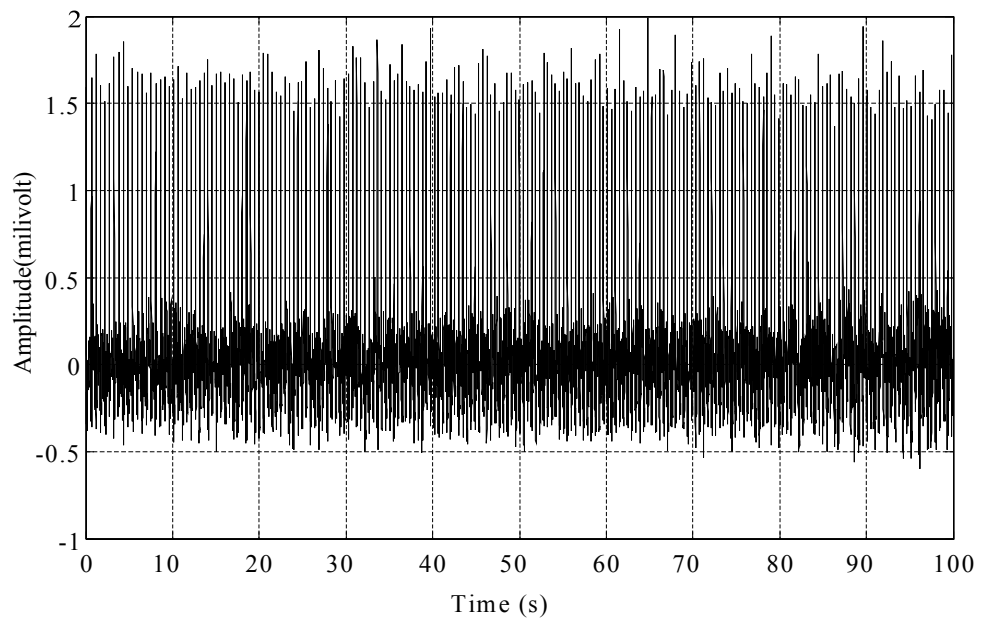


Figure 5.11: Baseline noise is suppressed with Blackman window FIR online filter.

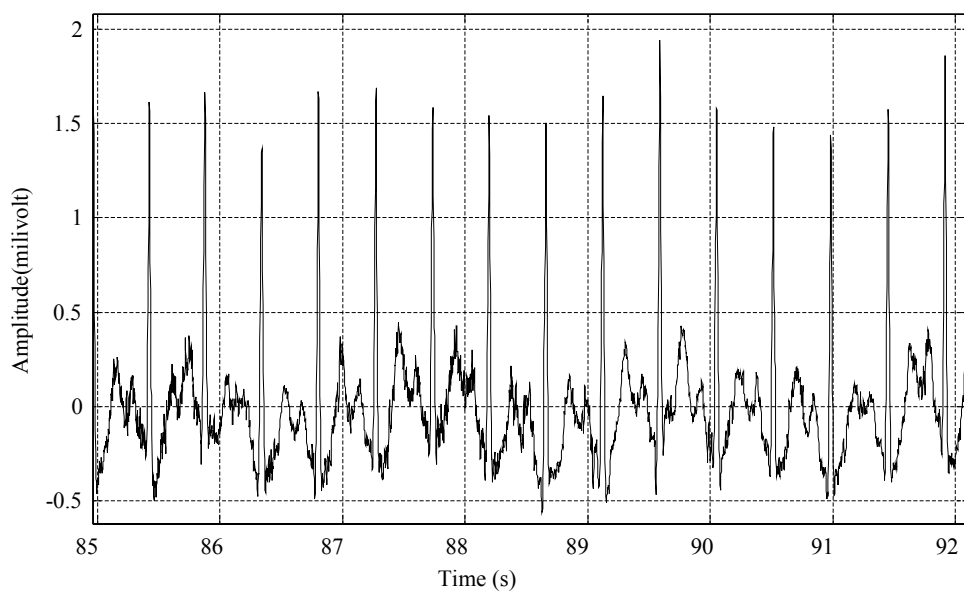


Figure 5.12: Baseline noise is suppressed with Blackman window FIR online filter.

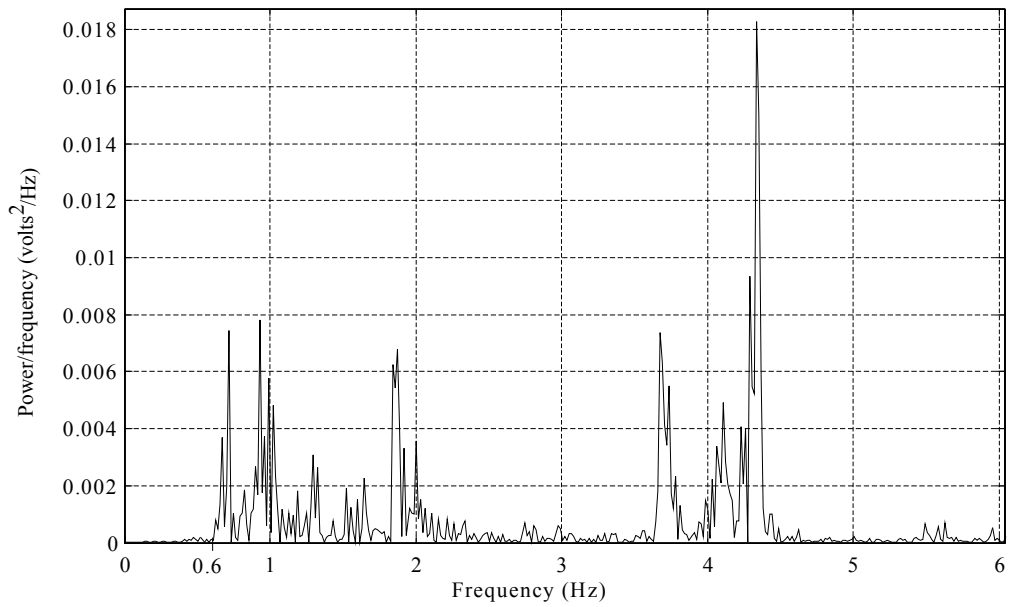


Figure 5.13: Power spectrum density estimation of Blackman window FIR online filter. Frequency range is from 0 to 6 Hz to show cut off frequency and suppression of the filter. The performed cut off frequency is 0.6 Hz.

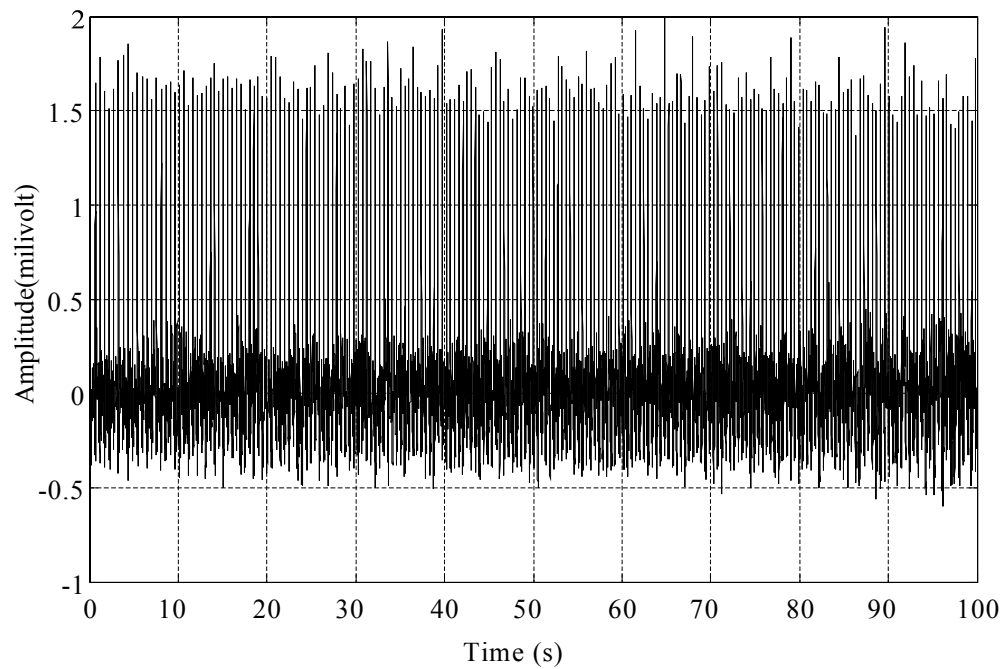


Figure 5.14: Baseline noise is suppressed with Bidirectional IIR online filter.

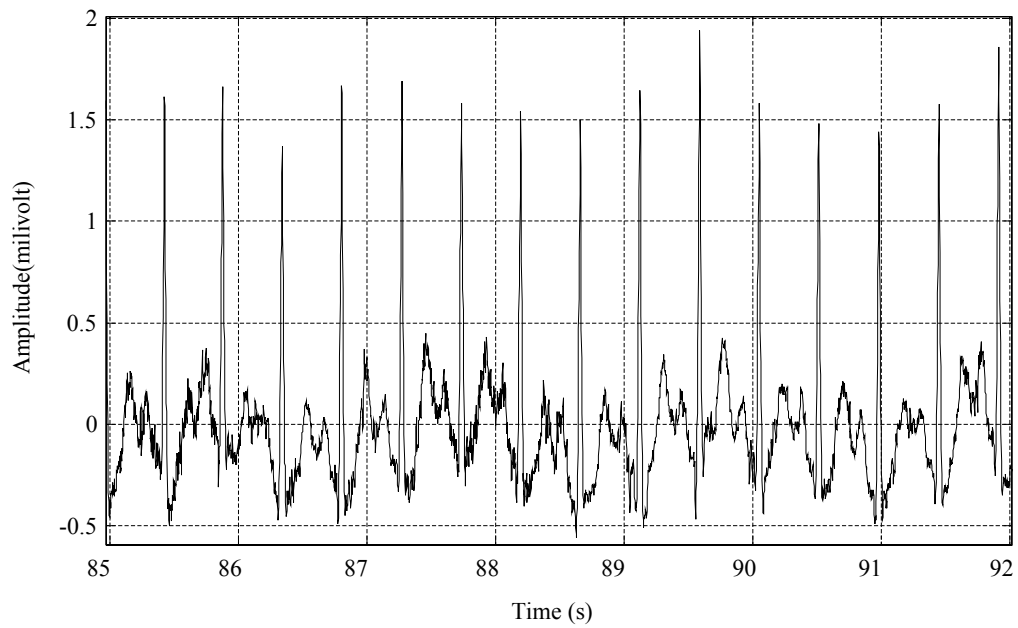


Figure 5.15: Baseline noise is suppressed with Bidirectional IIR online filter.

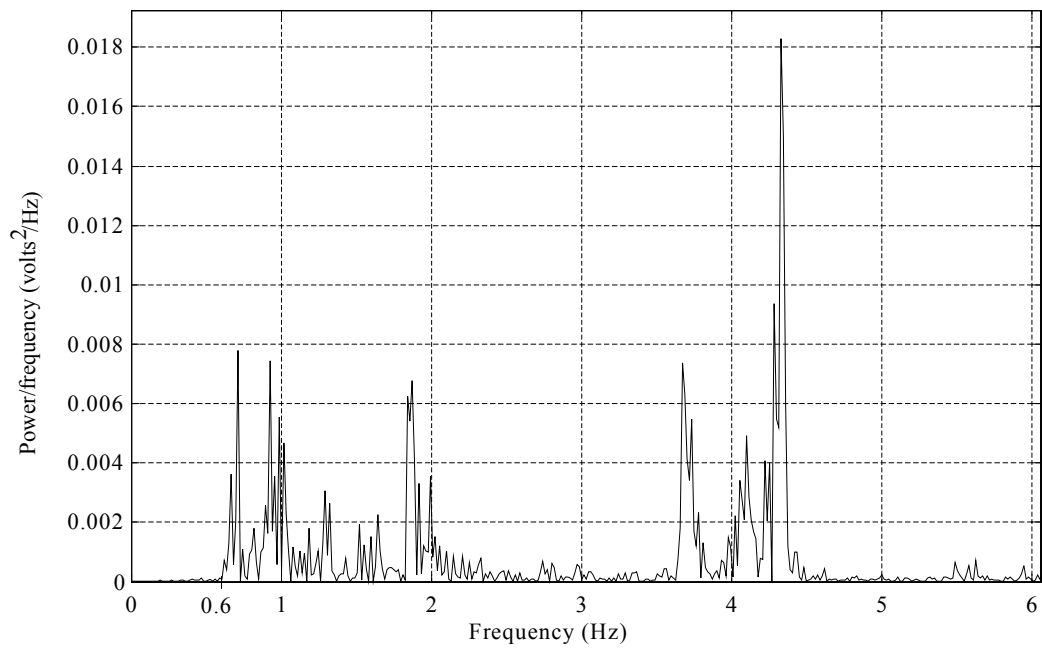


Figure 5.16: Power spectrum density estimation of bidirectional IIR online filter. Frequency range is from 0 to 6 Hz to show cut off frequency and suppression of the filter. The performed cut off frequency is 0.62 Hz.

CHAPTER 6

CONCLUSION AND DISCUSSION

Baseline wandering noise makes the analysis of ECG data difficult. It is desirable to remove this noise for proper analysis and display of the ECG signal. There are different filters to remove this noise. Finite Impulse Response (FIR) filters, Infinite Impulse Response (IIR) filters, interpolation filters and adaptive filters are implemented to suppress the baseline noise in this study.

Baseline wandering noise suppression may be carried out in two ways, offline and online. In offline filtering, the whole signal is recorded and the entire record is filtered. In online filtering, the signal is filtered as it is being recorded. It is necessary when real time processing and visualization are required as in an ECG stress test, in which the signal is simultaneously filtered and monitored in order to examine the effects of stress on the electrical activity of heart.

The main purpose of this study was first to implement various offline baseline noise filters and to discuss the advantages and disadvantages of each offline filter; then to apply successful offline filters for online filtering case. Also the suppression performances of both online and offline filters were investigated on real ECG data.

6.1 Comparison of FIR Filters

Sharp transition band, no ripple in pass-band and no ripple in stop-band is expected to eliminate the noise without changing the content of ECG signal for FIR filters. Thus, the order of the filter will be high to obtain such filter conditions. For

the applied FIR filters, this order equals 7412. This high order causes some implementation problems, such as hardware density, memory size, required time for the process etc. Also the group delay is high and it is approximately 3.7 seconds for FIR filters. A window of length having 7413 samples is used for windowing FIR filters given in Chapter 4. The optimal FIR filter is optimal in minimum error (difference between magnitude response of desired filter and designed filter) sense and it does not have the minimum RRSE. Root relative square error (RRSE) of offline type Blackman window FIR filter is 0.45 % and this is the minimum error result among the applied FIR filters. In fact, Blackman window FIR filter produces the best results among all filters used in this study.

6.2 Comparison of IIR filters

The order of performed Butterworth IIR filter is 5 and it is a recursive filter. Thus, IIR filters require less computation-power, and their implementation is easier than that of FIR filters. However, IIR filters have a phase distortion that is caused by nonlinear phase response of IIR filters and the RRSE is 64.46 %. It is the highest error and we observed that this filter disturbed the ECG signal. Phase distortion problem is solved by applying the IIR filter to the ECG signal in both directions. Reverse direction filtering is performed after forward direction filtering in order to correct the distortion of the ECG signal caused by the forward filtering phase distortion with non linear phase. This procedure is named as “zero-phase” or “bidirectional IIR filtering”. The RRSE of offline type zero-phase IIR filter is calculated as 0.7 %. It is slightly higher than the RRSE of the FIR filters; however it is still less than 1 %, which makes this filter a successful filter. Moreover, its computational complexity is low, therefore it is easy to implement, which makes this filter valuable for some applications, including online filtering.

6.3 Cubic Spline Interpolation Filters

When we implemented cubic spline interpolation filters, it was observed that the noise estimates constructed by using Q, R and S points as nodes do not match the actual baseline noise exactly. This mismatch between the actual noise and the interpolated noise decreases the performance of spline interpolation filters (SIF). As a result, RRSE in SIF is 3.52 % and it is higher than that of the FIR filters, and the bidirectional IIR filter. On the other hand, since SIF is not a frequency selective method, it does not negatively affect the power spectrum density of the ECG compared to the other methods. The frequency components at the frequencies of 1, 2, 3 and 4 Hz deviated from the original spectral peaks by approximately 1 %.

6.4 Adaptive Filters

NLMS filter is implemented as an adaptive filtering method. The normalized step size ' β ' is 0.1 and NLMS offset ' ε ' is 0.0001. Length of the filter is 1024. The RMSE and the RRSE were found to be equal to 30.26 micro-volt (μV) and 14.01 %, respectively. The performance of this filter is not satisfactory due to selection of inappropriate desired signal; RMSE and RRSE values are quite high.

6.5 Online Filtering

Online filtering is the case when real time processing and visualization are required and the signal is simultaneously filtered. Two successful offline filters performed on synthetic ECG are bidirectional IIR and Blackman window FIR. These offline filters had the smallest RMSE and RRSE values among all filters examined during the thesis study. Therefore, we chose these filters for online type filtering. The RMSE and the RRSE are calculated as 1 micro-volt (μV) and 0.45 %, respectively.

respectively for the online Blackman window FIR output. This means that the online Blackman window FIR filter has the same error as the offline case. We also observe that the signal's frequency components are not disturbed. The RMSE and the RRSE were calculated as 1.54 micro-volt (μV) and 0.7 %, respectively for the online bidirectional IIR output. The online bidirectional IIR filter has the same error as the offline case, and the signal's frequency components are not disturbed, as well. Although the suppression performance of Blackman window FIR filter is successful, the computational complexity of this filter is not appropriate for online filtering where fast implementation is important. Computational complexity of bidirectional IIR filter is much less than that of FIR filters, thus, it is more preferable for online filtering applications.

6.6 Real ECG Data Filtering

Two successful filters applied to synthetic ECG data are bidirectional IIR and Blackman window FIR. These filters are implemented and applied to real ECG signals and their performances are evaluated for both online offline cases. It is demonstrated that the signal's frequency components are suppressed (at both online and offline cases) up to 0.6 Hz with Blackman window FIR filter and up to 0.62 Hz with bidirectional IIR filter. The signal's frequency components are not disturbed, while the noise related low frequency components are suppressed.

6.7 Effects of the Cut-off Frequency

When the heart rate and respiration frequency changes, the cut-off frequency of the baseline wander filters should also change. In this study, we examined the effects of cut-off frequency on an ST segment depressed-baseline noisy data by using an offline Bidirectional IIR filter. Four different cut-off frequencies, 0.4 Hz,

0.67 Hz, 0.85 Hz and 1.2 Hz, are used in order to observe the effects of the cut-off frequency. 0.4 Hz cut-off frequency did not suppress baseline wander noise properly. When the frequency components between 0 and 1.2 Hz are filtered, the ST segment interval is changed and some vital ECG frequency components are suppressed. The suppression performance of 0.85 Hz is higher than 0.67 Hz, when time domain result and PSD estimate are examined carefully. Cut-off frequency varies corresponding to the heart rate and baseline noise spectra. Thus, constant cut-off frequency is not always appropriate for baseline wandering suppression and adaptive cut-off frequency selection should be more stable.

6.8 Summary of Conclusions

When we examine the filtering results in this thesis, we observe that Blackman window FIR filter yields the smallest RRSE value among all the filters. This observation is valid for both offline and online applications. However, high filter orders are required to obtain this satisfactory result, and this increases the computational complexity of the filter. Furthermore, there is significant delay in the filter results, thus this filter can be applied to long data windows. Therefore, this filter is appropriate for offline applications, but for online applications, in which short intervals of data is filtered and displayed and fast implementation is important, FIR filtering is not an appropriate filtering method. Bidirectional IIR filtering is more appropriate for online filtering applications due to its lower computational complexity, and its RRSE value for the simulated data is within an acceptable range.

The performance of interpolation methods is not satisfactory when compared to FIR and bidirectional IIR methods. However, since spline interpolation filtering is not a frequency selective method, frequency components of the ECG signal corresponding to large frequencies are not distorted. This method has some area of usage when the 2 Hz, 3 Hz frequencies' energies are desired to be very similar to the

original signal's energies. This method is considered as a reference method for comparison of the filtering performances.

The performance of applied adaptive filter is not satisfactory compared to FIR and bidirectional IIR methods. This filter is more suitable when there is random noise added to the ECG signal. Selection of proper reference signal is the main problem of this filter.

We have also observed that the choice of the cut-off frequency is very important; a lower than required cut-off frequency does not filter the actual ECG signal components, however some of the noise components remain as well. A higher cut-off frequency on the other hand, filters the noise successfully, but the ECG signal is distorted in the process. Cut-off frequency varies corresponding to the heart rate and baseline noise spectra. Thus, constant cut-off frequency is not always appropriate for baseline wandering suppression; it should be selected adaptively after a careful examination of the signal spectrum.

6.9 Future Work

As future work, spectrum adaptive cut-off frequencies could be studied for online type ECG applications. It would be better to study ST segment, other sensitive intervals in the ECG and the frequency spectrum of these segments. Also online baseline filtering of the ECG could be studied in detail in order to improve the performance of the filters for hardware implementations.

REFERENCES

- [1] Gulrajani, Ramesh M., “*Bioelectricity and Biomagnetism*”, John Wiley and Sons Publishing Company, 1998.
- [2] Dubin, D., Murat, S. N., “*Hızlı EKG Yorumu*”, Türkiye Klinikleri Yayınevi, 2003.
- [3] “Physiology of nerve homepage,”
<http://artsandscience.concordia.ca/psychology/psyc358/Lectures/APfigure.htm>, Last accessed date August 2006.
- [4] “EE416 Lecture homepage,”
<http://www.eee.metu.edu.tr/~yserin>, Last accessed date August 2006.
- [5] “Digital Filter design laboratory homepage,”
<http://www.seas.upenn.edu/~kfoster/kfoster.htm>, Last accessed date June 2006.
- [6] “Applied Signal processing homepage,”
<http://www.es.oersted.dtu.dk/staff/jaj/31610>, Last accessed date June 2006.
- [7] “Bookrags Electronic Encyclopedia homepage,”
<http://www.bookrags.com/research/electrocardiograph-ecg-woi/>, Last accessed date August 2006.
- [8] “Kardiosis WinEKG pro software homepage,”
<http://www.tepa.com.tr/PDFs/DownloadPage.htm>, Last accessed date August 2006.

- [9] "Health Encyclopedia Stress Test homepage,"
http://www.healthatoz.com/healthatoz/Atoz/ency/stress_test.jsp, Last accessed date August 2006.
- [10] Lisheng, X., Kuanquan, W., "Adaptive Baseline Wander Removal in the Pulse Waveform", IEEE, 1063-7125/02, 2002.
- [11] Rangayyan, Rangaraj M., "*Biomedical Signal Analysis*", John Wiley and Sons Publishing Company , 2002.
- [12] US Patent, "US5318036", Hewlett Packard.
- [13] Jane, R., Laguna, P., "Adaptive Baseline Wander Removal in the ECG:Comparative Analysis with Cubic Spline Technique", IEEE, 0276-6547/92, 1992.
- [14] "Ragnar Granit Institute ECG analysis lecture homepage,"
<http://ee.tut.fi/rgi/kurssit/71222/>, Last accessed date June 2006.
- [15] Pottala, E. W., Gradwohl, J. R., "*Comparison of Two Methods for Removing Baseline Wander In The ECG*", Pub Med National Library of Medicine,1992.
- [16] Pottala, E. W., "*Suppression of Baseline Wander in the ECG Using a Bilinearly Transform, Null-Phase Filter*", Journal of E.cardiology, vol. 22,1989.
- [17] US Patent, "US5402795", DellMar-Avionics.
- [18] Laguna, P., Jane, R., "Adaptive Filtering of ECG Baseline Wander" , IEEE, 0-7803-0785-2/92, 1992.

- [19] Rossi, R., “*Fast FIR Filters for a Stress Test System*”, IEEE, 0-8186-2485-X/92-6547/92, 1992.
- [20] Pandit, S., “*ECG Baseline Drift Removal through STFT*”, IEEE, 0-7803-3811-1/97, 1997.
- [21] Frau, D., Novak, D., “*Electrocardiogram Baseline Removal Using Wavelet Approximations*”, Proceeding of the 15th Biennial Eurasip Conference Biosignal, pp.136-138, 2000
- [22] Shusterman, V., “*Enhancing the Precision of ECG Baseline Correction*”, Computers and Biomedical Research, vol. 33, 2000.
- [23] “Biomedical Signal Processing lecture homepage,”
<http://www.cis.hut.fi/~aksela/javahome.html>, Last accessed date August 2006.
- [24] Sornmo, L., “*Time-Varying Digital Filtering of ECG Baseline Wander*”, Med. Biol. Eng. Computing, vol. 31, pp.503-504, 1993.
- [25] Oppenheim, A. V., Schafer R. W., “*Discrete-Time Signal Processing*”, Prentice Hall Publishing Company, 1999.
- [26] Lai, Edmund, “*Practical Digital Signal Processing*”, Newnes Publishing Company, 2003.
- [27] Mitra, Sanjit K., “*Digital Signal Processing a Computer Based Approach*”, McGraw-Hill Publishing Company, 1998.
- [28] Proakis, J. G., Monolakis, D. G., “*Digital Signal Processing Principles, Algorithms and Applications*”, Macmillan Publishing Company, 1999.

- [29] Lasada, R. A., "*Practical FIR Filter Design in MATLAB*", MathWorks, 2003.
- [30] Oppenheim, A. V., Schafer, R. W., Burrus, C. S., "*Computer-Based Exercises for Signal Processing Using Matlab*", Prentice Hall Publishing Company, 1994.
- [31] Dotsinsky, I., Stoyanov, T., "*Optimization of bi-directional digital filtering for drift suppression in electrocardiogram signals.*", Journal of Medical Eng. Tech., Volume 28, vol. 4, 2004.
- [32] Kohler, B. U., "*The principles of software QRS detection*", IEEE Eng. in Medicine and Biology, 2002
- [33] Kunzmann, U., Wagner, G., "*Parameter Extraction of ECG Signals in Real Time*", Biomedizinische Technik, 2002.
- [34] Tompkins, W. J., Pan, J., "*A Real-Time QRS Detection Algorithm*", IEEE Trans. Biomed. Eng., vol. 32, 1985.
- [35] Tompkins, Willis J., "*Biomedical Digital Signal Processing*", Prentice Hall Publishing Company, 1993.
- [36] Gomez, N., Gonzalez, R. I., "*A New Method for Electrocardiogram Study.*", IEEE, 0-7803-7789-3/03, 2003.
- [37] Harting, L., "*Baseline Suppression in ECG-Signals*", University of Twente, 2006.
- [38] Haykin, S., "*Adaptive Filter Theory*", Prentice Hall Publishing Company, 1996.
- [39] Hayes, M. H., "*Statistical Digital Signal Processing and Modeling*", John Wiley and Sons Publishing Company, 1996.

APPENDIX A

MATLAB BASED GRAPHICAL USER INTERFACE

MATLAB based graphical user interface (GUI) is prepared and function of filtering is executed with this GUI as shown in Figure A.1.

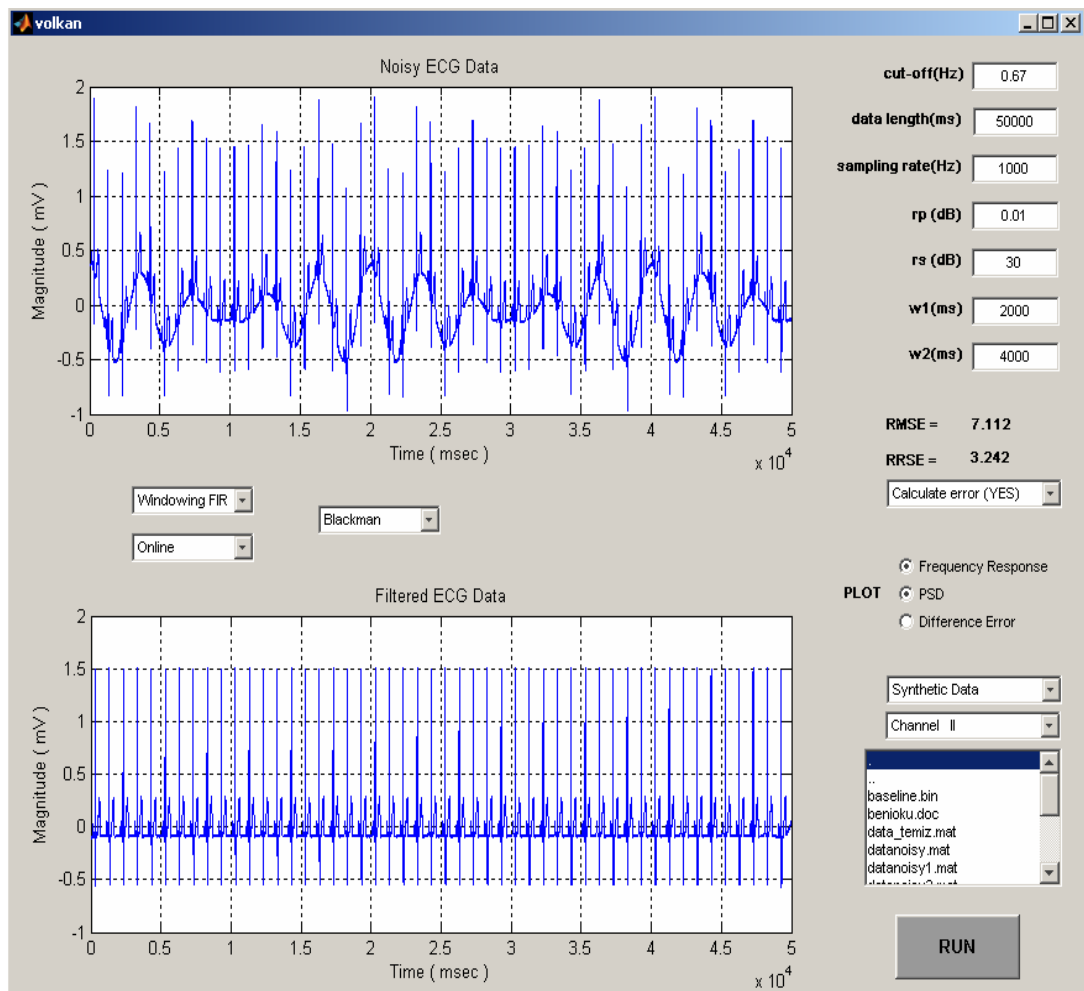


Figure A.1: Prepared graphical user interface (GUI). The graph on the top of GUI is noisy data and graph at the bottom is the filtered data.

cut-off(Hz)	0.67
data length(ms)	50000
sampling rate(Hz)	1000
rp (dB)	0.01
rs (dB)	30
w1(ms)	2000
w2(ms)	4000

(a)

1	<ul style="list-style-type: none"> Hamming Hamming Hanning Blackman 	6	<ul style="list-style-type: none"> Bidirectional IIR Optimal FIR Windowing FIR IIR Bidirectional IIR Interpolation Adaptive
2	<ul style="list-style-type: none"> Online Offline Online 	7	<ul style="list-style-type: none"> Calculate error (YES) Calculate error (NO) Calculate error (YES)
3	<ul style="list-style-type: none"> Q Q R S isoelectric 	8	<ul style="list-style-type: none"> Channel I Channel II Channel III Channel aVR Channel aVL Channel aVF Channel V1 Channel V2 Channel V3 Channel V4 Channel V5 Channel V6
4	<ul style="list-style-type: none"> Real Data Synthetic Data Real Data 	9	<input type="radio"/> Frequency Response <input type="radio"/> PSD <input type="radio"/> Difference Error
5	<ul style="list-style-type: none"> baseline.bin benioku.doc data_temiz.mat datanoisy.mat datanoisy1.mat datanoisy2.mat 		

(b)

Figure A.2: Filter design parameters are shown in (a) and property selection boxes are shown in (b).

Cut-off frequency (Hz), sampling rate (Hz), ripples (dB), length of windows (w1, w2) are selected in order to design required filter. Parameters can be selected within the edit boxes shown in Figure A.2 (a). The signal will be selected within selection box shown in Figure A.2 (b-5). If signal contains noise, the box shown in Figure A.2 (b-4) should be selected as 'real data'. If signal does not contain noise, the box shown in Figure A.2 (b-4) should be selected as 'synthetic data' and the synthetic noise will be added to the synthetic data selected in Figure A.2 (b-5). The channel type can be selected by Figure A.2 (b-8) because the binary signal contains data of 12 channels. Filter type can be selected as demonstrated in Figure A.2 (b-1, b-3, b-6). The online or offline type of filtering is selected by using list box shown in Figure A.2 (b-2). Error can be calculated by the box shown in Figure A.2 (b-7). Frequency response of filter, PSD estimation of filtered data, difference error, can be plotted when the radio buttons had been selected shown in Figure A.2 (b-9). After filter type and filter design parameters are selected, program executes the filtering process by selecting the run button on the screen as shown in Figure A.1.